

Investigation of the Adsorption of Model and Oil Sands Process-Affected Water Naphthenic  
Acids on Graphite

by

Ahmed Mohamed Abdel-Hakim Moustafa

A thesis submitted in partial fulfillment of the requirements for the degree of

Doctor of Philosophy

in

Environmental Engineering

Department of Civil and Environmental Engineering

University of Alberta

© Ahmed Mohamed Abdel-Hakim Moustafa, 2015

## ABSTRACT

Naphthenic acids (NAs) are constituents of bitumen in the oil sands deposits in northern Alberta, Canada. The extraction process of bitumen creates an enormous amount of wastewater called oil sands process affected waters (OSPW). This OSPW contains elevated concentrations of NAs, and other contaminants, that need removal in order to continue its reuse in the extraction process or eventually safe disposal into natural water streams. The research herein focusses on the understanding of NAs adsorption on the expanded graphite (EG) and highly-ordered pyrolytic graphite (HOPG). The adsorption of model NAs on EG was evaluated using Langmuir/Freundlich adsorption models and free energy thermodynamics calculations. Following the model compounds, the mechanisms for NAs adsorption of a commercial Merichem mixture and OSPW were explored. The visualization of adsorption on the surface of EG was not possible due to its irregular surface morphology. Thus, the Amplitude Modulation - Frequency Modulation Atomic Force Microscopy (AM-FM-AFM) was used to characterize the adsorption of NAs on HOPG.

Preliminary experiments revealed inconsistencies in NAs quantification due to the OSPW filtration method used to remove suspended solids. Thus, prior to the investigation of NAs adsorption, various filters were evaluated (nylon, polyvinylidene fluoride and polytetrafluoroethylene) to determine their impact on NAs quantification. Overall, the nylon membranes were the most hydrophilic and exhibited no removal of the acid extractable fraction (AEF) and limited removal of NAs (4%) from raw OSPW. Given these results, only nylon membranes were used for all remaining experimental work in the current study.

The adsorption of 5 model NA compounds in mono/multi-compound solutions was investigated to determine adsorption mechanisms. Overall, the NAs in both mono- and multi-compound solutions fit the Freundlich adsorption isotherms ( $R^2 > 0.89$ ). Thermodynamic

calculations were used to assign the formation of the negatively charged assisted hydrogen bond (–CAHB) between ionized solutes and the negatively charged functional groups (FGs) on the EG as the possible adsorption mechanism. The similar  $pK_a$  values of the model NAs resulted in comparable free energies for –CAHB formation ( $\Delta G^{-CAHB}$ ) being less than solvation free energies ( $\Delta G_{Solv}$ ). Thus, additional  $\Delta G$  is supplemented by increased hydrophobicity due to proton exchange of ionized acids with water ( $\Delta\Delta G_{Hydrophobicity}$ ). Adsorption capacities and competition coefficients indicated that  $\Delta\Delta G_{Hydrophobicity}$  values depend directly on hydrophobicity as indicated by  $\text{Log } K_{ow}$  values. Competitive adsorption implies the occurrence of multilayer adsorption via hydrophobic bonding with  $\text{CH}_3$  ends of the self-assembled layer of NAs to the EG surface.

Further study visually characterized the adsorption of decanoic acid (DA) on the surface of HOPG using AM-FM-AFM. The AM-FM-AFM images showed that DA molecules formed aggregates at the functionalized steps of HOPG and over the entire functionalized HOPG (F-HOPG). This DA adsorption to FGs in HOPG and F-HOPG confirmed the previous thermodynamics findings. The last step of this research was to understand the mechanism of NAs adsorption from complex mixtures including the Merichem NAs solution and raw OSPW. Adsorption results showed that higher  $\text{Log } K_{ow}$  NAs have higher removal efficiency for all solutions. The calculated free energy required for the formation of –CAHB was lower than the free energy of solvation for NAs; however the –CAHB formation was still triggered by the need for additional free energy  $\Delta\Delta G_{Hydrophobicity}$  as observed for model compounds. The presence of a large number of NAs species in both mixtures did not impact the reported mechanism.

In the current work, we confirmed that adsorption via the –CAHB governs the adsorption mechanism for ionized weak acids, such as NAs, to graphite-type surfaces. This knowledge is

essential for the development of possible engineered adsorbents for NAs and similar emerging pollutants of environmental concern. The identification of adsorption mechanisms (e.g., surface locations) could contribute to the development of specialized adsorbents that can significantly enhance the initial cost savings, efficiency and regeneration cost of wastewater treatment. It also contributes to the understanding of the aquatic fate and transport of NAs as impacted by their attachment on waste graphite nanomaterials that can be released into natural streams. Further, this research can be applied to various ionized acids and adsorbent combinations for treatment of other commercial and industrial wastewaters to allow for safe environmental effluent discharges.

## PREFACE

All of the research conducted in this thesis was designed and planned by myself and supervised by Professor Mohamed Gamal El-Din at the University of Alberta. Some of the research conducted for this thesis was done in collaboration with Dr. Hongbo Zeng at the University of Alberta and Professor Scott Smith at the Wilfrid Laurier University with Professor Mohamed Gamal El-Din being the lead collaborator at the University of Alberta. All the research work was conducted by myself except the following contribution from collaborators and coauthors:

### Chapter 2:

- Dr. EunSik Kim and Dr. Alla Alpatova contributed to the manuscript edits.
- Miss Nian Sun performed samples analysis using the Ultra pressure liquid chromatography-high resolution mass spectrometry (UPLC/HRMS)
- Professor Scott Smith provided us with his linear programming method (LPM) software to process our acid base titration results.
- Dr. Seoktae Kang was my co-supervisor at the University of Alberta and contributed to planning and manuscript edits.

### Chapter 3:

- Dr. Kerry N. McPhedran contributed to the manuscript edits.
- Dr. Jesús Moreira developed the MATLAB code for the Multi-compound Freundlich isotherm equation.

### Chapter 4:

- Mr. Jun Huang performed the Amplitude Modulation - Frequency Modulation Atomic Force Microscopy (AM-FM AFM) experiments on the samples previously processed by myself at Professor Mohamed Gamal El-Din's laboratory. Mr. Jun Huang wrote the

materials and methods for the AM-FM AFM section and contributed to the writing of the AM-FM AFM results explanation.

- Dr. Kerry N. McPhedran contributed to the manuscript edits.
- Professor Hongbo Zeng supervised Mr. Jun Huang's experimental and writing work. .

Chapter 5:

- Dr. Kerry N. McPhedran contributed to the manuscript edits.
- Miss Nian Sun performed samples analysis using the Ultra pressure liquid chromatography-high resolution mass spectrometry (UPLC/HRMS).

All the research work was conducted by myself except the above mentioned contribution from collaborators and coauthors.

*I dedicate my thesis work to*

*my very kind parents, my very patient wife,*

*my two beautiful daughters Nour & Salma and my super hero Yaseen*

*Kids: Thanks for the charming trips to EPL!*

## ACKNOWLEDGEMENTS

First and foremost, I thank Allah the almighty for providing me with guidance, patience, power and most importantly amazing people during my PhD years.

My deep gratitude is to my supervisor, Dr. Mohamed Gamal El-Din who gave me unique opportunities at the University of Alberta and supported me during my PhD years both academically and in my volunteer work at the Egyptian Students' Association. Thank you for allowing me to choose my research topic and for the continuous support to novel research ideas.

My deep thanks are due to Dr. Kerry N. McPhedran for his always open doors, for helping me improving my writing skills and for proof reading of my thesis.

My sincere appreciation is to Dr. Seoktae Kang, Dr. Lukas Wick, Dr. Hongbo Zeng and his PhD student Mr. Jun Huang, Dr. Scott Smith, Dr. Yang Liu, Dr. Ania Ulrich, Dr. Salma Guigard, Dr. Phillip Fedorak, Dr. Randy Whittal and Dr. Karen Dow for their help and support. I thank my group members, Dr. Pamela Chelme-Ayala, Dr. Alla Alpatova, Dr. Eun-Sik Kim, Dr. Parastoo Pourrezaie, Dr. Atefeh Afzal, Dr. Shahinoor Islam, Ms. Jingxin Wang, Ms. Nian Sun, Mr. Mohamed Ibrahim, Ms. Somaye Naser, Mr. Mohamed Meshref and Mr. Haitham Elnakar. I am indebted for the amazing technical support provided by Mrs. Maria Demeter and to valuable discussions with Mr. Mohammadreza Fayaz and Mr. Masoud Lashaki. I also thank my friends Ahmed Farag and Ehab Hamzah for all the great support during my PhD journey.

I am very grateful for the Alberta Innovates Technology Futures for a very generous Ph.D. Student Scholarship (2010-2013) and the funding provided by Helmholtz-Alberta Initiative (HAI) and NSERC Industrial Research Chair in Oil Sands Tailings Water Treatment.

Finally, I owe very special thanks to my family. To my parents, my wife, my daughters and my son, PhD could not be possible without you.

## TABLE OF CONTENT

<b>1 GENERAL INTRODUCTION AND RESEARCH OBJECTIVES .....</b>	<b>1</b>
1.1 MOTIVATION.....	1
1.2 BACKGROUND.....	3
1.2.1 Composition of the OSPW .....	3
1.2.2 NAs.....	3
1.2.3 Adsorption .....	6
1.3 SCOPE OF RESEARCH AND OBJECTIVES .....	8
1.4 THESIS ORGANIZATION.....	11
1.5 REFERENCES.....	13
<b>2 IMPACT OF POLYMERIC MEMBRANE FILTRATION OF OIL SANDS PROCESS WATER ON ORGANIC COMPOUNDS QUANTIFICATION<sup>1</sup> .....</b>	<b>17</b>
2.1 INTRODUCTION .....	17
2.2 MATERIALS AND METHODS .....	19
2.2.1 Oil sands process-affected water (OSPW).....	19
2.2.2 Chemicals and reagents .....	19
2.2.3 Filtration set-up and membranes .....	19
2.2.4 Quantification of acid-extractable fraction (AEF) and classical NAs.....	20
2.2.5 Synchronous fluorescence spectroscopy (SFS) analysis.....	21
2.2.6 X-ray photoelectron spectroscopy (XPS).....	21
2.2.7 Characterizations of the surfaces of polymeric membranes.....	21
2.3 RESULTS AND DISCUSSION.....	22
2.3.1 Identification of functional groups in AEF by acid-base titration and LPM....	22

2.3.2	Surface characterization of pristine polymeric membranes .....	23
2.3.3	Effects of centrifugation and solution pH on the adsorption of AEF on membrane during filtration .....	26
2.3.4	Identification of adsorbed aromatic compounds from OSPW and Merichem NAs solutions .....	28
2.3.5	ATR FT-IR analysis of membrane surfaces .....	30
2.3.6	Measurement of classical NAs using UPLC/HRMS .....	34
2.4	CONCLUSIONS .....	37
2.5	REFERENCES .....	38
<b>3</b>	<b>INVESTIGATION OF MONO/COMPETITIVE ADSORPTION OF ENVIRONMENTALLY RELEVANT IONIZED WEAK ACIDS ON GRAPHITE: IMPACT OF MOLECULAR PROPERTIES AND THERMODYNAMICS<sup>1</sup> .....</b>	<b>41</b>
3.1	INTRODUCTION .....	41
3.2	MATERIALS AND METHODS .....	44
3.2.1	Chemicals and reagents .....	44
3.2.2	Preparation and characterization of adsorbent and quantification of NAs .....	45
3.2.3	Sorption experiments .....	46
3.3	RESULTS AND DISCUSSION .....	48
3.3.1	EG characterization .....	48
3.3.2	Mono-compound adsorption .....	52
3.3.3	Multi-compound adsorption .....	55
3.3.4	Thermodynamics of mono-compound adsorption .....	59
3.3.5	Competitive adsorption .....	63

3.4 ENVIRONMENTAL SIGNIFICANCE.....	68
3.5 REFERENCES.....	70
<b>4 PROBING ADSORPTION OF WEAK ACIDS ON GRAPHITE USING AMPLITUDE MODULATION-FREQUENCY MODULATION ATOMIC FORCE MICROSCOPY<sup>1</sup> .....</b>	<b>74</b>
4.1 INTRODUCTION .....	74
4.2 MATERIALS AND METHODS .....	75
4.2.1 Chemicals and reagents.....	75
4.2.2 HOPG functionalization and characterization.....	76
4.2.3 Adsorption and AM-FM-AFM.....	76
4.3 RESULTS AND DISCUSSION.....	77
4.3.1 HOPG and F-HOPG characterization.....	77
4.3.2 DA adsorption thermodynamics.....	78
4.3.3 AM-FM-AFM imaging before/after DA adsorption.....	81
4.4 ENVIRONMENTAL SIGNIFICANCE.....	88
4.5 REFERENCES.....	89
<b>5 INVESTIGATION OF THE ADSORPTION OF IONIZED CARBOXYLIC ACIDS ON GRAPHITE: USING SIMPLE MODEL COMPOUNDS TO UNDERSTAND COMPLEX MIXTURES<sup>1</sup> .....</b>	<b>92</b>
5.1 INTRODUCTION .....	92
5.2 MATERIALS AND METHODS .....	94
5.2.1 Chemicals, Reagents and Oil Sands Process-Affected Water (OSPW).....	94
5.2.2 Expanded Graphite Characterization and Analytical Methods.....	95

5.2.3 Sorption Experiments.....	96
5.3 RESULTS AND DISCUSSION.....	97
5.3.1 EG characterization.....	97
5.3.2 Mono- and multi-compound model NA adsorption.....	99
5.3.3 EG adsorption of Merichem and OSPW NAs.....	102
5.3.4 Thermodynamics of adsorption of model compounds.....	113
5.3.5 Thermodynamics of adsorption of NAs in Merichem and OSPW.....	115
5.4 CONCLUSIONS.....	117
5.5 REFERENCES.....	118
<b>6 CONCLUSIONS AND RECOMMENDATIONS .....</b>	<b>121</b>
6.1 THESIS OVERVIEW.....	121
6.2 CONCLUSIONS.....	122
6.2.1 Chapter 2: Preliminary membrane study.....	122
6.2.2 Chapters 3, 4 and 5: Adsorption study.....	123
6.3 RECOMMENDATIONS.....	126
<b>7 APPENDIX A (SUPPORTING MATERIALS FOR CHAPTER 2) .....</b>	<b>128</b>
<b>8 APPENDIX B (SUPPORTING MATERIALS FOR CHAPTER 3).....</b>	<b>131</b>
<b>9 APPENDIX C (SUPPORTING MATERIALS FOR CHAPTER 4) .....</b>	<b>133</b>
<b>10 APPENDIX D (SUPPORTING MATERIALS FOR CHAPTER 5) .....</b>	<b>135</b>
<b>11 BIBLIOGRAPHY.....</b>	<b>137</b>

## LIST OF TABLES

<b>Table 2-1.</b> pK <sub>a</sub> values and percentage of functional groups in AEF from OSPW 1 and Merichem NAs as measured by LPM.....	23
<b>Table 3-1.</b> Physiochemical properties of the 5 model naphthenic acids calculated using SPARC software ( <a href="http://archemcalc.com/sparc/index">http://archemcalc.com/sparc/index</a> ; accessed January 17, 2014).....	44
<b>Table 3-2.</b> Experimental C <sub>e</sub> and calculated q <sub>e</sub> values for each model compound from the multi-compound adsorption.....	58
<b>Table 3-3.</b> Competition coefficients and adsorption parameter 1/n calculated from the multi-compound Freundlich isotherm equation along with 95% confidence intervals...	59
<b>Table 3-4.</b> Summary of the adsorption capacities for the mono-compound and multi-compound experiments shown in Figure 3-8 .....	67
<b>Table 5-1.</b> Monocompound Langmuir and Freundlich adsorption isotherm parameters for DA, Trans-4-IsoPCHA and Trans-4-PCHA as obtained from Chapter 2. ....	101
<b>Table 5-2.</b> Physiochemical properties of the 3 model naphthenic acids calculated using SPARC software ( <a href="http://archemcalc.com/sparc/index">http://archemcalc.com/sparc/index</a> ; accessed November 15, 2014).....	102
<b>Table 5-3.</b> Langmuir and Freundlich adsorption isotherm parameters for AEF in Merichem and OSPW. ....	103

## LIST OF FIGURES

<b>Figure 2-1.</b> Deconvolution of C1s XPS peak for (a) nylon, (b) PVDF, and (c) PTFE membranes.....	25
<b>Figure 2-2.</b> FT-IR results for the adsorption of AEF from a) OSPW 1 by different membranes (The original concentration of AEF in OSPW 1 was $80.00 \pm 0.48$ mg/L), b) FT-IR results for the adsorption of AEF from Merichem NAs solution by different membranes (The original concentration of AEF was $50.10 \pm 0.63$ mg/L).....	27
<b>Figure 2-3.</b> The synchronous fluorescence spectroscopy of a) OSPW 1 and b) Merichem NAs filtered through the different membranes.....	30
<b>Figure 2-4.</b> The ATR FT-IR spectra for (a) nylon, (b) PVDF, and (c) PTFE membranes before and after filtration of OSPW 1 and Merichem NAs solution. ....	32
<b>Figure 2-5.</b> The ATR FT-IR spectra of (a) nylon, (b) PVDF, and (c) PTFE membranes before and after filtration of OSPW 1 and Merichem NAs. An inset shows ATR FT-IR spectra of nylon membrane after filtration of OSPW 1 at pH 5.3. ....	33
<b>Figure 2-6.</b> Distribution and estimated concentration of classical NAs (Trial #1) in (a) OSPW 1 at pH 8.7 (11.9 mg/L), and permeates after filtration through (b) nylon membrane at pH 8.7 (11.4 mg/L), (c) PVDF membrane at pH 8.7 (11.6 mg/L), (d) PTFE membrane at pH 8.7 (11.8 mg/L), (e) Nylon membrane at pH 5.3 (8.8 mg/L) and (f) summary of the estimated concentrations of NAs. The concentration of classical NAs was measured by UPLC/HRMS.....	35
<b>Figure 2-7.</b> Distribution and estimated concentration of classical NAs (Trial #2) in (a) OSPW 1 at pH 8.7 (12.2 mg/L), and permeates after filtration through (b)	

nylon membrane at pH 8.7 (11 mg/L), (c) PVDF membrane at pH 8.7 (11 mg/L), (d) PTFE membrane at pH 8.7 (12 mg/L), (e) nylon membrane at pH 5.3 (8.8 mg/L), and (f) summary of the estimated concentrations of classical NAs. The concentration of classical NAs was measured by UPLC/HRMS. .... 36

**Figure 3-1.** SEM images for (a) graphite intercalated compounds (GIC), (b) an expanded graphite particle image shows the extreme alteration of GIC thickness due to expansion (yellow arrows) and (c) the surface morphology of expanded graphite. TOF-SIMS mapping of (d) C-C/C=C groups, (e) phenolic functional groups and (f) carboxylic functional groups..... 50

**Figure 3-2.** Deconvolution of C1s peak for EG (XPS results)..... 51

**Figure 3-3.** BET surface area and pore size distribution of EG..... 51

**Figure 3-4.** Mono compound Langmuir adsorption isotherm for (a) decanoic acid, (b) Trans-4-IsoPropylCHA (c) Trans-4-PropylCHA and mono compound Freundlich adsorption isotherm for (d) decanoic acid, (e) Trans-4-IsoPropylCHA (f) Trans-4-PropylCHA using the HPLC/MS ( $C_0 = 50\text{mg/L}$ )..... 53

**Figure 3-5.** a) Freundlich and b) Langmuir adsorption isotherms for the mixture of five model compounds ( $C_0 = 50\text{ mg/L}$ ,  $10\text{ mg/L}$  each) ..... 56

**Figure 3-6.** Experimental vs. modeled profiles for the multi-compound Freundlich adsorption isotherm values of  $q_{eq}$  ..... 59

**Figure 3-7.** The NAs concentration (total  $C_0 = 50\text{ mg/L}$ ;  $10\text{ mg/L}$  for each NA) during mixing for 24 hours with  $2.5\text{ g (EG) /L}$ ..... 63

**Figure 3-8.** (a) Mono-compound and (b) multi-compound adsorption of model naphthenic acids after mixing with  $2.5\text{ g (EG) /L}$  for 24 hours. MC = model compound..... 66

<b>Figure 4-1.</b> TOF-SIMS mapping of (a) HOPG and (b) F-HOPG surface. Deconvolution of C1s XPS peak for (c) HOPG and (d) F-HOPG. ....	78
<b>Figure 4-2.</b> Speciation diagram for decanoic acid (according to the online SPARC software ( <a href="http://archemcalc.com/sparc/index">http://archemcalc.com/sparc/index</a> ; accessed January 17 <sup>th</sup> , 2014).....	79
<b>Figure 4-3.</b> Log $K_{ow}$ values for decanoic acid at different pH (according to the online SPARC software ( <a href="http://archemcalc.com/sparc/index">http://archemcalc.com/sparc/index</a> ; accessed January 17 <sup>th</sup> , 2014).....	81
<b>Figure 4-4.</b> AM-FM AFM of HOPG surface before functionalization. a) Height image of fresh peeled HOPG surface ( $1\mu\text{m} \times 1\mu\text{m}$ ); b) corresponding frequency shift image of the HOPG surface shown in (a); c) height image of HOPG surface after adsorption of DA for 24h ( $5\mu\text{m} \times 5\mu\text{m}$ ), d) corresponding frequency shift image of HOPG surface shown in (c); e) enlarged fine scan of adsorbed DA on HOPG surface shown in (c) ( $1\mu\text{m} \times 1\mu\text{m}$ ), f) corresponding frequency shift image for surface shown in (e); g) section profile of topography indicated by line and arrows shown in (e); and h) corresponding section of frequency shift of section indicated by line and arrows shown in (f).....	83
<b>Figure 4-5.</b> AM-FM AFM of F-HOPG surface after surface functionalization. a) Height image of fresh peeled F-HOPG surface ( $1\mu\text{m} \times 1\mu\text{m}$ ); b) corresponding frequency shift image of the F-HOPG surface shown in (a); c) height image of F-HOPG surface after adsorption of DA for 24h ( $5\mu\text{m} \times 5\mu\text{m}$ ), d) corresponding frequency shift image of F-HOPG surface shown in (c); e) enlarged fine scan of adsorbed DA on F-HOPG surface shown in (c) ( $1\mu\text{m} \times 1\mu\text{m}$ ), f) corresponding frequency shift image for surface shown in (e); g)	

section profile of topography indicated by line and arrows shown in (e); and h) corresponding section of frequency shift of section indicated by line and arrows shown in (f).....	84
<b>Figure 4-6.</b> Frequency shift images of the fine scan ( $1\mu\text{m} \times 1\mu\text{m}$ ) AM-FM AFM and the corresponding schematics for: a) HOPG; b) ionized SAL adsorbed on HOPG steps only (no frequency shift image); c) aggregates of DA adsorbed only on the steps of HOPG d) F-HOPG; e) SAL of DA adsorbed on the whole surface of F-HOPG (no frequency shift image) and f) DA multilayers adsorbed on the whole surface of F-HOPG. (green circles indicate FG on HOPG/F-HOPG steps; red circles indicate FG on the F-HOPG surface after functionalization) ....	87
<b>Figure 5-1.</b> SEM images for (a) graphite intercalated compounds and (b) expanded graphite (EG) .....	98
<b>Figure 5-2.</b> Deconvolution of C1s peak using XPS for the expanded graphite (figure) and TOF-SIMS (images).....	99
<b>Figure 5-3.</b> Multi-compound and mono-compound adsorption of model compound (MC) naphthenic acids after mixing with 2.5 g/L EG for 24 hours. (graph bars represent average of $n = 3$ and error bars represent standard deviations) .....	100
<b>Figure 5-4.</b> Freundlich adsorption isotherm (a & c) and Langmuir adsorption isotherm (b & d) for the acid extractable fraction from Merichem NAs solution ( $C_i=50.3 \pm 0.7$ ) (a & b) and OSPW ( $C_0=50.6 \pm 1.2$ ) (c & d) (FTIR results).....	104
<b>Figure 5-5.</b> NAs distribution in Merichem solution ( $C_i= 43 \text{ mg/L}$ ) a) before adsorption b) after adsorption after mixing with 2.5 g/L EG for 24 hours and c) % removal of NAs (see text for further details).....	106

**Figure 5-6.** NAs distribution in OSPW solution ( $C_i = 10.9$  mg/L) a) before adsorption b) after adsorption after mixing with 2.5 g/L EG for 24 hours and c) % removal of NAs (see text for further details). ..... 107

**Figure 5-7.** The Log  $K_{ow}$  of expected NAs in Merichem solution and OSPW ..... 109

**Figure 5-8.** Impact of number of rings (-Z) on the removal of a)  $C_{14}$ , b)  $C_{15}$  and c)  $C_{16}$  NAs in the Merichem solution during the mixing with EG for 24 hours. .... 111

**Figure 5-9.** The impact of the number of rings (-Z) on the removal of a)  $C_{14}$ , b)  $C_{15}$  and c)  $C_{16}$  NAs in OSPW during the mixing with EG for 24 hours ..... 112

**Figure 5-10.** Schematics for EG surface molecular properties in water and Gibbs free energies before and after adsorption..... 115

**Figure 5-11.** Expected structure for the  $C_9H_{14}O_2$  (octahydro-1-pentalenecarboxylic acid) in the Merichem mixture as obtained from Chemspider accessed accessed December, 15, 2014..... 116

## LIST OF ABBREVIATIONS

AC	Activated carbon
AEF	Acid extractable organic fractions
AFM	Atomic Force Microscopy
$a_{ij}$	Competition coefficients for compound 'j' on compound 'i'
AM-FM-AFM	Amplitude Modulation - Frequency Modulation Atomic Force Microscopy
ATR FT-IR	Attenuated total reflectance Fourier transform infrared spectroscopy
$C_0$	Initial concentration
-CAHB	Negatively charged assisted hydrogen bond
CHA	Cyclohexanoic acid
$C_i$	Final concentration
COOH	Carboxyl group
CNT	Carbon nanotubes
DA	Decanoic acid
DCM	Dichloromethane
EG	Expanded graphite
FGs	Functional groups
F-HOPG	Functionalized Highly-ordered pyrolytic graphite
FT-IR	Fourier transform infrared
$\Delta G^{-CAHB}$	Free energy required for -CAHB formation
$\Delta G_{Hydrophobicity}$	Hydrophobic free energy
$\Delta\Delta G_{Hydrophobicity}$	Partial contribution of $\Delta G_{Hydrophobicity}$
GIC	Graphite intercalated compounds

$\Delta G_{\text{Solv}}$	Free energy of solvation
$\Delta G_{\text{Total}}$	Total free energy
HOPG	Highly-ordered pyrolytic graphite
HPA	Heptanoic acid
HPLC	High-performance liquid chromatography
$\text{KH}_2\text{PO}_4$	Potassium phosphate monobasic
$\text{K}_2\text{HPO}_4$	Potassium phosphate dibasic
$K_{\text{ow}}$	Octanol-water partition coefficient
LC/MS	Liquid chromatography-mass spectrometry
LPM	Linear programming method
MeOH	Methanol
n	Carbon number
NaOH	Sodium hydroxide
NAs	Naphthenic acids
OH	Hydroxyl group
OSPW	Oil sands process-affected water
PAH	Polycyclic aromatic hydrocarbons
PTFE	Polytetrafluoroethylene
PVDF	Polyvinylidene fluoride
SAL	Self-assembled layer
SEM	Scanning electron microscope
SFS	Synchronous fluorescence spectroscopy
Trans-4-IsoPCHA	Trans-4-IsoPropylCycloHexanoic Acid

Trans-4-PCHA	Trans-4-PropylCycloHexanoic Acid
TOF-SIMS	Time of Flight Secondary Ion Mass Spectroscopy
UPLC/HRMS	Ultra pressure liquid chromatography-high resolution mass spectrometry
XPS	X-ray photoelectron spectroscopy
-Z	Hydrogen deficiency

# 1 GENERAL INTRODUCTION AND RESEARCH OBJECTIVES

## 1.1 Motivation

The oil sands deposits in Canada cover a 140 000 km<sup>2</sup> area of northern Alberta and are considered to be the largest unconventional oil resource reserves on earth [1]. An estimated 170 trillion barrels of bitumen contained in these reserves are important to the economy in Canada and affords a national security for oil-based energy. Bitumen is extracted by surface mining of these deposits if they are less than 100 m deep; on the other hand, in situ extraction methods are used for deeper deposits [2]. For surface mined oil sands, on average each extracted barrel of bitumen uses at least 3 barrels of hot caustic water (50-80 °C) in the extraction process [3]. The produced alkaline (pH 8.0 to 8.7) oil sands process-affected water (OSPW) contains high concentrations of both soluble and insoluble organic compounds which are of environmental concern.

OSPW is acutely, sub-chronically and chronically toxic to organisms in receiving environments which prohibits its discharge to natural water bodies without further treatment. In addition, these contaminants affect the recycling efficiency of OSPW for re-use in the extraction of bitumen due to the concentration of compounds impacting water chemistry. This limitation in re-use results in a higher dependency on the intake of fresh waters. In 2005, the oil sands industry required a fresh water intake rate of 11.5 m<sup>3</sup>/s (over 350 million m<sup>3</sup>/year) from the Athabasca River. According to Alberta Environment reports, this value can reach 34 m<sup>3</sup>/s which exceeds 40 % of the lowest winter flow rate estimated at 75 m<sup>3</sup>/s [1]. OSPW is currently stored in vast tailing ponds occupying an area larger than 70 km<sup>2</sup> in Alberta [1]. The unintentional release or leaching of OSPW from tailing ponds could result in severe contamination to the

surrounding environment or to the downstream areas of the Athabasca River. Consequently, the oil sands companies need to detoxify the OSPW prior to its release to natural streams according to their agreement with the government of Alberta. Therefore, the need for OSPW treatment is obvious for several motives but most importantly to reduce the enormous dependency of oil sands industry on the fresh water intake, decrease the potential risks of OSPW storage to the surrounding environment, and to allow the eventual release of stored OSPW to receiving environments.

Several treatments techniques have been considered for the removal of naphthenic acids (NAs), the most toxic compounds in OSPW, including membrane filtration, advanced oxidation processes, biological treatment, and adsorption [1]. Despite technological advances, the large number of OPSW constituents has been shown to lead to the early fouling of various membranes and the development of by-products after advance oxidation which may be more toxic than parent compounds. Biological treatment is the most cost effective and environmental friendly technique; nevertheless, recalcitrant NAs are a major concern that cannot be treated via biodegradation. Previously, the adsorption processes have suffered from extensive fouling and regeneration costs. However a combination of these processes, for example, biological treatment to remove easily biodegradable compounds followed by adsorption to remove the persistent and higher molecular weight NAs could enhance treatment efficiency. As of yet, understanding of the mechanisms governing the removal of NAs from the complex mixture of OSPW has not been fully developed for any of the remediation techniques.

## **1.2 Background**

### **1.2.1 Composition of the OSPW**

Many aspects govern the composition of OSPW including the mined ore quality, bitumen extraction method used, and the duration of storage [4, 5]. Initial OSPW has a high concentration of total dissolved solids (exceeding 1500 mg/L) that increases following its recycling for bitumen extraction [1]. Most of the dissolved solids are sodium and bicarbonate (>500 mg/L each) and chloride and sulfate (~300 mg/L each). OSPW is slightly alkaline (pH  $\approx$  8) and considered a hard water due to the presence of magnesium (5-10 mg/L) and calcium (15-25 mg/L). Ammonia has been detected in some OSPW waters and it ranges from 3-14 mg/L [1, 6-8]. The organic fractions in OSPW consist of non-dissolved compounds (3% bitumen by weight), and dissolved organic compounds. The soluble compounds includes polycyclic aromatic hydrocarbons (PAHs), benzene, toluene, phenols, phthalates, fulvic and humic acids, and naphthenic acids (NAs) [9]. Nelson et al. [10] reported that OSPW dissolved organic matter ranged from 50-150 mg/L and consist mostly of organic acids. The U.S. EPA's toxicity identification and evaluation protocol has identified organic acids as the most toxic compounds in OSPW. In particular, the NAs, a persistent fraction composing of up to 80% of the organic acids in OSPW, have been reported as primary sources of toxicity [9].

### **1.2.2 NAs**

#### **1.2.2.1 NAs properties in OSPW**

The NAs are a group of non-volatile aliphatic and alicyclic carboxylic acids present originally in bitumen and leached to OSPW during the bitumen extraction process [11]. NAs in OSPW are found at concentrations ranging from 40 to 125 mg/L as measured by the Fourier

transform infrared spectroscopy (FT-IR) [1, 9, 12-14]. Their dissociation constants are around  $10^{-5}$  ( $\text{pK}_a \approx 5$ ) which make them almost 99.9% dissociated at the slightly alkaline pH of OSPW [15]. The classical NAs are represented by the general formula,  $\text{C}_n\text{H}_{(2n+Z)}\text{O}_2$ , where  $n$  is the carbon number,  $-Z$  is the hydrogen deficiency and  $-Z/2$  represent the number of rings [16]. OSPW characterization reveals that ‘oxidized’ NAs could contain more than two oxygen atoms following the formula  $\text{C}_n\text{H}_{(2n+Z)}\text{O}_x$  where  $x = 3$  to  $5$  [17]. Although NAs in OSPW are of known molecular weights, carbon numbers and number of rings, their specific structures are not known or easily identified. On the other hand, their diversity in molecular weight, number of rings and structure offers non-uniformity in chemical and physical properties such as  $\text{Log K}_{ow}$  and solubility. For example, suggested  $\text{Log K}_{ow}$  values of NAs in OSPW can range from 2.5 for the very soluble and lower molecular weight compounds to 8.5 for poorly soluble and higher molecular weight NAs [18].

#### **1.2.2.2 Toxicity of NAs**

Both inhibitory and toxic impacts for NAs in OSPW were reported for zooplankton, fish, rats, and bacteria [14]. However, due to the diversity in single NAs molecular properties and initial concentrations, the discrimination of the individual impact of each compound to the overall toxicity of OSPW cannot be easily accomplished. This is in addition to possible synergic effect on toxicity of NAs imposed by the presence of the high concentration of soluble inorganics and other organics. Frank et al. [19] found that the toxicity of model NAs depends on their  $\text{Log K}_{ow}$  values with higher  $\text{Log K}_{ow}$  values leading to higher toxicity. The potency of  $\text{Log K}_{ow}$  on the toxicity of individual NAs was confirmed using an EPA ecological structure activity relationship model [20]. The model suggested that linear compounds (higher  $\text{Log K}_{ow}$ ) are the most toxic in OSPW and the increase in number of rings (lower  $\text{Log K}_{ow}$ ) significantly decreases

the toxicity. Jones et al. [21] also observed that the lower the solubility (higher Log  $K_{ow}$ ) of NAs, the lower the toxicity of NAs.

### **1.2.2.3 Biodegradability of NAs**

Given the natural aging of OSPW while in storage in the tailing ponds, the understanding of NAs biodegradation is essential to optimize the application of further treatment techniques for this stored OSPW. For the purpose of the current work, identifying the classes of NAs impacted and removed by biodegradation would be useful to focus efforts on the removal of recalcitrant NAs. Biodegradation of NAs in OSPW has been found to be impacted by their molecular structure and molecular weight [22, 23]. The characterization of on-site biodegradation of NAs in OSPW revealed that lower molecular weight linear and one ring NAs were the most susceptible to biodegradation [8]. Similarly, lower molecular weight and ring-numbered NAs in a commercial Merichem mixture were found to be more vulnerable to aerobic biodegradation [14]. The observed trend of removal of lower molecular weight NAs will result in higher concentrations of the higher molecular weight compounds (higher Log  $K_{ow}$ ) in tailing ponds over time. In addition, aging of OSPW could result in the production of more recalcitrant NAs from the degradation of the residual bitumen in OSPW [24].

Given this discussion, an excellent treatment process to decrease the toxicity of OSPW would be to implement a remediation technique for the removal of NAs of higher molecular weight and higher Log  $K_{ow}$  values. A potentially viable treatment process may be the use of carbonaceous materials as adsorbents which may be useful for all OSPW NAs. These types of materials, most commonly activated carbon (AC), have been useful for removal of other organic compounds, including ionized organic acids, in matrices including water treatment and industrial wastewaters [25-29].

### **1.2.3 Adsorption**

#### **1.2.3.1 Adsorption of NAs from OSPW**

Recently, the use of carbonaceous materials for adsorption of NAs has been of great interest. For example, a recent study compared the impact of raw and chemically treated AC on the adsorption of NAs with the treated AC able to remove up to 90% of NAs (35 mg NAs removed per gram AC) [30]. In addition, Mohamed et al. [31] found that commercial AC can remove up to 142 mg NAs/g AC. Based on these results, a huge amount of activated carbon (high capital cost) would be required for remediation of OSPW given its high NAs concentrations. In addition, the high abundance of micropores in AC allows for the size removal of NAs, accordingly, the AC regeneration costs will be high to remove these NAs [32]. Due to the high potential costs of AC, several studies have examined the use of petroleum coke, a waste by-product of the oil refining process, for NAs removal [6, 18, 33]. Despite its availability at no cost, the raw petroleum coke removal capacity for NAs was extremely low as compared to commercially available activated carbon. It should be noted that for all previous studies the mechanism(s) of adsorption were not adequately reported and/or investigated. Thus, in order to develop an economically feasible and efficient adsorbent for NAs removal, the adsorption mechanism of those acids on carbonaceous adsorbents should be thoroughly investigated to determine the best possible material for OSPW treatment. Functionalized expanded graphite (EG) contains mesopores that will not allow for the size removal of NAs and contains phenolic and carboxyl groups that may allow for adsorption of the NAs on the EG surface [34]. Given the lack of mesopores, the EG was considered for use as an adsorbent in the current study.

### 1.2.3.2 EG properties

Crystalline flake graphite is a natural material that occurs as isolated, flat, plate-like particles with hexagonal edges. Prior to use for adsorption, these flat particles need to be intercalated to form the graphite intercalated compounds (GIC) with markedly higher surface areas. GIC can be created by exposure to a sudden thermal shock with the heating resulting in conversion of the intercallant to the gas phase [35]. The pressure generated by gas formation forces the adjacent layers to separate, resulting in the worm-like particles termed EG. The specific surface area of this EG graphite ranges from 28 - 1600 m<sup>2</sup>/g [36-40]. The preparation technique is the main factor controlling the specific surface area, while this large surface area works in addition to the EG hydrophobic characteristics to promote the adsorption of compounds such as hydrocarbons.

The extremely high hydrophobic properties of EG result in an enormous adsorption capability of this material. For example, hydrocarbons were shown to be sorbed on the surface of the worm-like particles, inside them and in the spaces in between the particles [41-44]. The adsorption capacity of EG for crude oil was 80 g/g and 80 % of the oil recovered after the adsorption process. The pores in worm-like particles were reported to have higher sorption capacity for light oil than heavy oil, while the sorption capacity in the spaces between the worm-like particles is higher for heavy oils with 60% of the heavy oil sorbed in these spaces [41-44]. Moustafa et al. [45] optimized the fabrication conditions for EG in terms of expansion time and temperature that resulted in a maximum sorption capacity of 103 g/g of insoluble hydrocarbons. However, few studies have investigated the use of EG for the removal of soluble organic contaminants [46-48]. These studies suggested that the presence of positive charges on the surface of reduced EG at low pH values attracted the negatively charged dyes. On the other hand,

the functionalization of EG via oxidation in air at 400°C (increased the negatively charged functional groups on EG surface) increased the adsorption of Methyl orange and did not impact the adsorption capacity of Methylene blue [36]. The adsorption behaviour of soluble organics on EG was not evidently characterized or understood as for the insoluble organics. More research is required to understand the adsorption of ionized organics on EG.

### **1.3 Scope of research and objectives**

The removal of neutral acids can occur via adsorption on carbonaceous materials being governed mainly by hydrophobic interactions and van der Waals forces which have been extensively studied and well characterized [49-51]. However, much less attention has been focussed on the assessment of the adsorptive performance of ionized weak acids on hydrophobic carbon surfaces [52-56]. The adsorption of ionized organic acids was previously thought to be governed solely by bridging via metal ions due to the repulsion between negatively charged ionized acids and surface functional groups of carbon adsorbent surfaces [57, 58]. However, more recent studies by Ni et al. [54] and Teixido et al. [55] have evaluated the potential role of hydrogen bonding (HB) in the adsorption of ionized weak acids. Some studies were able to identify the role of the strong HB between negatively charged groups of the weak acid and the adsorbent surface. More specifically, the weak acid was able to form a negatively charged assisted hydrogen bond (–CAHB). Li et al. [53] performed an extensive study confirming the role of the –CAHB for a range of pH values for benzoic acid, phthalic acids and 2, 6-dichloro-4-nitrophenol. At pH 7, they established via OH<sup>-</sup> release stoichiometry that almost 100% adsorption was due to the –CAHB. However, a limitation of these previous studies is that they included only mono-compound solutions. In addition, pK<sub>a</sub> values for the mono-solutions examined were diverse which resulted in distinct free solvation energies in water, while NAs in

OSPW have similar  $pK_a$  values making the thermodynamics of adsorption understanding more difficult. To date, no studies had investigated the removal of ionized model NAs having the same  $pK_a$  values from single or multi-compound mixtures. In addition, none of the studies in the literature had characterized the adsorption of the ionized acids on the surface of adsorbents, they only attempt to describe the impact of adsorption in solutions.

Accordingly, there is a research gap in the understanding the mechanism(s) of adsorption of environmentally relevant ionized NAs on carbonaceous materials. To fill this gap, the investigation of the adsorption of ionized model NAs with similar  $pK_a$ , followed by OSPW NAs on the EG may help to reveal important information regarding their adsorption mechanism. In addition, the further investigation of adsorption on the surface of adsorbent after adsorption would aid in the visual confirmation of our findings. Therefore, the main objective of this Ph.D. research was to investigate the adsorption mechanism(s) of ionized NAs on EG and to characterize the adsorption behaviour on the surface of adsorbent. Accordingly we can designate four stages for the work as follows:

- Chapter 2: Three commercial 0.45  $\mu\text{m}$  polymeric membranes with different hydrophilicity [nylon, polyvinylidene fluoride (PVDF), and polytetrafluoroethylene (PTFE)] were tested for their impact on NAs and AEF quantification. The main objective of this phase was to report the impact of the interactions between the organic fraction in both Merichem and OSPW mixtures and polymeric membranes during the filtration of OSPW on further quantifications of AEF and NAs filtration at different pH.
- Chapter 3: The adsorption of 5 model NAs in mono/multi-compound solutions on EG was investigated. The main objective of this phase was to study the thermodynamics of mono-compound adsorption for NAs with similar  $pK_a$  values with knowledge gained

used in further evaluation of the competition of NAs in multi-compound solutions. In addition, the multi-compound Freundlich adsorption isotherm was used to fit the multi-compound adsorption data for the mixture of 5 model compounds. The impact of structure reactivity on the adsorption behaviour was also reported.

- Chapter 4: The characterization and visualization of the adsorption of NAs on the surface of a carbon adsorbent in a flat sheet formation (highly-ordered pyrolytic graphite, HOPG) was conducted. This HOPG was considered since the EG surfaces were too irregular to allow for the visualization technique. The main objectives of this phase were to assess the adsorption potential of DA on HOPG thermodynamically and then use Amplitude Modulation Frequency Modulation Force Microscopy (AM-FM-AFM) to image HOPG surfaces before and after DA adsorption. As well, AM-FM-AFM was used to assess the change in surface mechanical properties after functionalization using water plasma treatment for the determination of occupied adsorption regions.
- Chapter 5: The adsorption of NAs from the commercial Merichem mixture and OSPW was investigated. The main objective was to apply the knowledge gained from studying model compounds to evaluate and determine the adsorption mechanisms of complex NAs mixtures such as Merichem and OSPW. The advantage of using Merichem mixture is the isolation of the possible impact on adsorption of dissolved salts and minerals found in OSPW.

By understanding the behaviour of 5 ionized NAs, Merichem NAs mixtures and raw OSPW NAs, and characterizing the adsorption on graphite surfaces the above research objectives will be achieved. This study will provide fundamental scientific tools for future studies aimed to

develop and optimize an economic and efficient engineered adsorbent for the removal of recalcitrant and higher molecular weight NAs in OSPW in addition to other emerging organic acid pollutants from natural water streams. The study will present the impact of molecular properties of NAs on their adsorption behaviour on EG. In addition, this study will show how to thermodynamically assess the adsorption of organic acids which could assist in the development of mathematical models to predict the adsorption of compounds before conducting actual experiments. The study will provide information regarding the locations of the adsorption sites for ionized NAs on the surface of EG which never had been reported previously. This will allow engineers to fabricate and optimize adsorbents that are lower in cost and do not require high energy for regeneration which has been an issue with AC.

#### **1.4 Thesis Organization**

This thesis consists of six chapters. Chapter 1 contains research motivations followed by general background (OSPW, NAs and EG) and then scope of research and objectives. The currently considered phases of research for membranes assessment and understanding adsorption of NAs on EG, are presented in Chapters 2-5.

The evaluation of three commercial 0.45  $\mu\text{m}$  polymeric membranes was performed in Chapter 2 to test for their impact on NAs and AEF quantification. Merichem NAs solution and OSPW were prepared and pH values were adjusted to range from 2.5 to 10. Samples were filtered using nylon, PVDF and PTFE membranes and tested for PAH, AEF and NAs. Adsorption of organics on membranes was assessed using attenuated total reflectance FT-IR (ATR FT-IR).

Chapter 3 contains the adsorption evaluation of 5 model NAs on EG as obtained experimentally from mono/multi-compound solutions. The competitive adsorption was assessed experimentally using liquid chromatography-mass spectrometry (LC/MS) and structure reactivity was revealed. The multi-compound Freundlich adsorption isotherm was used to fit the multi-compound adsorption data for the mixture of 5 model compounds and to confirm the experimental findings. EG was characterized using X-ray photoelectron spectroscopy (XPS) and Time of Flight Secondary Ion Mass Spectroscopy (TOF-SIMS).

Chapter 4 contains detailed characterization of HOPG surfaces for the visualization of adsorbed NAs. AM-FM-AFM was used to image the freshly peeled and functionalized HOPG surfaces before and after DA adsorption. As well, AM-FM-AFM was used to assess the change in surface mechanical properties for the determination of occupied adsorption regions. HOPG was characterized using XPS and TOF-SIMS.

Chapter 5 contains the assessment of the adsorption of NAs from the commercial Merichem mixture and OSPW. Ultra pressure liquid chromatography-high resolution mass spectrometry (UPLC/HRMS) used to quantify NAs in both mixtures. Experimental competitive adsorptions were analysed and thermodynamics calculations were performed to help to determine the adsorption mechanism(s).

Chapter 6 contains the conclusions and recommendations. Each appendix covers some experimental methodologies for a specific chapter: Appendix A for chapter 2 and 5, Appendix B for chapter 3, Appendix C for chapter 4 and Appendix D for chapter 5.

## 1.5 References.

- [1] Allen EW. Process water treatment in Canada's oil sands industry: I. Target pollutants and treatment objectives. *Journal of Environmental Engineering and Science* 2008;7:123-138.
- [2] Smith BE, Lewis CA, Belt ST, Whitby C, Rowland SJ. Effects of Alkyl Chain Branching on the Biotransformation of Naphthenic Acids. *Environmental Science & Technology* 2008;42:9323-9328.
- [3] Holowenko FM, MacKinnon MD, Fedorak PM. Characterization of naphthenic acids in oil sands wastewaters by gas chromatography-mass spectrometry. *Water Research* 2002;36:2843-2855.
- [4] Kannel PR, Gan TY. Naphthenic acids degradation and toxicity mitigation in tailings wastewater systems and aquatic environments: a review. *Journal of environmental science and health Part A, Toxic/hazardous substances & environmental engineering* 2012;47:1-21.
- [5] Ityokumbul MT, Kasperski KL. Reactivity of caustic treated oil sand coke residues. *Fuel Processing Technology* 1994;37:281-294.
- [6] El-Din MG, Fu H, Wang N, Chelme-Ayala P, Perez-Estrada L, Drzewicz P, et al. Naphthenic acids speciation and removal during petroleum-coke adsorption and ozonation of oil sands process-affected water. *Science of the Total Environment* 2011;409:5119-5125.
- [7] Quagraine EK, Peterson HG, Headley JV. In situ bioremediation of naphthenic acids contaminated tailing pond waters in the Athabasca oil sands region-demonstrated field studies and plausible options: A review. *Journal of Environmental Science and Health Part a-Toxic/Hazardous Substances & Environmental Engineering* 2005;40:685-722.
- [8] Han X, MacKinnon MD, Martin JW. Estimating the in situ biodegradation of naphthenic acids in oil sands process waters by HPLC/HRMS. *Chemosphere* 2009;76:63-70.
- [9] MacKinnon M, Van Meer T, Verbeek A. Assessment of biological impact from a wet landscape option for the reclamation of fine tails from oil sands. *Canadian Technical Report of Fisheries and Aquatic Sciences* 1993;250:258.
- [10] Nelson PN, Baldock JA, Oades JM. Concentration and composition of dissolved organic-carbon in streams in relation to catchment soil properties. *Biogeochemistry* 1993;19:27-50.
- [11] Headley JV, McMartin DW. A review of the occurrence and fate of naphthenic acids in aquatic environments. *Journal of Environmental Science and Health Part a-Toxic/Hazardous Substances & Environmental Engineering* 2004;39:1989-2010.
- [12] Mackinnon MD, Retallack JT. Preliminary characterization and de toxification of tailings pond water at the syncrude canada limited oil sands plant. *Proceedings of the 4th Annual Meeting of the International Society of Petroleum Industry Biologists*, 1981 1982:P185-210.
- [13] Scott AC, MacKinnon MD, Fedorak PM. Naphthenic acids in athabasca oil sands tailings waters are less biodegradable than commercial naphthenic acids. *Environmental Science & Technology* 2005;39:8388-8394.
- [14] Clemente JS, Fedorak PM. A review of the occurrence, analyses, toxicity, and biodegradation of naphthenic acids. *Chemosphere* 2005;60:585-600.
- [15] Kaur K, Bhattacharjee S, Pillai RG, Ahmed S, Azmi S. Peptide arrays for detecting naphthenic acids in oil sands process affected water. *Rsc Advances* 2014;4:60694-60701.
- [16] Brient JA. Commercial utility of naphthenic acids recovered from petroleum distillates. *Abstracts of Papers of the American Chemical Society* 1998;215:018-PETR.
- [17] Barrow MP, Headley JV, Peru KM, Derrick PJ. Data Visualization for the Characterization of Naphthenic Acids within Petroleum Samples. *Energy & Fuels* 2009;23:2592-2599.
- [18] Pourrezaei P, Alpatova A, Chelme-Ayala P, Perez-Estrada LA, Jensen-Fontaine M, Le XC, et al. Impact of petroleum coke characteristics on the adsorption of the organic fractions from oil sands

process-affected water. *International Journal of Environmental Science and Technology* 2014;11:2037-2050.

[19] Frank RA, Fischer K, Kavanagh R, Burnison BK, Arsenault G, Headley JV, et al. Effect of carboxylic acid content on the acute toxicity of oil sands naphthenic acids. *Environmental Science & Technology* 2009;43:266-271.

[20] Frank RA, Sanderson H, Kavanagh R, Burnison BK, Headley JV, Solomon KR. Use of a (Quantitative) Structure-Activity Relationship (Q)SAR Model to Predict the Toxicity of Naphthenic Acids. *Journal of Toxicology and Environmental Health-Part a-Current Issues* 2010;73:319-329.

[21] Jones D, Scarlett AG, West CE, Rowland SJ. Toxicity of Individual Naphthenic Acids to *Vibrio fischeri*. *Environmental Science & Technology* 2011;45:9776-9782.

[22] Birkholz DA, Rogers RE, MacKinnon M. Molecular toxicology associated with natural naphthenic acids isolated from Syncrude tailings pond water and commercially available naphthenic acids. *Canadian Technical Report of Fisheries and Aquatic Sciences* 1997;0:109.

[23] Quagraine EK, Headley JV, Peterson HG. Is biodegradation of bitumen a source of recalcitrant naphthenic acid mixtures in oil sands tailing pond waters? *Journal of Environmental Science and Health Part a-Toxic/Hazardous Substances & Environmental Engineering* 2005;40:671-684.

[24] McKenzie N, Yue S, Liu X, Ramsay BA, Ramsay JA. Biodegradation of naphthenic acids in oils sands process waters in an immobilized soil/sediment bioreactor. *Chemosphere* 2014;109:164-172.

[25] Stackelberg PE, Gibs J, Furlong ET, Meyer MT, Zaugg SD, Lippincott RL. Efficiency of conventional drinking-water-treatment processes in removal of pharmaceuticals and other organic compounds. *Science of the Total Environment* 2007;377:255-272.

[26] Randtke SJ. Organic contaminant removal by coagulation and related process combinations. *Journal American Water Works Association* 1988;80:40-56.

[27] Rengaraj S, Moon SH, Sivabalan R, Arabindoo B, Murugesan V. Agricultural solid waste for the removal of organics: adsorption of phenol from water and wastewater by palm seed coat activated carbon. *Waste Management* 2002;22:543-548.

[28] Bousher A, Shen XD, Edyvean RGJ. Removal of coloured organic matter by adsorption onto low-cost waste materials. *Water Research* 1997;31:2084-2092.

[29] Zhang MM, Li C, Benjamin MM, Chang YJ. Fouling and natural organic matter removal in adsorbent/membrane systems for drinking water treatment. *Environmental Science & Technology* 2003;37:1663-1669.

[30] Iranmanesh S, Harding T, Abedi J, Seyedejn-Azad F, Layzell DB. Adsorption of naphthenic acids on high surface area activated carbons. *Journal of Environmental Science and Health Part a-Toxic/Hazardous Substances & Environmental Engineering* 2014;49:913-922.

[31] Mohamed MH, Wilson LD, Headley JV, Peru KM. Sequestration of naphthenic acids from aqueous solution using beta-cyclodextrin-based polyurethanes. *Physical Chemistry Chemical Physics* 2011;13:1112-1122.

[32] Lashaki MJ, Fayaz M, Wang H, Hashisho Z, Philips JH, Anderson JE, et al. Effect of Adsorption and Regeneration Temperature on Irreversible Adsorption of Organic Vapors on Beaded Activated Carbon. *Environmental Science & Technology* 2012;46:4083-4090.

[33] Zubot W, MacKinnon MD, Chelme-Ayala P, Smith DW, El-Din MG. Petroleum coke adsorption as a water management option for oil sands process-affected water. *Science of the Total Environment* 2012;427:364-372.

[34] Inagaki M, Suwa T. Pore structure analysis of exfoliated graphite using image processing of scanning electron micrographs. *Carbon* 2001;39:915-920.

[35] Toyoda M, Moriya K, Inagaki M. Temperature dependence of heavy oil sorption on exfoliated graphite. *Sekiyu Gakkaishi-Journal of the Japan Petroleum Institute* 2001;44:169-172.

- [36] Tryba B, Morawski AW, Kaleczuk RJ, Inagaki M. Exfoliated graphite as a new sorbent for removal of engine oils from wastewater. *Spill Science & Technology Bulletin* 2003;8:569-571.
- [37] Vieira F, Cisneros I, Rosa NG, Trindade GM, Mohallem NDS. Influence of the natural flake graphite particle size on the textural characteristic of exfoliated graphite used for heavy oil sorption *Carbon* 2006;44:2590-2592
- [38] Hristea G, Budrugaec P. Characterization of exfoliated graphite for heavy oil sorption *Journal of Thermal Analysis and Calorimetry* 2008;91:817-823.
- [39] Kalaitzidou K, Fukushima H, Drzal LT. Mechanical properties and morphological characterization of exfoliated graphite-polypropylene nanocomposites. *Composites Part a-Applied Science and Manufacturing* 2007;38:1675-1682.
- [40] Fukushima H, Drzal LT. Enhancement of the mechanical, electrical and thermal properties of nylon nanocomposites via addition of exfoliated graphite nanoplatelets (xGnP). *Proceedings of the Twelfth US-Japan Conference on Composite Materials* 2006:793-807.
- [41] Toyoda M, Inagaki M. Heavy oil sorption using exfoliated graphite - New application of exfoliated graphite to protect heavy oil pollution. *Carbon* 2000;38:199-210.
- [42] Inagaki M, Toyoda M, Kang FY, Zheng YP, Shen WC. Pore structure of exfoliated graphite - A report on a joint research project under the scientific cooperation program between NSFC and JSPS. *New Carbon Materials* 2003;18:241-249.
- [43] Inagaki M, Nagata T, Suwa T, Toyoda M. Sorption kinetics of various oils onto exfoliated graphite. *New Carbon Materials* 2006;21:97-102.
- [44] Toyoda M, Iwashita N, Inagaki M. Sorption of Heavy Oils into Carbon Materials. *Chemistry and Physics of Carbon, Vol 30* 2008;30:177-237.
- [45] Moustafa A. Fabrication characterization and oil spills remediation properties of the exfoliated graphite. *The Pennsylvania State University-Electronic thesis directory*; 2009.
- [46] Song Y-L, Li J-T, Chen H. Removal of acid brown 348 dye from aqueous solution by ultrasound irradiated exfoliated graphite. *Indian Journal of Chemical Technology* 2008;15:443-448.
- [47] Li JT, Li M, Li JH, Sun HW. Removal of disperse blue 2BLN from aqueous solution by combination of ultrasound and exfoliated graphite. *Ultrasonics Sonochemistry* 2007;14:62-66.
- [48] Ramesha GK, Kumara AV, Muralidhara HB, Sampath S. Graphene and graphene oxide as effective adsorbents toward anionic and cationic dyes. *Journal of Colloid and Interface Science* 2011;361:270-277.
- [49] Cornelissen G, Gustafsson O, Bucheli TD, Jonker MTO, Koelmans AA, Van Noort PCM. Extensive sorption of organic compounds to black carbon, coal, and kerogen in sediments and soils: Mechanisms and consequences for distribution, bioaccumulation, and biodegradation. *Environmental Science & Technology* 2005;39:6881-6895.
- [50] Allen-King RM, Grathwohl P, Ball WP. New modeling paradigms for the sorption of hydrophobic organic chemicals to heterogeneous carbonaceous matter in soils, sediments, and rocks. *Advances in Water Resources* 2002;25:985-1016.
- [51] Muller G, Radke CJ, Prausnitz JM. Adsorption of weak organic electrolytes from aqueous-solution on activated carbon - effect of pH. *Journal of Physical Chemistry* 1980;84:369-376.
- [52] Yang K, Wu W, Jing Q, Zhu L. Aqueous Adsorption of Aniline, Phenol, and their Substitutes by Multi-Walled Carbon Nanotubes. *Environmental Science & Technology* 2008;42:7931-7936.
- [53] Li X, Pignatello JJ, Wang Y, Xing B. New Insight into Adsorption Mechanism of Ionizable Compounds on Carbon Nanotubes. *Environmental Science & Technology* 2013;47:8334-8341.
- [54] Ni J, Pignatello JJ, Xing B. Adsorption of Aromatic Carboxylate Ions to Charcoal Black Carbon is Accompanied by Proton Exchange with Water (vol 45, pg 9240, 2012). *Environmental Science & Technology* 2012;46:5633-5633.

- [55] Teixido M, Pignatello JJ, Beltran JL, Granados M, Peccia J. Speciation of the Ionizable Antibiotic Sulfamethazine on Black Carbon (Biochar). *Environmental Science & Technology* 2011;45:10020-10027.
- [56] Hyun S, Lee LS. Hydrophilic and hydrophobic sorption of organic acids by variable-charge soils: Effect of chemical acidity and acidic functional group. *Environmental Science & Technology* 2004;38:5413-5419.
- [57] Fontecha-Camara MA, Lopez-Ramon MV, Alvarez-Merino MA, Moreno-Castilla C. Effect of surface chemistry, solution pH, and ionic strength on the removal of herbicides diuron and amitrole from water by an activated carbon fiber. *Langmuir* 2007;23:1242-1247.
- [58] Vinu A, Hossain KZ, Kumar GS, Ariga K. Adsorption of L-histidine over mesoporous carbon molecular sieves. *Carbon* 2006;44:530-536.

## 2 IMPACT OF POLYMERIC MEMBRANE FILTRATION OF OIL SANDS PROCESS WATER ON ORGANIC COMPOUNDS QUANTIFICATION<sup>1</sup>

### 2.1 Introduction

The oil sands in Canada are one of the largest unconventional oil resources in the world. Billion liters of oil sands process-affected water (OSPW) are produced yearly by the oil sands industry and are currently stored in huge tailing ponds [1]. According to the U.S. EPA's toxicity identification and evaluation protocol, organic acids are considered to be the most toxic compounds in OSPW [2]. In particular, naphthenic acids (NAs), a persistent fraction of organic acids in OSPW, have been reported as primary sources of toxicity and are considered as target pollutants [2].

Classical NAs are a group of aliphatic and alicyclic carboxylic acids, with a general empirical formula  $C_nH_{(2n-Z)}O_2$ , where  $n$  is the carbon number,  $-Z$  is the hydrogen deficiency [3]. Oxidized NAs with the formula  $C_nH_{2n+Z}O_x$  ( $x > 3$ ), where  $x$  represents the number of oxygen atoms, have also been detected in OSPW [4]. Few techniques have been used to qualitatively detect NAs in OSPW.

---

<sup>1</sup>A version of this chapter has been published previously: Ahmed M.A. Moustafa, EunSik Kim, Alla Alpatova, Nian Sun, Scott Smith, Seoktae Kang, Mohamed Gamal El-Din, Impact of polymeric membrane filtration of oil sands process water on organic compounds quantification. Water Science and Technology. 2014. 70 (5), 771-779.

Attenuated total reflectance Fourier transform infrared spectroscopy (ATR FT-IR) has been used to characterize different NAs mixtures or single NAs model compounds [5]. The evaluation of the aromatic organic content in OSPW, including naphtho-aromatic acidic compounds, can be done using synchronous fluorescence spectroscopy (SFS) [6]. The concentration of NAs in OSPW can also be estimated as a part of the extractable organic fraction (AEF) by FT-IR, which is based on the detection of carbonyl stretches [4, 7-9]. On the other hand, the estimated concentration and distribution of NAs in OSPW can be obtained by ultra/or high pressure liquid chromatography-high resolution mass spectrometry (UPLC/HRMS, HPLC/HRMS) [10-13]. However, FT-IR remains the most common technique for the estimation of the concentration of AEF compounds in OSPW due to its simplicity and low cost [14].

Raw OSPWs from different tailing ponds contain AEF at concentrations between 40 and 125 mg/L at different pH values (7 to 8.7) [3, 10]. In addition, the pH of OSPW could significantly change after treatment. Sample filtration using 0.45  $\mu\text{m}$  polymeric membranes precedes the analysis of OSPW to remove suspended solids. In this study, it is hypothesized that this filtration could bias the quantification of classical NAs. The main goal of this research was to report the impact of the interactions between the organic fraction in OSPW and polymeric membranes during the filtration of OSPW on further quantifications of AEF and NAs in solution. In addition to OSPW, commercial NAs (refined Merichem NAs mixture) were used to investigate the differences in behavior between a commercial NAs mixture and NAs in OSPW during filtration. Three commercial 0.45  $\mu\text{m}$  polymeric membranes with different hydrophilicity [nylon, polyvinylidene fluoride (PVDF), and polytetrafluoroethylene (PTFE)] were tested in this study.

## **2.2 Materials and Methods**

### **2.2.1 Oil sands process-affected water (OSPW)**

Three different OSPWs were obtained from two oil sands companies located in Fort McMurray, Alberta, Canada. OSPW 1 and OSPW 2 were collected from the same settling basin, but at different sampling period (September 2010 for OSPW 1 and June 2012 for OSPW 2), while OSPW 3 was collected from a second oil sands company. The pH values of the OSPWs ranged from 7.0 to 8.7.

### **2.2.2 Chemicals and reagents**

Refined Merichem NAs were provided by Merichem Chemicals and Refinery Services LLC (Houston, TX, USA). Sodium hydroxide (NaOH) and tetradecanoic acid-1-<sup>13</sup>C were purchased from Sigma Aldrich (Edmonton, AB, Canada). Sulfuric acid (H<sub>2</sub>SO<sub>4</sub>), potassium hydrogen phthalate (C<sub>8</sub>H<sub>5</sub>KO<sub>4</sub>), dichloromethane (CH<sub>2</sub>Cl<sub>2</sub>), methanol (CH<sub>3</sub>OH), sodium chloride (NaCl), and Optima-Grade water were purchased from Fisher Scientific (Edmonton, AB, Canada). Milli-Q water (Synergy® UV instrument, Millipore, Molsheim, France) was used through the entire study. Naphthenic acids (NAs) standards were purchased from Sigma-Aldrich (Edmonton, AB, Canada).

### **2.2.3 Filtration set-up and membranes**

The OSPW samples were centrifuged at 16 000 RPM to remove suspended solids. A 200 mg/L stock solution of Merichem NAs was prepared in 100 mM NaOH. The pH of OSPW and Merichem NAs mixture was adjusted with H<sub>2</sub>SO<sub>4</sub> or NaOH to 2.5, 5.5, 6.5, 9.2, 10 and 2.5, 5.5, 6.5, 8.2, 9.4, 10, respectively. The filtration set-up consisted of a 300-mL filtration funnel

(Gelman Sciences, MI, USA) and a 500-mL receiving Büchner volumetric flask connected to a vacuum pump. Three types of 0.45  $\mu\text{m}$  polymeric membranes (nylon: Cat. # HNWP04700; PVDF: Cat # HVL04700; and PTFE: Cat # FHLC04700, Millipore, ON, Canada) were used in the tests. Membranes were prewashed with 50 ml of MilliQ water. A 100 mL aliquot of each sample was filtered at a time; permeates were collected and used for AEF, SFS and classical NAs analyses.

#### **2.2.4 Quantification of acid-extractable fraction (AEF) and classical NAs**

AEF was quantified using FT-IR spectroscopy (Perkin Elmer Spectrum, 100 FT-IR Spectrometer, Waltham, MA, USA) based on a standard calibration curve ( $R^2=0.999$  for 9 points) as described elsewhere [15]. Stock solution was prepared by dissolving 0.2 g of NAs in 200 g of dichloromethane ( $\text{CH}_2\text{Cl}_2$ , DCM). The quantification of AEF was based on the absorbance of wavenumbers at  $1,743\text{ cm}^{-1}$  and  $1,706\text{ cm}^{-1}$  for the monomer and dimer carboxylic acids, respectively [7, 9]. Each analysis was performed in triplicate and the results are reported as an average  $\pm$  standard deviation (STD). A Waters Acquity UPLC System (Milford, MA, USA) was used for the chromatographic separation of classical NAs. 2 mL of each sample were centrifuged for 5 min at 10 000 RPM. 500  $\mu\text{L}$  of the supernatant were placed in a 2-mL glass vial with 400  $\mu\text{L}$  of Optima-grade methanol and 100  $\mu\text{L}$  of 400 mg/L tetradecanoic acid- $1\text{-}^{13}\text{C}$  (internal standard) to make a final 1-mL sample solution with 0.4 mg/L internal standard for the final injection. Further details can be found in Appendix A. An acid-base titration with the linear programming method (LPM) was used to identify and quantify the relative intensities of the functional groups present in AEF from OSPW and Merichem NAs as described previously [16, 17] with further details available in Appendix A.

### **2.2.5 Synchronous fluorescence spectroscopy (SFS) analysis**

SFS was used to evaluate the variation in aromatic residues of organic compounds in solution due to filtration. Duplicate fluorescence measurements were performed on a Cary Eclipse fluorescence spectrometer (Varian, Australia PTY LTD, Australia), and the synchronous fluorescence method was applied [6]. The  $\Delta$  offset value ( $\Delta = \lambda_{\text{Emission}} - \lambda_{\text{Excitation}}$ ) was 18 nm. The excitation wavelength ( $\lambda$ ) ranged from 200 to 600 nm. The excitation and emission slits were set at 5 nm. The scan speed was 10 nm/s, and the photomultiplier tube voltage was set at 800 V [18].

### **2.2.6 X-ray photoelectron spectroscopy (XPS)**

An AXIS 165 spectrometer (Kratos Analytical, Japan) analytical chamber was maintained below  $3 \times 10^{-8}$  Pa. Monochromatic Al K $\alpha$  source ( $h\nu = 1486.6$  eV) was used at a power of 210 W. The analyzed area had dimensions of  $400 \times 700$   $\mu\text{m}$ . Duplicate survey scans were collected for binding energies in a range of 1,100 eV to 0 with analyzer pass energy of 160 eV and a step of 0.4 eV and 20 eV with a step of 0.1 eV for the high-resolution spectra. No charge neutralization was required due to sample conductivity.

### **2.2.7 Characterizations of the surfaces of polymeric membranes**

The contact angles of pristine membranes were estimated using a sessile drop method (FTA-200, FOLIO Instruments Inc., Kitchener, ON, Canada). A 4  $\mu\text{L}$  of Milli-Q water was dropped on each membrane (five replicates) and the contact angle was determined by the FTA32 software. The chemical functionality of the membranes' surface before and after filtration was determined in duplicate by attenuated total reflectance (ATR) FT-IR using a multi-reflection

Smart Performer® instrument (Nicolet 8700, Thermo Electron Corp., West Palm Beach, FL, USA) with a zinc selenide (ZnSe) crystal at a nominal incident angle of 45°. The spectra were collected in the range of wavenumbers from 600 to 4 000  $\text{cm}^{-1}$  with 128 scans at a resolution of 4.0  $\text{cm}^{-1}$ .

## 2.3 Results and Discussion

### 2.3.1 Identification of functional groups in AEF by acid-base titration and LPM

Table 2-1 showed the  $\text{pK}_a$  values and relative percentages of the detected groups in OSPW 1 and Merichem NAs, respectively. Site 1 with a  $\text{pK}_a$  value of 5.8 and  $5.5 \pm 0.1$  for OSPW 1 and Merichem NAs, respectively, was attributed to the presence of carboxylic functional groups [19]. Site 2 had a  $\text{pK}_a$  of  $6.4 \pm 0.1$  and  $6.6 \pm 0.2$  for OSPW 1 and Merichem NAs mixtures, respectively, and was attributed to the presence of phosphoryl functional groups [17]. The intensity of this site was lower than that of site 1 for both Merichem NAs mixture and OSPW 1 by 20% and 50%, respectively. Site 3 had a  $\text{pK}_a$  of  $7.9 \pm 0.1$  and  $7.8 \pm 0.1$  for OSPW 1 and Merichem NAs mixture, respectively. It was suggested that this could be attributed to the presence of amine functional groups as both amine and phosphoryl functional groups have been reported previously using LPM for a water matrix at similar pH values [17]. Sites 2 and 3 had the lowest intensity among all four detected sites in both Merichem NAs mixture and OSPW 1. However, further studies are required to confirm that sites 2 and 3 belong to phosphoryl and amine functional groups, respectively. Site 4 was ascribed to hydroxyl functional groups, with  $\text{pK}_a$  values of 9.9 and  $9.4 \pm 0.1$  for OSPW 1 and Merichem NAs mixture, respectively. The presence of hydroxyl functional groups could be an indication of the oxidized NAs [4, 8, 14, 17]. This site had the highest intensity in OSPW 1, but its intensity was significantly lower in

Merichem NAs mixture. This alteration in site percentages could significantly affect the further quantification processes due to the corresponding formation of different bonds with membrane surfaces [20]. More specifically, focus on the carboxyl and hydroxyl groups would be useful as they characterize classical and oxidized NAs [4, 8, 14].

**Table 2-1.** pK<sub>a</sub> values and percentage of functional groups in AEF from OSPW 1 and Merichem NAs as measured by LPM.

Sample	Site number	pK <sub>a</sub>	Relative response	Percentage (Average)
<b>OSPW</b>	(1)	5.8 ± 0.0	3.4 ± 0.2	32
	(2)	6.4 ± 0.1	1.8 ± 0.4	17
	(3)	7.9 ± 0.1	1.0 ± 0.3	10
	(4)	9.9 ± 0.0	4.3 ± 0.3	41
<b>Merichem</b>	(1)	5.5 ± 0.1	6.1 ± 0.6	64
	(2)	6.6 ± 0.2	1.1 ± 0.5	12
	(3)	7.8 ± 0.1	0.6 ± 0.5	7
	(4)	9.4 ± 0.1	1.7 ± 0.6	17

### 2.3.2 Surface characterization of pristine polymeric membranes

The nylon membrane composed of 77% carbon, 10% oxygen and 13% nitrogen atoms (Figure 2-1). The curve fitting of C1s peak resulted in binding energies (E<sub>B</sub>) of 284.9, 285.6 and 287.8 eV, attributed to C-C, C-N and O=C-N species, respectively [21]. PVDF membrane consisted of 56% carbon, 10% oxygen and 34% fluoride atoms. The deconvolution of C1s peak resulted in four E<sub>B</sub> at 284.8, 286.2, 288.7 and 290.7 eV, assigned to C-H, H-C-H, C=O and F-C-F groups, respectively [21]. The PTFE membrane consisted of 56% carbon, 20% oxygen and 24% fluorine atoms. The deconvolution of C1s peak resulted in peaks with E<sub>B</sub> of 284.8, 286.1, 288.7, and 291.9 eV. These binding energies were assigned to C-C, C-O, O-C=O and F-C-F

groups, respectively [22, 23]. Contact angles measurements indicated that nylon membrane was the most hydrophilic, having a contact angle of  $34.5 \pm 3.1$ . The PTFE membrane was the less hydrophilic with contact angle of  $82.0 \pm 5.5$  and the PVDF membrane slightly higher at  $69.8 \pm 1.5$ . The XPS and contact angle results indicate that nylon membranes should be the best for filtration due to their relatively high hydrophilicity as indicated by previous work [24-26].

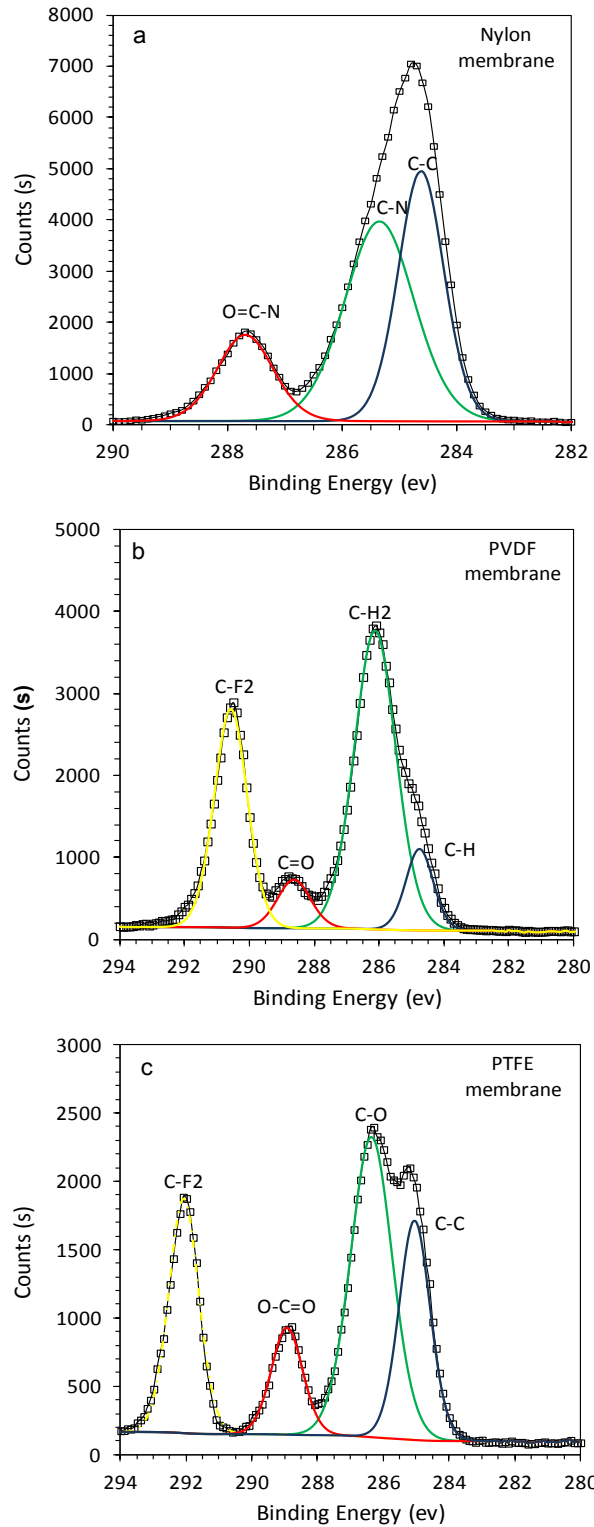


**Figure 2-1.** Deconvolution of C1s XPS peak for (a) nylon, (b) PVDF, and (c) PTFE membranes.

### **2.3.3 Effects of centrifugation and solution pH on the adsorption of AEF on membrane during filtration**

It was found that centrifugation did not affect the quantification of AEF, with the AEF concentrations being  $80.1 \pm 0.5$  mg/L and  $79.9 \pm 0.5$  mg/L for as-received and centrifuged OSPW 1, respectively. This may be attributed to the very low insoluble matter concentration in the water matrix received as compared to OSPW matrices used in previous work [5]. The centrifuged OSPW 1 was further subjected to membrane filtration to evaluate the effect of pH on the adsorption of AEF (Figure 2-2). The highest reduction in AEF concentration after filtration of OSPW 1 was observed at pH 2.5, with  $33.0 \pm 0.5\%$ ,  $26.0 \pm 0.8\%$  and  $24.0 \pm 0.5\%$  adsorption on nylon, PVDF and PTFE membranes, respectively. Because the sizes of AEF molecules are significantly smaller than the pore sizes of polymeric microfiltration membranes used in this study, the removal due to size size is not expected to play a significant role in the adsorption of AEF at any tested pH.

As shown by the LPM results (Table 2-1), at pH 2.5 the functional groups in AEF molecules were mostly protonated. Hence, the hydrophobic interactions between the non-charged AEF molecules and membrane surface could result in the adsorption of AEF molecules on the membrane surface, decreasing the concentration of AEF in permeate. The adsorption of AEF decreased when the pH increased from 2.5 to 5.5. This is consistent with the LPM results, which indicated that carboxylic functional groups became totally or partially ionized at pH 5.8 (Table 2-1). The ionization reduced the hydrophobic interactions between the AEF molecules and the membrane surface, which resulted in more soluble AEF molecules passing through the membrane pores. Further deprotonation of functional groups in AEF at pHs 6.4 and 7.9 rendered higher net negative charge on AEF molecules. The development of a negatively charged assisted

hydrogen bond (-CAHB) between the ionized acids and carbonyl groups on the membrane surface depends on the pKa of organic acids [27]; however, nylon filters showed no removal at pH 8.7. For the Merichem NAs, the carboxylic acids functional group concentration was about two times higher than OSPW that caused the development of -CAHB and subsequent adsorption to the nylon membrane at pH 8.7 (Figure 2-2). On the other hand, the tested PVDF and PTFE membranes are expected to be negatively charged at the circumneutral and basic pHs due to the presence of the fluoride groups on the surface [28, 29]. As such, the electrostatic repulsion between the negatively charged AEF molecules and the membrane surface would be a primary adsorption mechanism in this pH range.

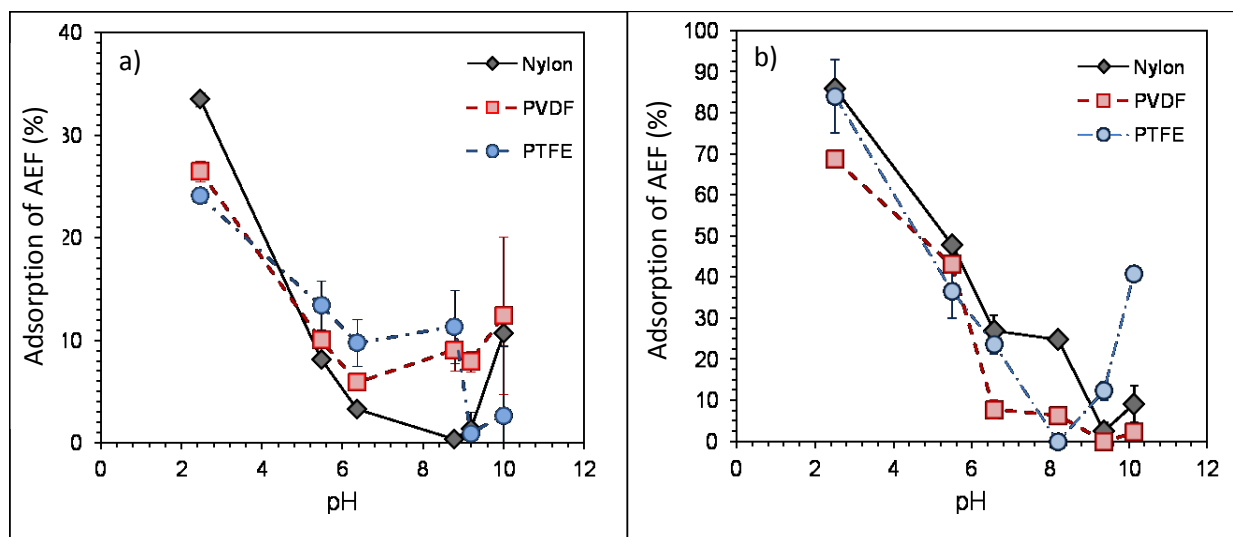


**Figure 2-2.** FT-IR results for the adsorption of AEF from a) OSPW 1 by different membranes (The original concentration of AEF in OSPW 1 was  $80.00 \pm 0.48$  mg/L), b) FT-IR results for the adsorption of AEF from Merichem NAs solution by different membranes (The original concentration of AEF was  $50.10 \pm 0.63$  mg/L).

According to the contact angle measurements, the adsorption of AEF molecules by the nylon membrane was the lowest, with no rejection observed at pH 8.7 (natural pH of OSPW 1)

due to its higher hydrophilicity. Taking into account that PTFE and PVDF membranes are more hydrophobic than the nylon one, the hydrophobic interactions between the surfaces of PTFE and PVDF membranes and AEF molecules would be higher, resulting in an increase in AEF rejection on these membranes at pH 8.7. When pH was further increased to 10.0, the adsorption of AEF molecules increased for all membrane types. This can be explained by the LPM results, which indicated that hydroxyl (OH) functional groups in AEF are deprotonated at pH 9.9. Given the prevalence of OH groups in AEF (41%, Table 2-1), the complete ionization of AEF molecules increased its net negative charge. Therefore, the repulsive forces between the membrane surface and the AEF molecules will repel AEF molecules from the membrane surface during filtration, increasing their rejection by all tested membranes. The PTFE membrane, which had the lowest hydrophilicity, had 100% recovery of AEF from the Merichem NAs mixture ( $50.4 \pm 1.2$  mg/L) at pH 8.2. This is due to the higher content of carboxylic groups in the Merichem mixture which may not be able to form -CAHB with the low concentration of carbonyl groups on the PTFE membrane.

#### **2.3.4 Identification of adsorbed aromatic compounds from OSPW and Merichem NAs solutions**

The FT-IR analysis which was used for the quantification of AEF, is based on the detection and quantification of carbonyl stretches. However, these stretches could represent NAs and other organics in AEF, including aromatic compounds [4, 6]. To investigate the impact of aromatic fraction in AEF on FT-IR measurements, the SFS analyses of OSPW 1 and Merichem NAs were performed at pH 8.7 and 8.2, respectively (Figure 2-3).

The characteristic peaks of aromatic compounds were obtained in OSPW 1 at the emission wavelengths of  $273\text{ cm}^{-1}$ ,  $310\text{ cm}^{-1}$  and  $325\text{ cm}^{-1}$ , indicating the presence of one and two aromatic rings (Figure S2) [6]. The observed wavelengths slightly deviated from the reported values ( $282.5\text{ cm}^{-1}$ ,  $320\text{ cm}^{-1}$  and  $340\text{ cm}^{-1}$ ) likely due to the pH effect on the peak shape [30, 31]. The intensity of the peaks for non-filtered and PVDF- and PTFE- filtered OSPW 1 was similar, indicating that there was no adsorption of aromatic compounds by these membranes. However, the intensity of the peaks corresponding to the compounds with two rings was lower for the nylon-filtered OSPW 1, indicating that some of the two-ring compounds were removed during filtration. Comparing this finding with the results of FT-IR analysis, it can be concluded that the compounds in the removed fraction did not contain carboxyl groups (COOH) in their structure which is corroborated in the NAs quantification section below.

To evaluate the impact of low pH on the adsorption of aromatic compounds from OSPW 1 during filtration, filtration on the nylon membrane was performed at pH 5.3. At this pH, the carboxyl functional groups are expected to be partially protonated ( $\text{pK}_a$  5.8) (Table 2-1). As shown in Figure 2-3, the intensity of the peaks detected in OSPW 1 after filtration on the nylon membrane was lower at pH 5.3 as compared to pH 8.7 for both one- and two-ring compounds. This implies that the aromatic compounds were removed from OSPW 1 during filtration on the nylon membrane as the pH decreased. The SFS of Merichem NAs mixtures revealed three peaks at  $287\text{ cm}^{-1}$ ,  $329\text{ cm}^{-1}$  and  $410\text{ cm}^{-1}$  corresponding to the compounds with one, two and four or more rings, respectively (Figure 2-3) [6]. The intensity of the first peak did not change in the PTFE- and PVDF-filtered solutions at both studied pHs (5.5 and 8.2); however, it decreased after filtration using the nylon membrane. The intensity of the peaks corresponding to the compounds with two rings decreased after filtration on all membranes. Consistently with the SFS of OSPW

1, it can be concluded that the removed aromatic compounds at the studied pHs (8.7 for OSPW 1 and 8.2 for Merichem NAs) did not contain carboxyl groups in their structure. No peaks corresponding to the compounds with four or more rings were detected after filtration on all membranes, suggesting that this type of organics was fully removed during the filtration. These results indicate the insignificant impact of adsorption to membranes for the OSPW aromatic compounds in addition to a minimal impact on the Merichem NAs mixture.

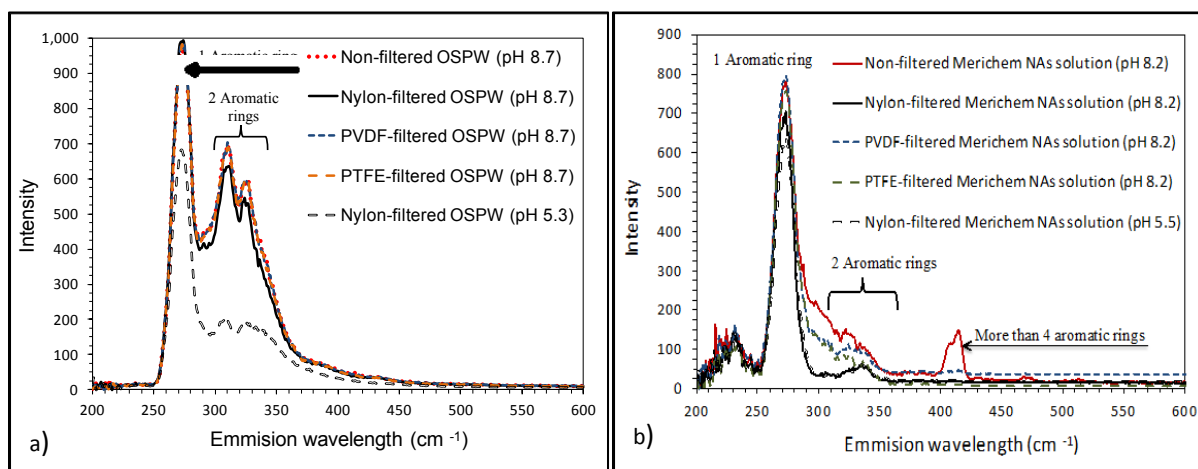


**Figure 2-3.** The synchronous fluorescence spectroscopy of a) OSPW 1 and b) Merichem NAs filtered through the different membranes.

### 2.3.5 ATR FT-IR analysis of membrane surfaces

The decrease in AEF concentration was observed after filtration of OSPW 1 and Merichem NAs solutions using different membranes (Figure 2-2). The nylon and PTFE membranes did not show adsorption of AEF at pHs 8.7 and 8.2 in OSPW 1 and Merichem NAs mixture, respectively. The ATR FT-IR spectra of nylon, PVDF and PTFE membranes before and

after filtration of OSPW 1 and Merichem NAs are shown in Figures 2-5 and 2-4, respectively. Two adsorption bands (C=O and OH) can indicate the presence of carboxyl functional groups on a surface, with the adsorption band near  $1,670\text{ cm}^{-1}$  characterizing C=O stretching vibration, and adsorption band between  $3\,300$  and  $2\,500\text{ cm}^{-1}$  characterizing OH stretching vibration [5, 32]. As shown in Figure 2-4 two adsorption peaks at  $1\,670\text{ cm}^{-1}$  and  $3\,300\text{--}2\,500\text{ cm}^{-1}$  were detected in all membranes. The wide peak appeared in  $3\,300\text{--}2\,500\text{ cm}^{-1}$  region could be ascribed either to hydroxyl groups in carboxyl group or to any possible residual moisture remaining in the membranes after air-drying [5]. The intensity of the adsorption band at  $1,670\text{ cm}^{-1}$  increased two to five times after filtration on all membranes (Figure 2-5), with the adsorption bands for OSPW 1 and Merichem NAs mixture having similar intensities. The FT-IR analysis showed no losses of AEF in permeate from the nylon-filtered OSPW 1 at natural pH 8.7. The ATR FT-IR results confirmed the adsorption of AEF compounds on the membrane surface at natural pH 8.7. It should be noted that  $\text{CH}_2\text{Cl}_2$  solvent is used for AEF extraction while ATR FT-IR allows for the direct analysis of AEF compounds retained on the membrane surface. As such, the difference between ATR FT-IR and FT-IR results might imply that FT-IR did not account for a certain fraction of carboxylic acids due to the extraction step. The  $\text{CH}_2\text{Cl}_2$  might not fully extract carboxylic acids from a solution and the organic fraction of OSPW 1 reported as AEF may not account for all NAs present in OSPW 1.

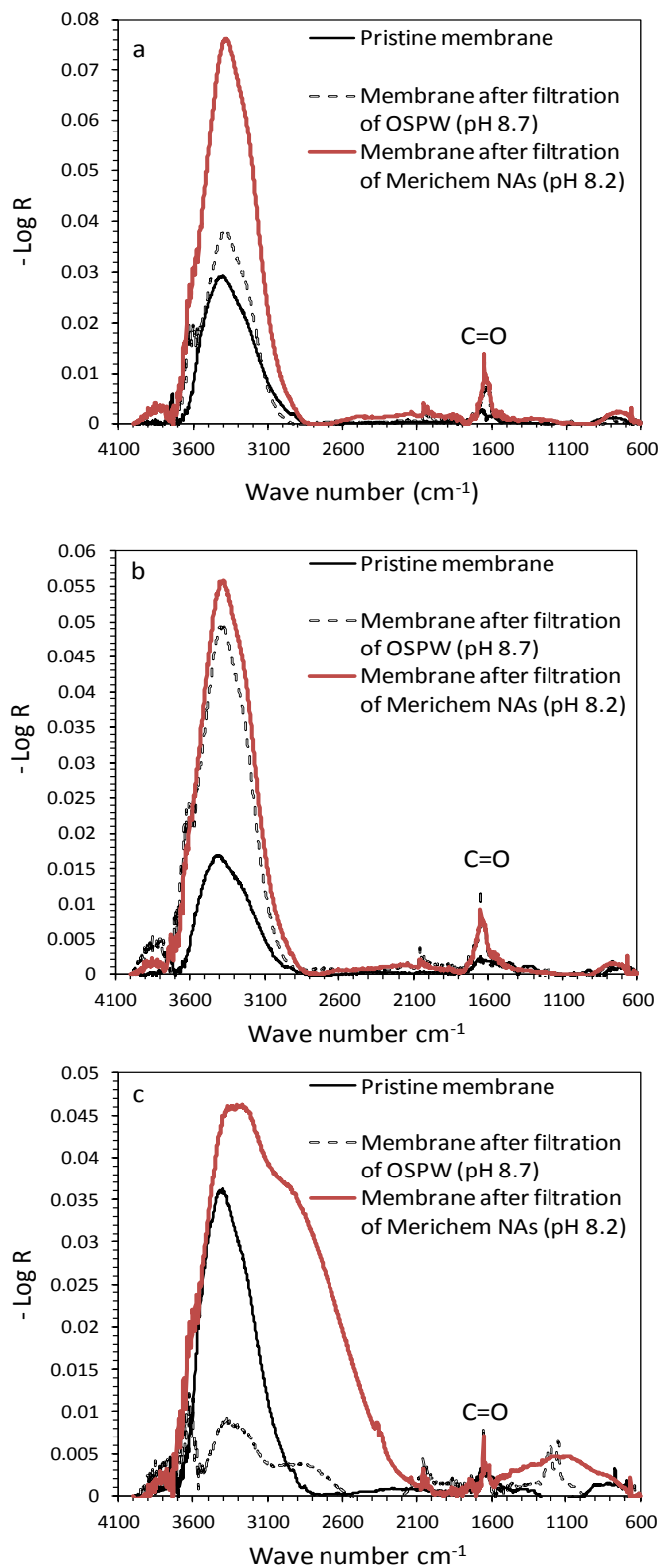


**Figure 2-4.** The ATR FT-IR spectra for (a) nylon, (b) PVDF, and (c) PTFE membranes before and after filtration of OSPW 1 and Merichem NAs solution.

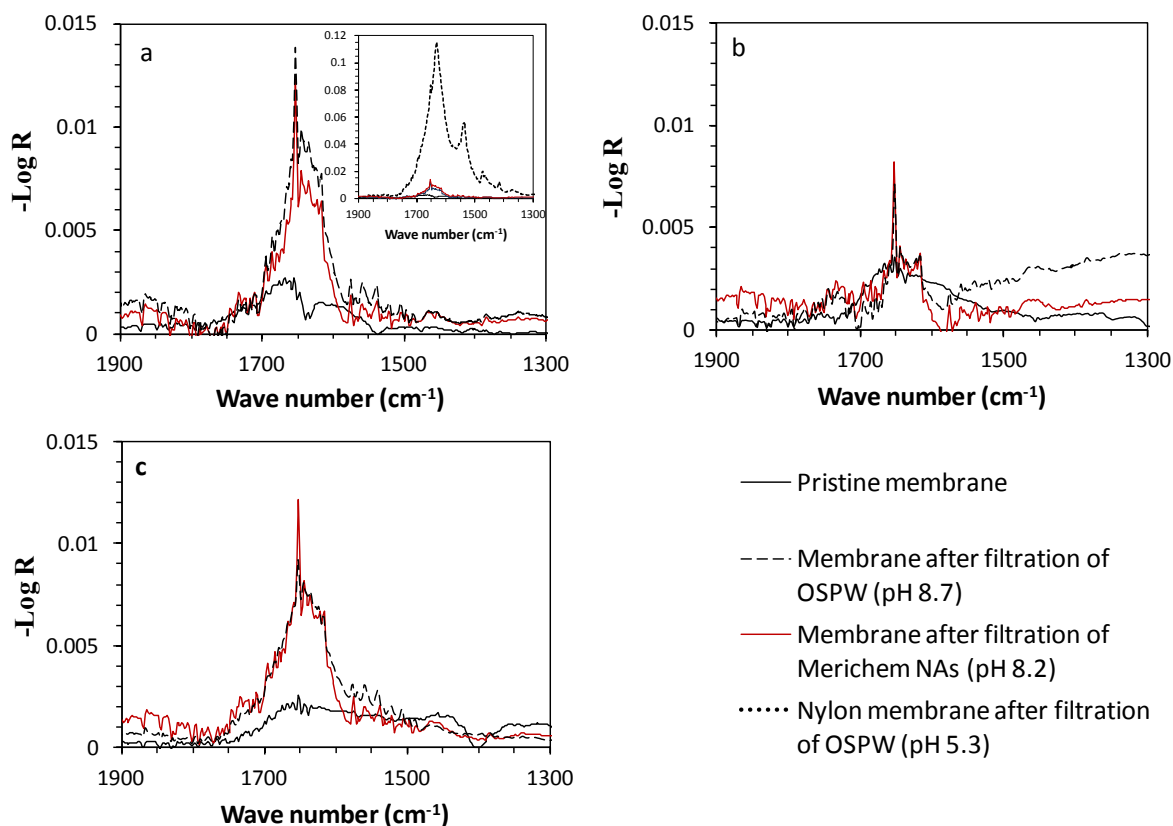


**Figure 2-5.** The ATR FT-IR spectra of (a) nylon, (b) PVDF, and (c) PTFE membranes before and after filtration of OSPW 1 and Merichem NAs. An inset shows ATR FT-IR spectra of nylon membrane after filtration of OSPW 1 at pH 5.3.

To investigate the effect of low pH on the surface composition of the studied membranes due to filtration, the surface of a nylon membrane was analyzed by ATR FT-IR after filtration of OSPW 1 at pH of 5.3. Consistently with the FT-IR analysis of membranes' permeates, which showed higher adsorption of AEF in the acidic pH range, the intensity of carbonyl peak on the membrane surface was almost eight times higher as compared to the peak detected after filtration of OSPW 1 at pH 8.7. This is caused by the higher hydrophobicity of the protonated organic fraction in OSPW 1 at the acidic conditions (pH 5.3) (Table 2-1) [9, 33]. It is noted that FT-IR results for the same sample (pH 5.3) showed  $8.0 \pm 0.3\%$  adsorption of AEF, while no adsorption

was observed for filtered OSPW 1 at pH 8.7. Comparing these observations with the ATR results, it might be concluded that the detected C=O groups on the filter surface could be a leftover or any possible residual moisture remaining in the membranes. An additional technique is required in order to quantify the percentage of AEF removed by the membranes.

### **2.3.6 Measurement of classical NAs using UPLC/HRMS**

The effect of membrane filtration on the adsorption of classical NAs was evaluated by quantifying classical NAs in OSPW 1 before and after filtration. The results were reported in terms of the carbon number (n) and hydrogen deficiency/number of rings (-Z) (Figures 2-6 and 2-7). The observed -Z numbers for OSPW 1 were even, ranging from 2 to 12 rings, and n ranging from 9 to 20 carbons. These findings agreed with the results reported in previous studies where nylon membrane filters were used for filtration of various water matrices [5, 30]. The total relative responses of classical NAs did not significantly change after filtration at the natural pH of OSPW 1 (Figures 2-6b and 2-7b). A maximum of 10% adsorption of NAs was detected for nylon and PVDF membranes and less than 2% for PTFE membrane (Figures 2-6c, 2-6d, 2-7c and 2-7d). Consistently with the FT-IR analysis, the adsorption of classical NAs increased with the decrease in the OSPW pH. The filtration experiment conducted on nylon membrane at pH 5.3 resulted in  $26\% \pm 2.4$  adsorptions of classical NAs from OSPW 1 as shown in Figures 2-6e and 2-7e.

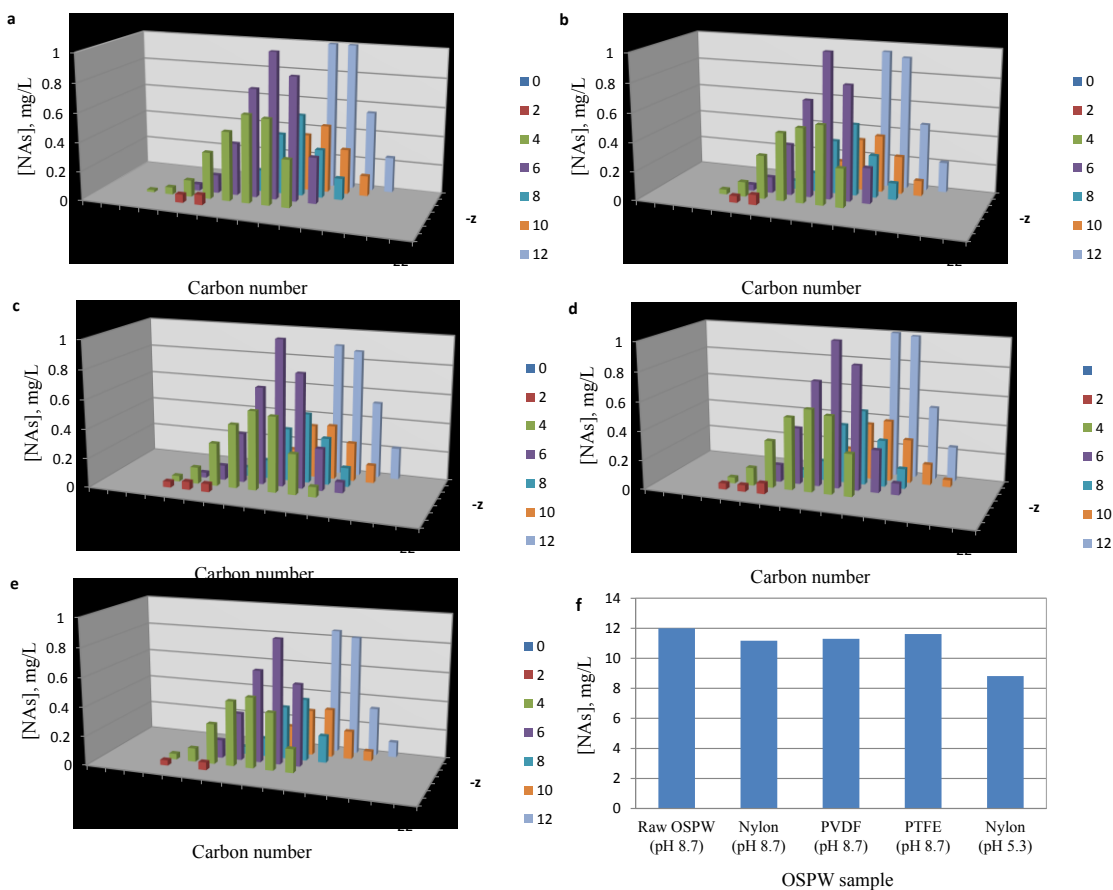


**Figure 2-6.** Distribution and estimated concentration of classical NAs (Trial #1) in (a) OSPW 1 at pH 8.7 (11.9 mg/L), and permeates after filtration through (b) nylon membrane at pH 8.7 (11.4 mg/L), (c) PVDF membrane at pH 8.7 (11.6 mg/L), (d) PTFE membrane at pH 8.7 (11.8 mg/L), (e) Nylon membrane at pH 5.3 (8.8 mg/L) and (f) summary of the estimated concentrations of NAs. The concentration of classical NAs was measured by UPLC/HRMS.

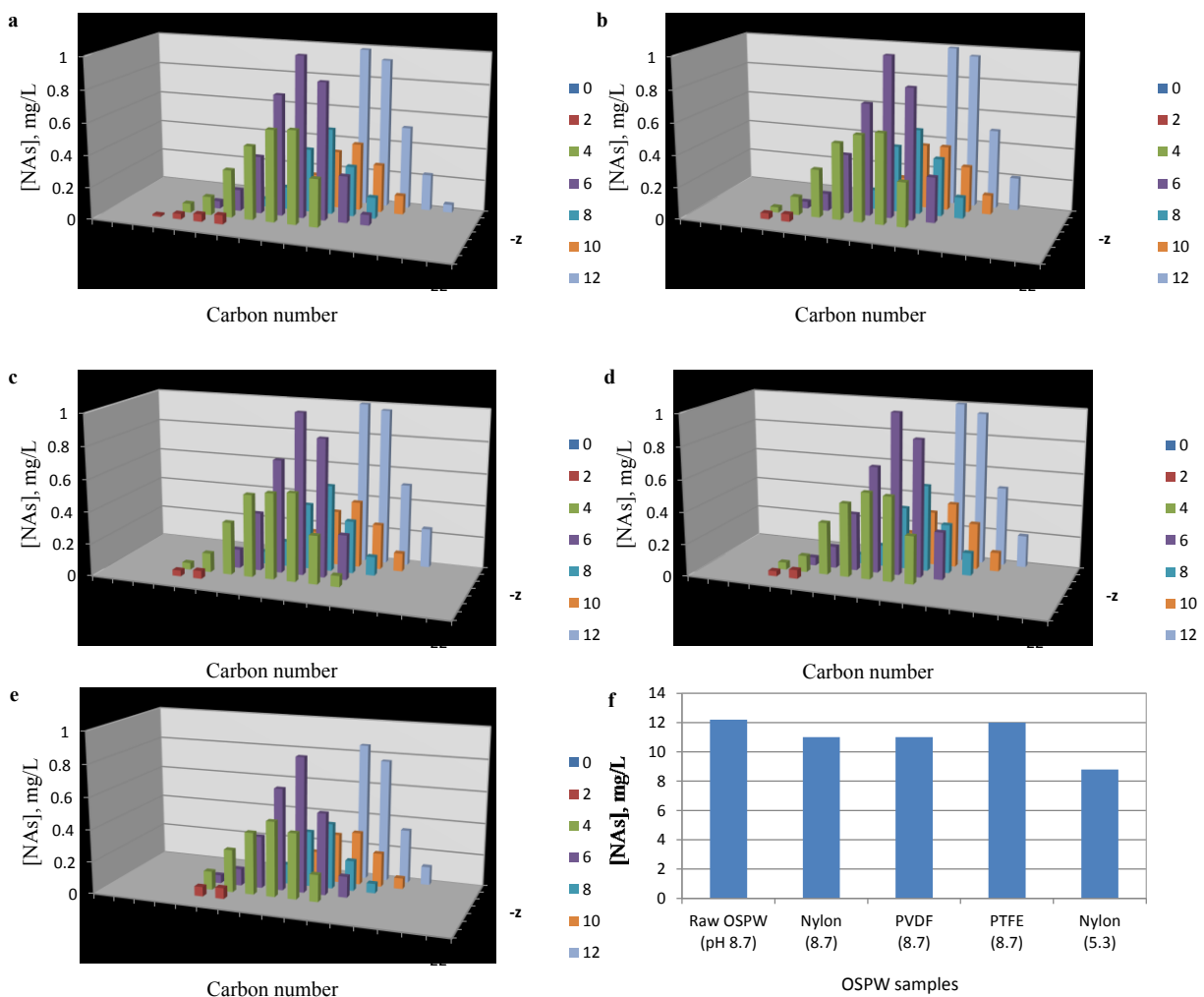


**Figure 2-7.** Distribution and estimated concentration of classical NAs (Trial #2) in (a) OSPW 1 at pH 8.7 (12.2 mg/L), and permeates after filtration through (b) nylon membrane at pH 8.7 (11 mg/L), (c) PVDF membrane at pH 8.7 (11 mg/L), (d) PTFE membrane at pH 8.7 (12 mg/L), (e) nylon membrane at pH 5.3 (8.8 mg/L), and (f) summary of the estimated concentrations of classical NAs. The concentration of classical NAs was measured by UPLC/HRMS.

## 2.4 Conclusions

The treatment techniques of OSPW such as adsorption and advanced oxidation are assessed based on the reduction in the concentration of NAs species and their associated toxicity. Therefore, the concentration of these compounds should not be underestimated. This study showed that the use of membranes for filtration of insoluble compounds before AEF extraction can bias the quantification results especially when OSPW pH is reduced to less than 6.2. In addition, it is interesting to note that the higher concentration of carboxylic acids in commercial NAs significantly increases the adsorption to the nylon membrane versus the OSPW due to the formation of -CAHB. Therefore, the use of membranes for filtration of OSPW, commercial NAs mixtures or other oily wastewaters before the quantification analysis should be thoroughly investigated before their application. This finding should be applicable to any water matrix containing a mixture of soluble carboxylic hydrocarbons such as the tailings water for the conventional oil and gas industries and contaminated groundwater impacted by leaking underground and aboveground storage tanks.

## 2.5 References.

- [1] Del Rio LF, Hadwin AKM, Pinto LJ, MacKinnon MD, Moore MM. Degradation of naphthenic acids by sediment micro-organisms. *Journal of Applied Microbiology* 2006;101:1049-1061.
- [2] MacKinnon M, Van Meer T, Verbeek A. Assessment of biological impact from a wet landscape option for the reclamation of fine tails from oil sands. *Canadian Technical Report of Fisheries and Aquatic Sciences* 1993;0:258.
- [3] Allen EW. Process water treatment in Canada's oil sands industry: I. Target pollutants and treatment objectives. *Journal of Environmental Engineering and Science* 2008;7:123-138.
- [4] Grewer DM, Young RF, Whittal RM, Fedorak PM. Naphthenic acids and other acid-extractables in water samples from Alberta: What is being measured? *Science of the Total Environment* 2010;408:5997-6010.
- [5] Pourrezaei P, Drzewicz P, Wang Y, El-Din MG, Perez-Estrada LA, Martin JW, et al. The Impact of Metallic Coagulants on the Removal of Organic Compounds from Oil Sands Process-Affected Water. *Environmental Science & Technology* 2011;45:8452-8459.
- [6] Kavanagh RJ, Burnison BK, Frank RA, Solomon KR, Van Der Kraak G. Detecting oil sands process-affected waters in the Alberta oil sands region using synchronous fluorescence spectroscopy. *Chemosphere* 2009;76:120-126.
- [7] Frank RA, Kavanagh R, Burnison BK, Headley JV, Peru KM, Van Der Kraak G, et al. Diethylaminoethyl-cellulose clean-up of a large volume naphthenic acid extract. *Chemosphere* 2006;64:1346-1352.
- [8] Martin JW, Barri T, Han XM, Fedorak PM, El-Din MG, Perez L, et al. Ozonation of Oil Sands Process-Affected Water Accelerates Microbial Bioremediation. *Environmental Science & Technology* 2010;44:8350-8356.
- [9] Jivraj MN, MacKinnon, M.D., Fung, B. Naphthenic acid extraction and quantitative analysis with FTIR spectroscopy. Technical report; 1995 1995.
- [10] Han X, MacKinnon MD, Martin JW. Estimating the in situ biodegradation of naphthenic acids in oil sands process waters by HPLC/HRMS. *Chemosphere* 2009;76:63-70.
- [11] Martin JW, Han XM, Peru KM, Headley JV. Comparison of high- and low-resolution electrospray ionization mass spectrometry for the analysis of naphthenic acid mixtures in oil sands process water. *Rapid Communications in Mass Spectrometry* 2008;22:1919-1924.
- [12] He Y, Wiseman SB, Hecker M, Zhang X, Wang N, Perez LA, et al. Effect of Ozonation on the Estrogenicity and Androgenicity of Oil Sands Process-Affected Water. *Environmental Science & Technology* 2011;45:6268-6274.
- [13] Anderson JC, Wiseman SB, Wang N, Moustafa A, Perez-Estrada L, Gamal El-Din M, et al. Effectiveness of Ozonation Treatment in Eliminating Toxicity of Oil Sands Process-Affected Water to *Chironomus dilutus*. *Environmental science & technology* 2012;46:486-493.
- [14] Bataineh M, Scott AC, Fedorak PM, Martin JW. Capillary HPLC/QTOF-MS for characterizing complex naphthenic acid mixtures and their microbial transformation. *Analytical Chemistry* 2006;78:8354-8361.
- [15] El-Din MG, Fu H, Wang N, Chelme-Ayala P, Perez-Estrada L, Drzewicz P, et al. Naphthenic acids speciation and removal during petroleum-coke adsorption and ozonation of oil sands process-affected water. *Science of the Total Environment* 2011;409:5119-5125.
- [16] Brassard P, Kramer JR, Collins PV. Binding-site analysis using linear-programming. *Environmental Science & Technology* 1990;24:195-201.

- [17] Cox JS, Smith DS, Warren LA, Ferris FG. Characterizing heterogeneous bacterial surface functional groups using discrete affinity spectra for proton binding. *Environmental Science & Technology* 1999;33:4514-4521.
- [18] Peuravuori J, Koivikko R, Pihlaja K. Characterization, differentiation and classification of aquatic humic matter separated with different sorbents: synchronous scanning fluorescence spectroscopy. *Water Research* 2002;36:4552-4562.
- [19] Fein JB, Daughney CJ, Yee N, Davis TA. A chemical equilibrium model for metal adsorption onto bacterial surfaces. *Geochimica Et Cosmochimica Acta* 1997;61:3319-3328.
- [20] Ni H-G, Zeng H, Zeng EY. Sampling and analytical framework for routine environmental monitoring of organic pollutants. *Trac-Trends in Analytical Chemistry* 2011;30:1549-1559.
- [21] Xie R, Li Y, Chu L-Y. Preparation of thermo-responsive gating membranes with controllable response temperature. *Journal of Membrane Science* 2007;289:76-85.
- [22] Chandler-Temple A, Wentrup-Byrne E, Whittaker AK, Grondahl L. Graft Copolymerization of Methoxyacrylethyl Phosphate onto Expanded Poly(tetrafluoroethylene) Facial Membranes. *Journal of Applied Polymer Science* 2010;117:3331-3339.
- [23] Chebbi R, Beicha A, Daud WRW, Zaamouche R. Surface analysis for catalyst layer (PT/PTFE/C) and diffusion layer (PTFE/C) for proton exchange membrane fuel cells systems (PEMFCs). *Applied Surface Science* 2009;255:6367-6371.
- [24] Wang X, Tian Y, Wang Z, Tao Y. A Novel Hydrophilic Modification of PTFE Membranes Using In Situ Deposited PANI. *Journal of Macromolecular Science Part B-Physics* 2011;50:172-178.
- [25] Wang L, Zhang X, Hou S, Wang X, Wang A, Liu S. Preparation and Characterization of Hydrophilic PVDF Membrane via graft modification by Maleic Anhydride. *Manufacturing Science and Technology*, 2011. 286-291.
- [26] Yang X, Zhang B, Liu Z, Deng B, Yu M, Li L, et al. Preparation of the antifouling microfiltration membranes from poly(N,N-dimethylacrylamide) grafted poly(vinylidene fluoride) (PVDF) powder. *Journal of Materials Chemistry* 2011;21:11908-11915.
- [27] Ni J, Pignatello JJ, Xing B. Adsorption of Aromatic Carboxylate Ions to Charcoal Black Carbon is Accompanied by Proton Exchange with Water (vol 45, pg 9240, 2012). *Environmental Science & Technology* 2012;46:5633-5633.
- [28] Han MJ, Barona GNB, Jung B. Effect of surface charge on hydrophilically modified poly(vinylidene fluoride) membrane for microfiltration. *Desalination* 2011;270:76-83.
- [29] Lin A, Shao S, Li H, Yang D, Kong Y. Preparation and characterization of a new negatively charged polytetrafluoroethylene membrane for treating oilfield wastewater. *Journal of Membrane Science* 2011;371:286-292.
- [30] Cabaniss SE, Shuman MS. Synchronous fluorescence-spectra of natural-waters - tracing sources of dissolved organic-matter. *Marine Chemistry* 1987;21:37-50.
- [31] Pullin MJ, Cabaniss SE. Physicochemical variations in DOM-synchronous fluorescence: Implications for mixing studies. *Limnology and Oceanography* 1997;42:1766-1773.
- [32] B.H S. infrared spectroscopy: fundamentals and applications: John Wiley & Sons, Ltd., Chichester, UK; 2004.
- [33] Kannel PR, Gan TY. Naphthenic acids degradation and toxicity mitigation in tailings wastewater systems and aquatic environments: a review. *Journal of environmental science and health Part A, Toxic/hazardous substances & environmental engineering* 2012;47:1-21.

Ahmed Moustafa  
Department of Civil and Environmental Engineering  
6-023 Markin/CNRL Natural Resources Engineering Facility  
University of Alberta  
Alberta  
Canada  
T6G 2W2

4 February 2015

Dear Ahmed.

Permissions request relating to material published in *Water Science & Technology*:

In response to your request for copyright clearance to include the following publication as part of your thesis:

Ahmed M. A. Moustafa, Eun-Sik Kim, Alla Alpatova, Nian Sun, Scott Smith, Seoktae Kang and Mohamed Gamal El Din. Impact of polymeric membrane filtration of oil sands process water on organic compounds quantification. *Water Science & Technology* 70(5) 771-779.

We are very happy to grant you permission to reproduce the material specified above without charge, provided that:

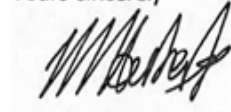
- the material to be used has appeared in our publication without credit or acknowledgement to another source;
- suitable acknowledgement to the source is given in accordance with standard editorial practice, e.g.,

"Reproduced from W. Gujer and A. J. B. Zehnder (1983) 'Conversion Processes in Anaerobic Digestion'. *Water Science & Technology* Vol. 15, pp. 127-167, with permission from the copyright holders, IWA Publishing".

- Reproduction of this material is confined to the purpose for which this permission is given.

I trust this permission will be satisfactory; if any point needs clarification or you have any further queries, please do not hesitate to contact us again.

Yours sincerely



Michelle Herbert  
Journals Editorial Co-ordinator  
IWA Publishing

### **3 INVESTIGATION OF MONO/COMPETITIVE ADSORPTION OF ENVIRONMENTALLY RELEVANT IONIZED WEAK ACIDS ON GRAPHITE: IMPACT OF MOLECULAR PROPERTIES AND THERMODYNAMICS<sup>1</sup>**

#### **3.1 Introduction**

Several emerging and classical pollutants are found in ionized forms in the pH ranges of natural water streams, including endocrine-disrupters (e.g., bisphenol A [1]), antibiotics (e.g., sulfonamides [2]) and pesticides (e.g., atrazine [3]). In addition to these more commonly studied pollutants, and of current concern, are the highly diverse ionized organic naphthenic acids (NAs) which are present during the extraction process of bitumen from the Athabaskan oil sands in Alberta, Canada [4]. Generally, the removal of these NAs and other neutral weak acids can occur via adsorption on carbonaceous materials being governed mainly by hydrophobic interactions, van der Waals forces and hydrogen bonding which have been extensively studied and well characterized [5-7]. However, much less attention has been focussed on the assessment of the adsorptive performance of ionized weak acids on hydrophobic carbon surfaces [2, 8-11].

---

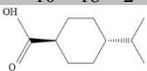
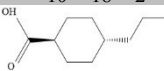
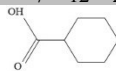
<sup>1</sup>A version of this chapter has been published previously: Ahmed M.A. Moustafa, Kerry N. McPhedran, Jesús Moreira and Mohamed Gamal El-Din, Investigation of mono/competitive adsorption of environmentally relevant ionized weak acids on graphite: Impact of molecular properties and thermodynamics. *Environmental Science & Technology*. 2014. 48 (24), 14472-14480.

Historically, the adsorption of deprotonated acids was thought to be governed solely by bridging via metal ions and repulsion between negatively charged acids and surface functional groups, both phenolic and carboxylic, of carbon adsorbent surfaces [12, 13]. However, more recent studies by Ni et al. [10] and Teixido et al. [2] have evaluated the potential role of hydrogen bonding (HB) in the adsorption of ionized weak acids. Both studies were able to identify the role of the strong HB between negatively charged groups of the weak acid and the adsorbent surface. More specifically, the weak acid was able to form a negatively charged assisted hydrogen bond (-CAHB). This -CAHB formation is accompanied by a rise in the pH of the solution indicating the formation of hydroxide ( $\text{OH}^-$ ) groups, however, this rise is not easily measured due to the use of buffered background solutions which conceal  $\text{OH}^-$  release. Subsequently, Li et al. [9] performed an extensive study confirming the role of the -CAHB for a range of pH values for benzoic acid, phthalic acids and 2, 6-dichloro-4-nitrophenol. At pH 7, they established via  $\text{OH}^-$  release stoichiometry that almost 100% adsorption was due to the -CAHB. However, a limitation of these previous studies has been that only mono-compound solutions were considered. In addition, the  $\text{pK}_a$  values for the weak acids examined were diverse which resulted in distinct free solvation energies in water. Thus, the potential competition for adsorption sites by weak acids found in mixtures and the impact of molecular properties of compounds (with similar  $\text{pK}_a$  values) have not been previously examined.

The alkaline ( $\text{pH } 8 \pm 0.7$ ) oil sands process affected water (OSPW) in Alberta contains persistent ionized weak organic NAs at concentrations ranging 10 to 120 mg/L [4, 14, 15]. NAs in OSPW include hundreds of species, both known and unknown, which does not allow for the appropriate investigation of their fundamental behaviour and interaction with carbon adsorbents. Given the limitations of using raw OSPW, 5 model NAs were chosen to be examined in the

current study including: decanoic acid (DA), trans-4-Isopropylcyclohexanecarboxylic acid (Trans-4-IsoPCHA), trans-4-propylcyclohexanecarboxylic acid (Trans-4-PCHA), heptanoic acid (HPA) and cyclohexanecarboxylic acid (CHA) (Table 3-1). The main objective of this work was to study the thermodynamics of mono-compound adsorption for NAs with similar  $pK_a$  values with knowledge gained used in further evaluation of the competition of NAs in multi-compound solutions. To meet these objectives, the 5 model NAs were assessed, both individually and in mixtures, using the following criteria: (a) similar structures with different molecular weights (MW): (DA vs HPA) and (CHA vs Trans-4-IsoPCHA and Trans-4-PCHA); (b) similar MW but completely different structures: (DA vs Trans-4-IsoPCHA and Trans-4-PCHA) and (CHA vs HPA); (c) similar MW with a slight difference in structure: (Trans-4-IsoPCHA vs Trans-4-PCHA). Functionalized expanded graphite (EG) containing phenolic and carboxyl groups was used as the adsorbent for all model compounds.

**Table 3-1.** Physiochemical properties of the 5 model naphthenic acids calculated using SPARC software (<http://archemcalc.com/sparc/index>; accessed January 17, 2014)

Model NA compounds	Compound (1) Decanoic acid	Compound (2) Trans-4-Isopropyl Cyclohexanoic acid	Compound (3) Trans-4-propyl Cyclohexanoic acid	Compound (4) Heptanoic acid	Compound (5) Cyclohexanoic acid
<b>CAS #</b>	334-48-5	7077-05-6	38289-27-9	111-14-8	98-89-5
<b>Abbreviation</b>	DA	Trans-4-IsoPCHA	Trans-4-PCHA	HPA	CHA
<b>Formula</b>	C <sub>10</sub> H <sub>20</sub> O <sub>2</sub>	C <sub>10</sub> H <sub>18</sub> O <sub>2</sub>	C <sub>10</sub> H <sub>18</sub> O <sub>2</sub>	C <sub>7</sub> H <sub>14</sub> O <sub>2</sub>	C <sub>7</sub> H <sub>12</sub> O <sub>2</sub>
<b>Structure</b>					
<b>Molecular weight</b>	172.3 g/mol	170.3 g/mol	170.3 g/mol	130.2 g/mol	128.2 g/mol
<b>Log K<sub>ow</sub></b>	3.92	2.89	3.05	2.54	2.36
<b>pH 7 - Water solubility</b>	47.89 mg/L	109 mg/L	94 mg/L	1955 mg/L	4919 mg/L
<b>pK<sub>a</sub></b>	4.9	4.82	4.82	4.8	4.91
<b>Boiling point</b>	269 °C	263.8 °C	270.3 °C	223 °C	232 °C
<b>Enthalpy of vaporization</b>	53.6 kJ/mol	55.23 kJ/mol	55.97 kJ/mol	48.50 kJ/mol	51.70 kJ/mol
<b>Log K<sub>ow</sub> for anions (pH 8)</b>	0.72	-0.28	-0.12	-1.06	-1.71
<b>Volume (nm<sup>3</sup>)</b>	0.312	0.294	0.293	0.238	0.207

## 3.2 Materials and Methods

### 3.2.1 Chemicals and reagents.

The graphite intercalated compounds (GIC: CAS# 12777-87-6) (Grade 3772, Lot# 6319-3) were a gift from Asbury Carbons (NJ, USA) and used to create expanded graphite (EG). Trans-4-propylcyclohexanecarboxylic acid (Trans-4-PCHA) and trans-4-Isopropylcyclohexanecarboxylic acid (Trans-4-IsoPCHA) were purchased from TCI Japan Organic Chemicals (Tokyo, Japan); heptanoic acid (HPA) was purchased from TCI America Organic Chemicals (Oregon, US); decanoic acid (DA) was purchased from Sigma Aldrich

(Malaysia) and cyclohexanecarboxylic acid (CHA) was purchased from Sigma-Aldrich Canada (Oakville, ON, Canada). The 50-52% sodium hydroxide was purchased from Sigma-Aldrich Canada (Oakville, ON, Canada). The dichloromethane, methanol, ammonium acetate, acetic acid, potassium phosphate monobasic ( $\text{KH}_2\text{PO}_4$ ) and potassium phosphate dibasic ( $\text{K}_2\text{HPO}_4$ ) were purchased from Fisher Scientific (Edmonton, AB, Canada). Ultrapure water was obtained from a Millipore and Elga system (Synergy<sup>®</sup> UV instrument, Millipore, Molsheim, France).

### **3.2.2 Preparation and characterization of adsorbent and quantification of NAs.**

GIC were expanded by a thermal shock at  $1000 \pm 25$  °C for one minute using a Lindberg/Blue box furnace (Model BF51800 Thermo Scientific Edmonton, AB). The total pore volume and BET surface area of EG were performed at 77 K using nitrogen gas on a IQ2MP Quantachrome system for surface analysis [16]. Duplicate X-ray photoelectron spectroscopy (XPS) analyses (AXIS 165 spectrometer; Kratos Analytical, Japan) were used to characterize the elemental composition and surface functional groups of EG at a depth = 2–5 mm and area of  $400 \times 700$   $\mu\text{m}$ . The analytical chamber was sustained under  $3 \times 10^{-8}$  Pa and a monochromatic Al K $\alpha$  source ( $h\nu = 1486.6$  eV) was used at 210 W, while survey scans were collected for binding energies from 1100 to 0 eV with analyzer pass energy of 160 eV and a step of 0.4 eV. For high-resolution spectra, pass energy was 20 eV with a 0.1 eV step with no charge neutralization required for conducting samples. To study the morphology of GIC and EG, a Hitachi scanning electron microscopy (SEM) (S-2500, Tokyo, Japan) was used on dried samples scattered onto a stub pasted with silicon. Imaging acquisition was conducted using a Time of Flight Secondary Ion Mass Spectroscopy instrument (GmbH, Germany). Bi<sup>+</sup> ions were used as analytical source, operated at 25 kV in a static mode. Triplicate zeta potential measurements were performed to acquire the EG surface charge using a Malvern Zetasizer Nano device. The contact angle of EG

was estimated using a sessile drop method (FTA-200, FOLIO Instruments Inc., Kitchener, ON, Canada). A 4  $\mu$ L of Milli-Q water was dropped on EG (three replicates) and the contact angle was determined by the FTA32 software. All NAs quantifications were done in duplicate with methods described in Appendix B.

### **3.2.3 Sorption experiments.**

Solutions of each model NA (50 mg/L) were prepared in MilliQ water adjusted to pH 8 using 0.1 M phosphate buffer. Duplicate samples of EG (0.15, 0.3, 0.6, and 0.9 g) were added to 60 mL of each NA solution in a 250 mL glass vial with a Teflon screw cap. This resulted in EG concentrations from 2.5 to 15 g/L. Samples were mixed for 24 hours using a wrist action shaker with an oscillation rate of  $385 \pm 10\%$  at the highest degree of agitation (Model 75; Burrell Scientific, Pittsburgh, PA, USA) at room temperature ( $22 \pm 2$  °C). Initial control experiments without EG indicated no loss of NAs (e.g., to surfaces) after 24 h. The three highest EG masses (0.3, 0.6, 0.9 g) were used for fitting the adsorption isotherm models to avoid adsorbance saturation. Multi-compound adsorption experiments were performed similarly with 50 mg/L solution (10 mg/L of the 5 NA model compounds (5MC)). For competitive adsorption experiments, all samples (60 mL each) were mixed with 2.5 g/L of EG in duplicate and removed from the shaker at 1, 5, 10, 15, 20, 25, 30, 45 and 60 minutes and 2, 6, 12, 18 and 24 hours. The initial concentration of the NAs mixture was 50 mg/L (10 mg/L each). Another set of adsorption experiments examining competitive adsorption were performed using mono/multi-compound solutions at pH 8. All those solutions (60 mL each) were mixed with 2.5 g/L of EG in duplicates for 24 hours at room temperature. More specifically, two initial concentrations of NAs were tested (50 and 10 mg/L) in the mono compound experiments. In addition, 5 different mixtures were prepared as follows:

- 1- 5MC: (10 mg/L each)
- 2- 3MC: DA, Trans-4-IsoPCHA and Trans-4-PCHA (10 mg/L each)
- 3- 3MC: DA, Trans-4-IsoPCHA and Trans-4-PCHA (16.67 mg/L each)
- 4- 4MC: Trans-4-IsoPCHA, Trans-4-PCHA, HPA and CHA (10 mg/L each)
- 5- 4MC: Trans-4-IsoPCHA, Trans-4-PCHA, HPA and CHA (12.5 mg/L each)

The Langmuir and Freundlich model isotherms were used to fit the mono-compound adsorption data. The Langmuir model was developed to describe monolayers on homogenous surfaces [17], while the Freundlich model considers the heterogenic nature of adsorbent surfaces and could represent mono and multilayer adsorption [18], linear regression was employed to determine the adsorption parameters for isotherm models according to the following:

$$\text{Langmuir model: } q_e = (q_{max}bC_e)/(1 + bC_e) \quad (1)$$

Where  $q_e$  ( $\text{mg g}^{-1}$ ) and  $C_e$  ( $\text{mg/L}$ ) are the mass of sorbed NA on EG and NAs concentration in solution; respectively, at equilibrium.  $q_{max}$  ( $\text{mg g}^{-1}$ ) is the maximum adsorption capacity at equilibrium and  $b$  ( $\text{L mg}^{-1}$ ) is a constant related to the strength of the adsorption bond.

$$\text{Freundlich model: } q_e = KC_e^{(1/n)} \quad (2)$$

Where  $K$  ( $\text{mg/L}$ ) is an adsorption capacity related constant and  $n$  is an adsorption strength related constant. In addition, the multi-compound Freundlich adsorption isotherm [19] was used to fit the multi-compound adsorption data for the mixture of 5 model compounds as per the following:

$$q_{1(DA)} = k_1C_1(C_1 + a_{12}C_2 + a_{13}C_3 + a_{14}C_4 + a_{15}C_5)^{(1/n_1-1)} \quad (3)$$

$$q_{2(Trans-4-ISOPCHA)} = k_2C_2(a_{21}C_1 + C_2 + a_{23}C_3 + a_{24}C_4 + a_{25}C_5)^{(1/n_2-1)} \quad (4)$$

$$q_{3 (Trans-4-PCHA)} = k_3 C_3 (a_{31} C_1 + a_{32} C_2 + C_3 + a_{34} C_4 + a_{35} C_5)^{(1/n_3-1)} \quad (5)$$

$$q_{4 (HPA)} = k_4 C_4 (a_{41} C_1 + a_{42} C_2 + a_{43} C_3 + C_4 + a_{45} C_5)^{(1/n_4-1)} \quad (6)$$

$$q_{5 (CHA)} = k_5 C_5 (a_{51} C_1 + a_{52} C_2 + a_{53} C_3 + a_{54} C_4 + C_5)^{(1/n_5-1)} \quad (7)$$

Where the  $K_i$  and  $n_i$  values are obtained from the mono-compound Freundlich adsorption isotherms the  $q_i$  and  $C_i$  values are calculated from the multi-compound adsorption isotherms. Each  $a_{ij}$  is the competition coefficient related to the intermolecular interaction within EG. By definition:  $a_{ij} = 1/a_{ji}$  (e.g.,  $a_{31} = 1/a_{13}$ ). The estimation of adsorption parameters (a's and n's in multi-compound Freundlich adsorption isotherm) was performed applying nonlinear least-squares fitting using MATLAB software student version (R2013a) as described in Appendix B.

### 3.3 Results and Discussion

#### 3.3.1 EG characterization.

The SEM images show an extreme alteration in surface morphology of EG due to expansion of GIC (Figure 3-1). GIC occurs as isolated plate-like particles that have a dark grey surface (Figure 3-1a). After expansion, the GIC transforms to significantly larger worm-like particles (EG) having crevice-like pores on the surface (Figures 3-1b and 3-1c). As well, the density of EG (4.8 g/L) decreased to only 0.8% of the initial GIC (630 g/L) [20]. The chemical mapping of the EG surface using the TOF-SIMS indicated that the C-C/C=C groups were the most dominant with total ion counts (TC) of 273 377 (Figure 3-1d), while the detection of the developed oxygen containing groups C-OH and COOH was minimal with TC of 69 and 371, respectively (Figure 3-1e and 3-1f) confirming the observation of Krawczyk [21]. Although the limited oxygen groups imply that the surface is mainly hydrophobic [21], there is still a potential

for electrostatic effects or hydrogen bonding with the surface following the deprotonating of C-OH and COOH groups in aqueous alkaline solutions which is confirmed by the contact angle measurements ( $74.6 \pm 2.5$ ) [9]. The XPS indicated that EG is composed of 96% carbon and 4% oxygen (Figure 3-2). The curve fitting of C1s peak resulted in binding energies ( $E_B$ ) of 284.8, 286.2 and 288.7 which can be attributed to C-C, C-OH and C=O groups, respectively (Figure 3-2) [21, 22]. These most abundant groups are consistent with the TOF-SIMS mapping results indicated previously. The BET surface area of EG is  $76.9 \pm 1.4 \text{ m}^2 \text{ g}^{-1}$  and the pore size distribution shows that 100% of pores are mesopores (pore diameter is  $> 2 \text{ nm}$ ) (Figure 3-3). The pore size of the EG is important to determine the potential for compounds to enter/exit the pores via adsorption/desorption processes. Therefore, by considering the minimum pore diameter to be 2 nm, it is suggested that no removal of NAs due to size on the EG surface may occur, since the maximum kinetic dimension of any NA employed currently is less than 0.8 nm [23]. These large pores should promote faster kinetics for adsorption due to easier molecular diffusion and the accordingly earlier breakthrough [24]. They also have the potential to maximize the possibility of competition between different compounds in aqueous mixture [24].

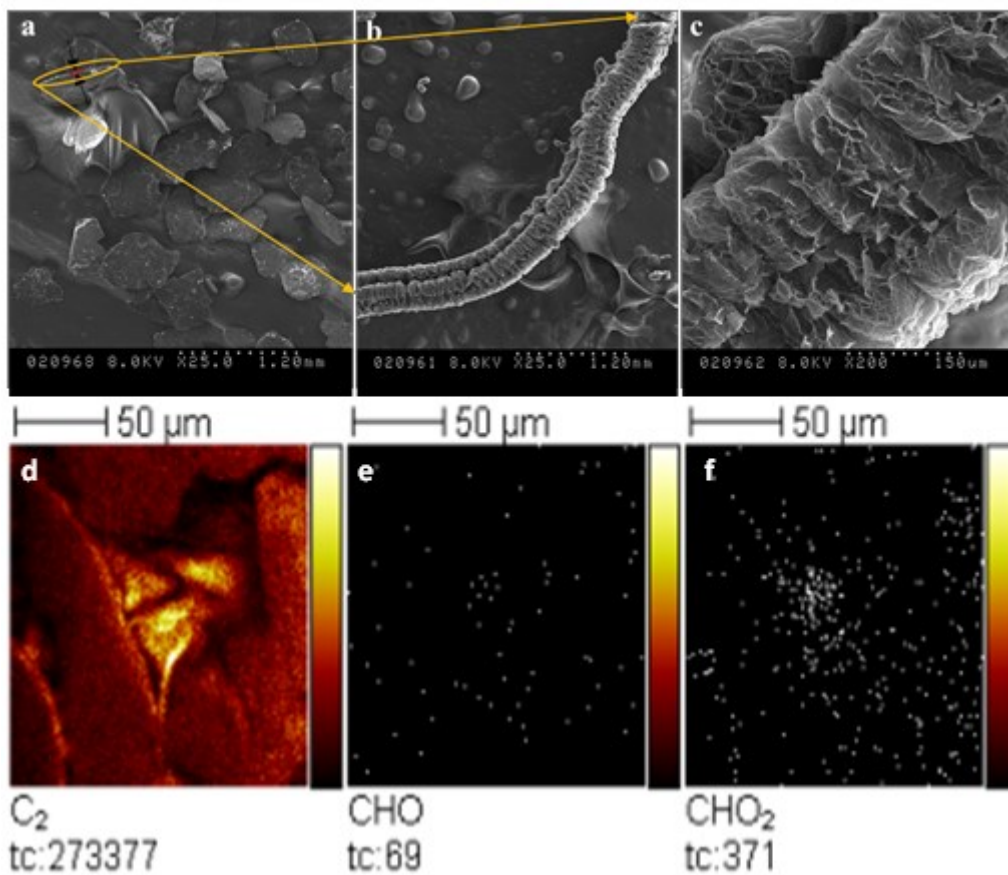


**Figure 3-1.** SEM images for (a) graphite intercalated compounds (GIC), (b) an expanded graphite particle image shows the extreme alteration of GIC thickness due to expansion (yellow arrows) and (c) the surface morphology of expanded graphite. TOF-SIMS mapping of (d) C-C/C=C groups, (e) phenolic functional groups and (f) carboxylic functional groups

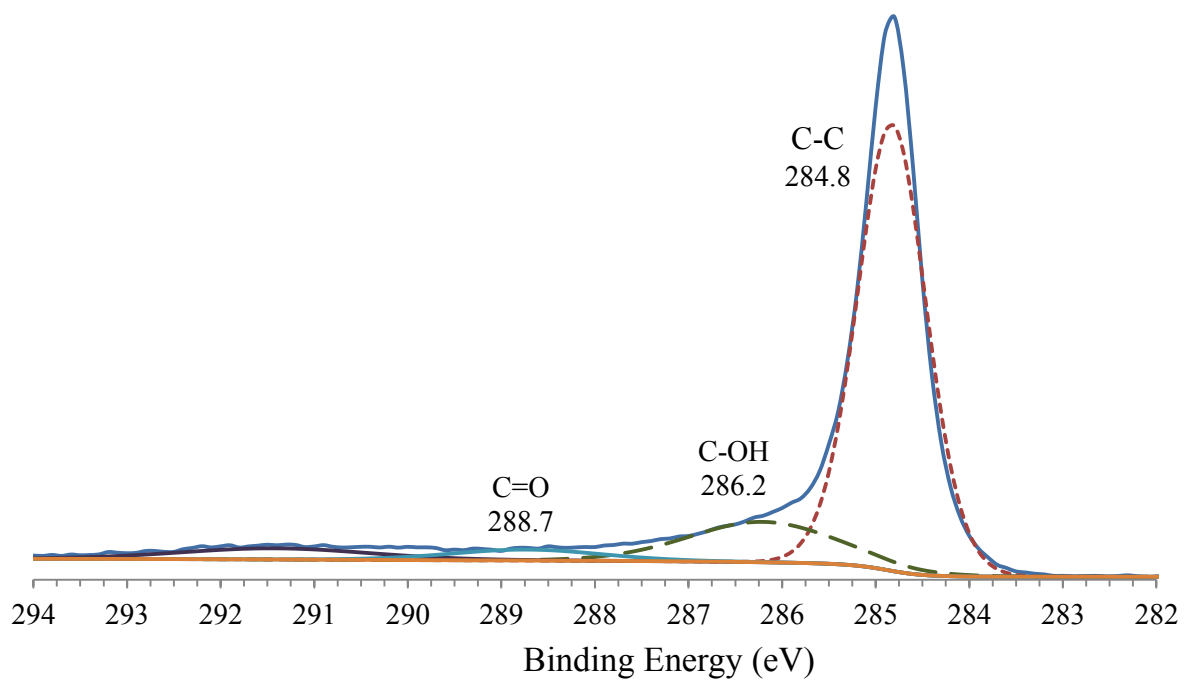


**Figure 3-2.** Deconvolution of C1s peak for EG (XPS results)

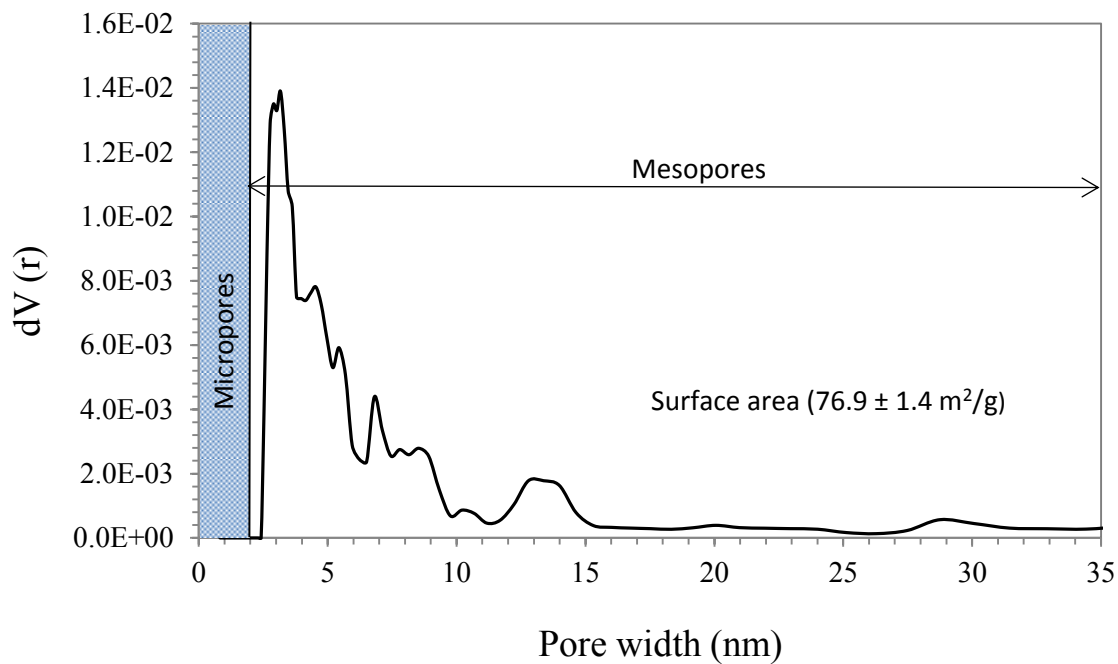


**Figure 3-3.** BET surface area and pore size distribution of EG.

### 3.3.2 Mono-compound adsorption.

The linear regression of the adsorption data indicated that generally the Langmuir and Freundlich isotherm models both fit the adsorption data for three model compounds (DA, Trans-4-IsoPCHA and Trans-4-PCHA;  $R^2 \geq 0.91$ ) (Figure 3-4). The only exception was the Trans-4-IsoPCHA Langmuir isotherm which is considered invalid given the negative  $q_{\max}$  of -24.8 (Figure 3-4c). It should be noted that CHA and HPA did not show any significant adsorption on EG after 24 hours, consequently no isotherms for these compounds were acquired for the mono-compound adsorption study. These results were unexpected given the adsorption of the other model NAs, thus, further discussion regarding this lack of sorption is included in the following sections. The Langmuir model would suggest the need for a homogenous EG surface for adsorption [17], however, the analysis of XPS results and TOF-SIMS mapping indicated a heterogeneous surface with the presence of O=C-OH and C-OH. Given the heterogeneity of the EG surface currently, the mono-compound Freundlich adsorption model is considered a better representation of the adsorption data since it was developed based on a diversity of sites affinity toward adsorbates [18].

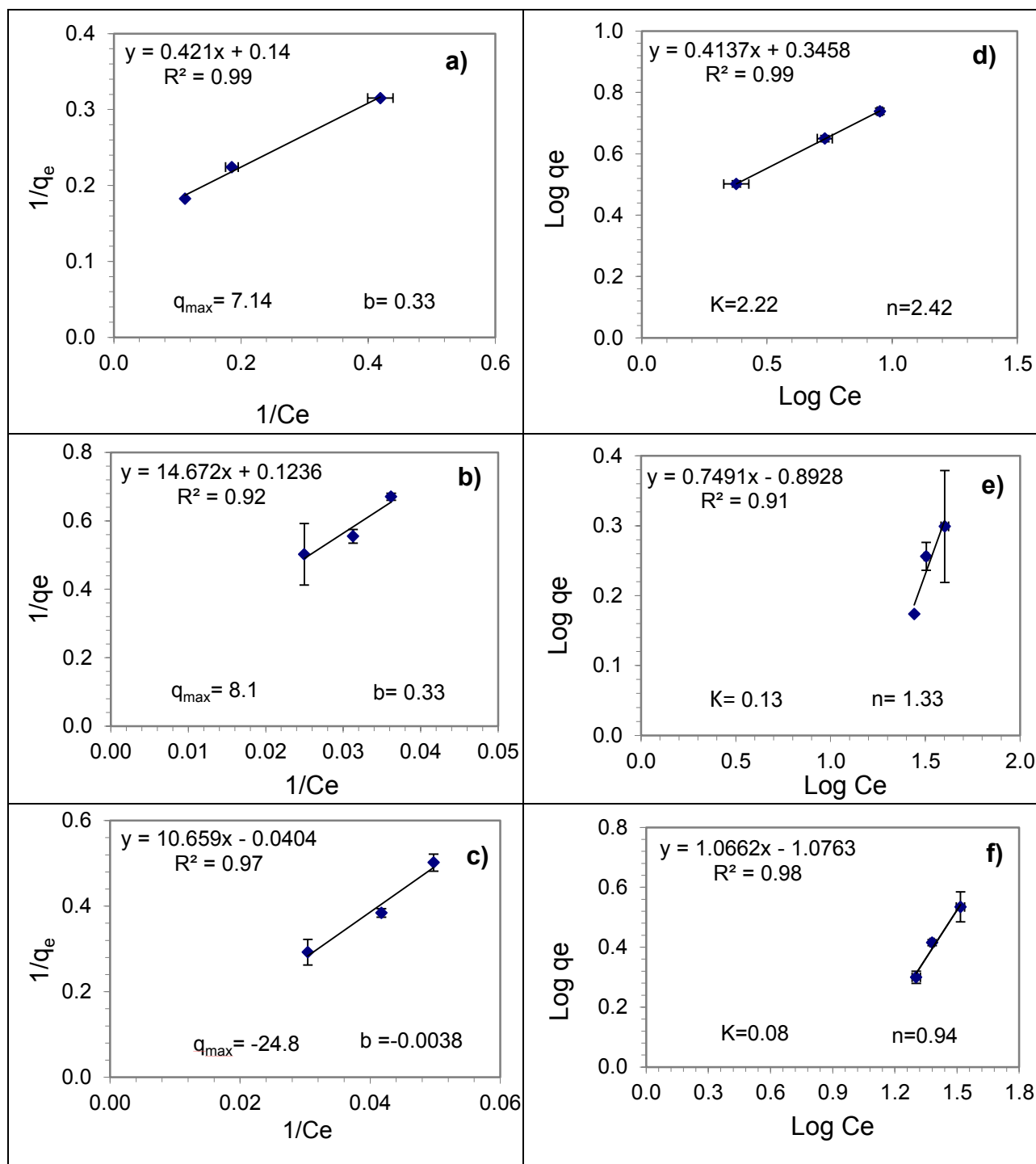
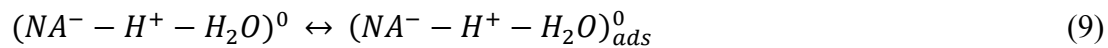


**Figure 3-4.** Mono compound Langmuir adsorption isotherm for (a) decanoic acid, (b) Trans-4-IsoPCHA (c) Trans-4-PCHA and mono compound Freundlich adsorption isotherm for (d) decanoic acid, (e) Trans-4-IsoPCHA (f) Trans-4-PCHA using the HPLC/MS ( $C_0 = 50\text{mg/L}$ ).

The physicochemical properties included in Table 3-1 may be used to further describe the mono-compound adsorption. Speciation diagrams in water for each acid demonstrates that they are more than 99.9% ionized at pH 8 according to the online SPARC software (<http://archemcalc.com/sparc/index>; accessed January, 17, 2014). In anionic form, the log  $K_{ow}$  values for NAs are more than 3 orders of magnitude lower than those of their neutral forms (Table 3-1). The values of log  $K_{ow}$  decrease according to DA > Trans-4-IsoPCHA > Trans-4-PCHA > HPA > CHA, with very low or negative values indicating their extreme affinity to water over the polar/nonpolar environment in octanol. Additionally, the surface charge of EG is negative due to the deprotonation of surface functional groups C-OH and O=C-OH [9, 25, 26], as confirmed by the zeta potential measurement ( $-25.6 \pm 2.3$  mV). This excessive presence of negative charges for both the adsorbate and adsorbent would suggest the reduction or elimination of adsorption due to strong electrostatic repulsion [9]. However, significant adsorption capacities for 3 NAs were still observed with EG adsorption capacities decreasing according to DA<sup>-</sup> (11 200 mg/kg) > Trans-4-PCHA<sup>-</sup> (5 130 mg/kg) > Trans-4-IsoPCHA<sup>-</sup> (2 460 mg/kg) as calculated by the mono-compound Freundlich adsorption isotherm eq. 2. A potential mechanism for this adsorption is the anion exchange or bridging due to the presence of K<sup>1+</sup> (less than 0.25 M) from the phosphate buffer, however, anion exchange has been shown to be inhibited by the ionic strength via charge screening mechanism [11, 27-30]. Moreover, Li et al. [9] observed no impact on adsorption of weak organic acids at pH 7 in solution with ionic strengths up to 0.3 M Ca<sup>2+</sup>. Therefore, it is unlikely that this bridging adsorption was occurring for the current NAs. Thus, the observed adsorption of NAs on the negatively charged EG surfaces is currently hypothesized to occur via the negatively charged assisted hydrogen bond (–CAHB).

The establishment of a –CAHB has been considered a possible mechanism for adsorption of weak acids onto carbon adsorbents [2, 9, 31, 32]. This type of bond occurs between the negatively charged carboxyl groups of NAs and the negatively charged carboxyl or phenolic groups on EG surfaces. As discussed previously, the formation of the –CAHB is accompanied by a rise in the pH [2, 9] determined by:



Previous studies have indicated that the determination of  $OH^{-}$  may be used to stoichiometrically determine the potential –CAHB formation [2, 9]. However, the measurement of moles hydroxide released versus moles of NAs adsorbed currently was not probable due to the use of a 0.1 M phosphate buffer solution limiting the detection of pH changes as mentioned previously. Therefore, the use of thermodynamics calculations, developed herein, is essential to help explain the formation of the –CAHB.

### 3.3.3 Multi-compound adsorption.

The first step in the assessment of multi-compound adsorption data was the application of the mono-compound isotherm models for the overall mixture (i.e.,  $C_0 = 50$  mg/L). The adsorption parameters values obtained from the mono-compound Freundlich and Langmuir models indicated that only the Freundlich isotherm model fit the adsorption data given the negative  $q_{max}$  of the Langmuir isotherm (Figure 3-5). Overall, the EG adsorption capacity was 4 839 mg/kg for the mixture which is less than the average for the three adsorption capacities calculated in the mono-compound experiments (6 263 mg/kg). This lower adsorption capacity

indicates the presence of competition between the mixture compounds which negatively impacted the overall adsorption capacity.

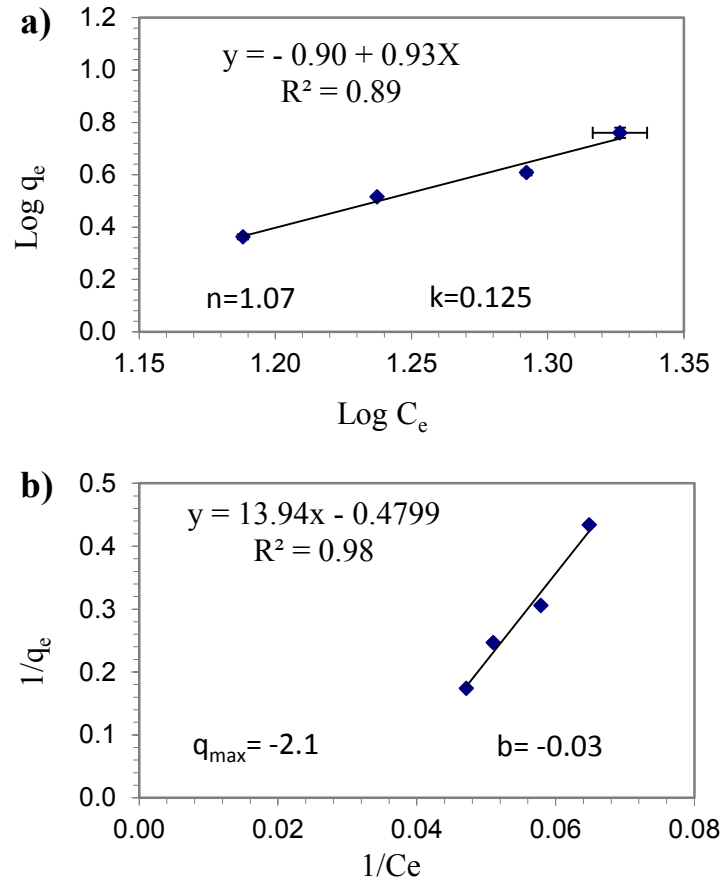


**Figure 3-5.** a) Freundlich and b) Langmuir adsorption isotherms for the mixture of five model compounds ( $C_0 = 50 \text{ mg/L}$ ,  $10 \text{ mg/L}$  each)

In order to understand the competition of NAs for the available adsorption sites, the multi-compound Freundlich adsorption isotherm was implemented to fit the multi-compound adsorption data. Given the negligible removal of HPA and CHA from the mixture after 24 hours, equations 3, 4, 5, 6 and 7 were reduced to the following:

$$q_{1(DA)} = k_1 C_1 (C_1 + a_{12} C_2 + a_{13} C_3)^{(1/n_1-1)} \quad (10)$$

$$q_{2(Trans-4-ISOPCHA)} = k_2 C_2 (a_{21} C_1 + C_2 + a_{23} C_3)^{(1/n_2-1)} \quad (11)$$

$$q_{3(Trans-4-PCHA)} = k_3 C_3 (a_{31} C_1 + a_{32} C_2 + C_3)^{(1/n_3-1)} \quad (12)$$

The individual  $k_i$  values were taken from the mono-compound adsorption results while the experimentally determined  $C_e$  and calculated  $q_e$  for each model compound were taken from the multi-compound adsorption experiments (Table 3-2). These  $k_i$ ,  $C_e$  and  $q_e$  values were used for the estimation of adsorption parameters, namely the  $a_{ij}$ 's and  $n_i$ 's in the multi-compound Freundlich adsorption isotherm eqs. 10, 11 and 12, by applying nonlinear least-squares fitting as outlined in the 'Sorption experiments' section. Table 3-3 reports the six parameters calculated after performing non-linear regression with  $a_{ij}$ 's and  $n_i$ 's and their 95% confidence intervals. For the experimental and calculated results optimization, good correlations were obtained with  $R^2$  values of 0.99, 0.76, and 0.89 for  $q_1$ ,  $q_2$ , and  $q_3$  respectively (Figure 3-6). Given the high  $R^2$  values and small span in confidence intervals it can be stated that the multi-compound model is able to accurately predict the experimental data. As well, the obtained values of the calculated  $n$ 's in Table 3-3 are in good agreement with experimental values shown in Figure 3-4 (d, e and f). When the competition coefficients ( $a_{ij}$ 's) approach zero this signifies the lack of competitive interaction of compound 'j' on compound 'i', while values equal to or greater than 10 indicate extreme competition conditions which compound 'j' outcompetes compound 'i' [19, 33]. Thus, the low values of  $a_{12}$  ( $1 \times 10^{-5}$ ) and  $a_{13}$  ( $8 \times 10^{-3}$ ) indicated that compound 1 (DA) has an extremely high competitive impact on compounds 2 and 3 (Trans-4-IsoPCHA and Trans-4-PCHA), while both have no competitive impact on compound 1 (DA). The value of  $a_{23}$  ( $1.4 \times 10^{16}$ ) indicates an extreme competitive impact of compound 3 (Trans-4-PCHA) on the

adsorption of compound 2 (Trans-4-IsoPCHA) and the negligible impact of the inverse relationship. Based on these competition coefficients, the affinity of NAs to the EG surface is DA > Trans-4-PCHA > Trans-4-IsoPCHA. Further assessment of the multi-compound mixtures using thermodynamics to describe competitive adsorption is found in the following sections.

**Table 3-2.** Experimental  $C_e$  and calculated  $q_e$  values for each model compound from the multi-compound adsorption

<b>DA</b>	<b>Trans-4-IsoPCHA</b>	<b>Trans-4-PCHA</b>	<b>HPA</b>	<b>CHA</b>
<b>C<sub>1</sub></b>	<b>C<sub>2</sub></b>	<b>C<sub>3</sub></b>	<b>C<sub>4</sub></b>	<b>C<sub>5</sub></b>
0.75	7.27	5.29	10	10
0.50	6.75	4.96	10	10
0.35	6.02	4.13	10	10
0.18	5.33	3.44	10	10
<b>q<sub>1</sub></b>	<b>q<sub>2</sub></b>	<b>q<sub>3</sub></b>	<b>q<sub>4</sub></b>	<b>q<sub>5</sub></b>
1.85	0.55	0.94	0	0
1.27	0.43	0.67	0	0
0.97	0.40	0.59	0	0
0.65	0.31	0.44	0	0

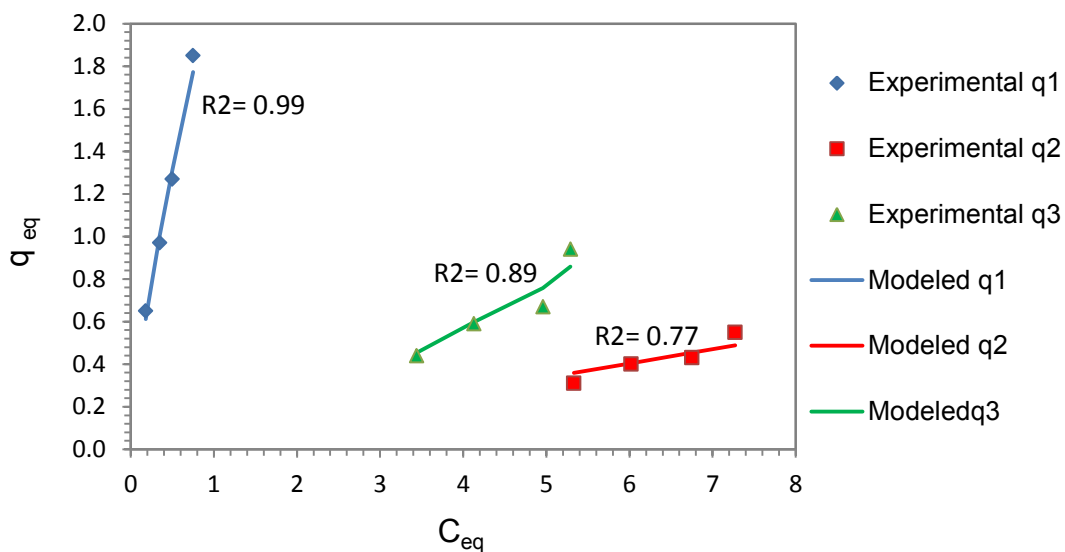


**Figure 3-6.** Experimental vs. modeled profiles for the multi-compound Freundlich adsorption isotherm values of  $q_{eq}$

**Table 3-3.** Competition coefficients and adsorption parameter  $1/n$  calculated from the multi-compound Freundlich isotherm equation along with 95% confidence intervals

Parameter	value	95% Confidence Interval
$a_{12}$	$1 \times 10^{-5}$	$5.9 \times 10^{-6}$
$a_{13}$	$8 \times 10^{-3}$	$1.9 \times 10^{-3}$
$a_{23}$	$1.4 \times 10^{16}$	$5.5 \times 10^{15}$
$1/n_1$	0.73	0.042
$1/n_2$	0.98	0.058
$1/n_3$	1.15	0.045

### 3.3.4 Thermodynamics of mono-compound adsorption.

In the absence of direct measurement of the –CAHB formation, the probability of –CAHB formation can be determined via thermodynamics. The free energy required for –CAHB

formation ( $\Delta G^{-CAHB}$ ) needs to overcome water competition for the adsorption sites ( $\Delta G_{H_2O}^{HB}$ ) and the solvation energy of NA in water ( $\Delta G_{Solv}$ ) according to:

$$\Delta G^{-CAHB} > \Delta G_{Solv} > \Delta G_{H_2O}^{HB} \quad (13)$$

The high concentration of water as a solvent affords an extremely strong competition with NAs to bond with the EG surface [34]. The following reaction describes the expected competition [9]:



The free energy of adsorption ( $\Delta G^{HB}$ ) can be calculated as follows:

$$\Delta G^{HB} = -RT \ln \left[ \frac{(NA^- - H^+ - EG^-)(H_2O)^2}{(NA^- - H^+ - H_2O)(EG - H_2O)} \right] \quad (15)$$

Given the overwhelming contribution of the water (55.5 M) in eqn. 15 and assuming 99.9% dissociation of the 50 mg/L NAs,  $\Delta G^{HB}$  can be reduced and assigned to water according to the following:

$$\Delta G_{H_2O}^{HB} = -RT \ln \left[ \frac{(H_2O)^2}{(NA^- - H^+ - H_2O)} \right] \quad (16)$$

Calculated  $\Delta G_{H_2O}^{HB}$  values are  $-40.1 \text{ kJ mole}^{-1}$  for  $DA^-$ ,  $Trans\text{-}4\text{-IsoPCHA}^-$  and  $Trans\text{-}4\text{-PCHA}^-$  and  $-39.4 \text{ kJ mole}^{-1}$  for  $HPA^-$  and  $CHA^-$ , respectively. This implies that the free energy requirement for  $-CAHB$  formation ( $\Delta G^{-CAHB}$ ) should be higher than the calculated water contribution in order to overcome its bond to the EG surface. In addition,  $\Delta G^{-CAHB}$  must be high enough to compensate for the free energy resulting from the proton exchange of  $NA^-$  with water for solvation ( $\Delta G_{Solv}$ ) described in the following equation:

$$\Delta G_{Solv} = -RT \ln \left[ \frac{K_{a\text{water}}}{K_{aNA}} \right] \quad (17)$$

Hence, using eq. 17 the solvation free energies are  $\Delta G_{\text{Solv}} = -52.8 \text{ kJ mole}^{-1}$  for DA and HPA, and  $-52.4 \text{ kJ mole}^{-1}$  for Trans-4-IsoPCHA, Trans-4-PCHA and CHA, respectively. Although  $\Delta G^{\text{CAHB}}$  is not known for the current compounds, reported values were found to rely on the difference in  $\text{pK}_a$  between the bonded species with  $\Delta G^{\text{CAHB}} = -50.2 \text{ kJ mole}^{-1}$  observed for acetate/phenolic ( $\Delta \text{pK}_a = 5.2$ ) and  $-56.2 \text{ kJ mole}^{-1}$  for carboxyl/carboxyl ( $\Delta \text{pK}_a = 0$ ) [32]. Therefore, it is expected that  $\Delta G^{\text{CAHB}}$  values for the current compounds should be in a similar range due to their similar  $\text{pK}_a$  values (i.e.,  $\text{pK}_a \approx 4.8$  for all compounds) (Table 3-1) [9, 35, 36]. Since no adsorption was observed for HPA and CHA, it can be postulated that  $\Delta G^{\text{CAHB}}$  for these NAs is lower than their  $\Delta G_{\text{Solv}}$  values ( $-52.8$  and  $-52.4 \text{ kJ mole}^{-1}$ , respectively), thus, their  $\Delta G^{\text{CAHB}}$  values are not high enough to overcome their solvation energy in water making an additional free energy contribution vital for the  $-\text{CAHB}$  formation. Li et al. [9] and Teixido et al. [2] suggested that a portion of the increase in the hydrophobicity of NAs due to proton exchange of  $\text{NA}^-$  with water could contribute to the energy gain required for the  $-\text{CAHB}$  formation. To determine this hydrophobicity increase we must first consider  $K_{\text{ow}}$  as an adequate measure for hydrophobicity then the following equation describes the hydrophobic free energy ( $\Delta G_{\text{Hydrophobicity}}$ ):

$$\Delta G_{\text{Hydrophobicity}} = -RT \ln \left[ \frac{K_{\text{ow NA}}}{K_{\text{ow NA}^-}} \right] \quad (18)$$

Therefore, using eq. 19 the  $\Delta G_{\text{Hydrophobicity}} = -18.3, -18.1, -18.1, -20.5$  and  $-23.2 \text{ kJ mole}^{-1}$  for  $\text{DA}^0$ ,  $\text{Trans-4-IsoPCHA}^0$ ,  $\text{Trans-4-PCHA}^0$ ,  $\text{HPA}^0$  and  $\text{CHA}^0$ , respectively. It should be noted that the contributions of the  $\Delta G_{\text{Hydrophobicity}}$  for each  $\text{NA}^0$  toward  $-\text{CAHB}$  formation will not be expected to occur in equal proportions despite their similar  $\Delta G_{\text{Hydrophobicity}}$  values since the contributions are also dependent on the bond length and water affinity (as expressed by  $K_{\text{ow}}$ ) of each NA [37-40]. Assuming the same bond lengths for the current NAs, in conjunction with the

$K_{ow}$  values from Table 3-1, the partial contribution of  $\Delta G_{Hydrophobicity}$  (designated as  $\Delta\Delta G_{Hydrophobicity}$ ) would be expected to be  $DA^0 > Trans\text{-}4\text{-PCHA}^0 > Trans\text{-}4\text{-IsoPCHA}^0 > HPA^0 > CHA^0$  (Table 3-1). The result of this contribution to  $-CAHB$  is a total free energy gain  $\Delta G_{Total} = \Delta\Delta G_{Hydrophobicity} + \Delta G^{-CAHB}$  which can be included in eq. 13 as:

$$\Delta G_{Total} > \Delta G_{Solv} > \Delta G_{H_2O}^{HB} \quad (20)$$

As a result of a combination of these free energies, and given the  $\Delta G^{-CAHB}$  values are similar for the current NAs, the estimated  $\Delta G_{Total}$  values would be  $DA^0 > Trans\text{-}4\text{-PCHA}^0 > Trans\text{-}4\text{-IsoPCHA}^0 > HPA^0 > CHA^0$  based on the thermodynamics of adsorption. Thus, these theoretical results are in pronounced agreement with the adsorption capacities observed in mono-compound solutions and the calculated competitive interactions in the multi-compound solution. Additionally, the insignificant adsorption observed for HPA and CHA in the mono-adsorption experiments could be due to the insignificant contribution of their  $\Delta\Delta G_{Hydrophobicity}$  as a result of their lower  $K_{ow}$  values. Interestingly, given the  $\Delta pK_a = 0$  for any two identical NAs, one may consider the possibility of forming  $-CAHB$  between  $NA-NA$  is more advantageous thermodynamically than that between  $NA^-EG^-$  [9, 35, 36]. However, Vembanur et al. [41] demonstrated that the gain in the solvation barrier for hydrophobic compounds,  $\Delta G_{Hydrophobicity}$ , increases near hydrophobic surfaces, which favors the  $-CAHB$  formation between  $NA^-EG^-$  over  $NA^-NA^-$  in solution. These results imply that for similar  $pK_a$  values, the molecular weight and general structure of NAs has no direct impact on their adsorption from mono/multi-compound solutions, with the adsorption being almost solely dependent on the  $K_{ow}$  of both  $NA$  and  $NA^-$  species.

### 3.3.5 Competitive adsorption.

In order to evaluate the competitive interactions of NAs and to further investigate the impact of the molecular properties of NAs on adsorption, the adsorption of a 5MC mixture was monitored for 24 hours (Figure 3-7). The assessment of adsorption performance of each NA over time reveals the kinetics of the competitive adsorption process until equilibrium. For discussion, the adsorption may be considered in two distinct intervals with interval (1) up to 6 hours and interval (2) from 6 to 24 hours.

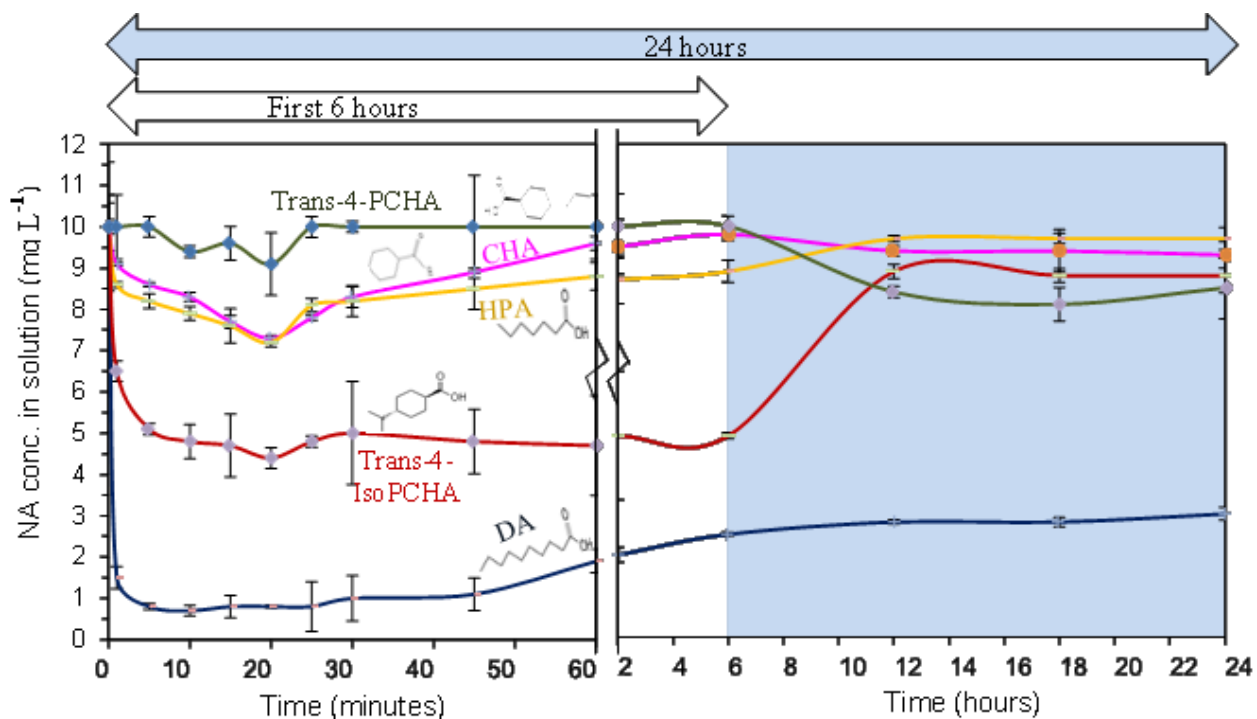


**Figure 3-7.** The NAs concentration (total  $C_0 = 50$  mg/L; 10 mg/L for each NA) during mixing for 24 hours with 2.5 g (EG) /L

For interval 1, at the onset of the experiment (up to 10 minutes), exceptionally high adsorption kinetics and removal were observed for DA and Trans-4-IsoPCHA (93% and 52%

adsorbed, respectively). Generally, fast kinetics for all NAs would be predicted due to the large sizes of the EG pores which assist the molecular diffusion [24]. The fast adsorption of DA was anticipated due to the maximum gain in free energy ( $\Delta G_{\text{Total}}$ ) and the lack of competition from other compounds ( $a_{12}$  and  $a_{13}$ ; Table 3-3) as identified previously. Of interest is the negligible removal of Trans-4-PCHA compared to 52% removal of Trans-4-IsoPCHA which was not expected given the higher  $\Delta G_{\text{Total}}$  for Trans-4-PCHA. However, the Trans-4-IsoPCHA has two  $\text{CH}_3$  groups at its hydrophobic end as compared to only one  $\text{CH}_3$  groups for Trans-4-PCHA which increases the possibility for Trans-4-IsoPCHA to bond with the hydrophobic end of the self-assembled layer (SAL) of DA already adsorbed via  $-\text{CAHB}$  with EG. Vembanur et al. [41] indicated that this bond is formed due to a significant decrease in the density of water molecules around the  $\text{CH}_3$  end of the SAL. As a result, fast contact between the hydrophobic ends ( $\text{CH}_3$ ) of the SAL and the compounds in the aqueous solution is developed due to the decrease in desolvation hindrance. It is also noted in interval 1 that more than 25% for both HPA and CHA were removed within 20 minutes before re-dissolving (in conjunction with 18% of DA) which suggests that the HPA and CHA species might be involved in hydrophobic bonds with DA's SAL which become broken upon DA desorption.

In interval 2, equilibrium is approached after 12 hours of mixing. The predictable competition exerted by the Trans-4-PCHA (as indicated by  $a_{23}$ ; Table 3-3) and desorption of a further 5% of DA are postulated to cause the drop in the adsorbed Trans-4-IsoPCHA from 50% to 12%. Assuming the same molarity for those 3 compounds, it is noted that the total amount of Trans-4-PCHA adsorbed (15%) plus the amount of re-solvated DA (5%) is 20%, which is not equivalent to the total desorption of Trans-4-IsoPCHA (50% - 12% = 38%). Accordingly, we suggest the remaining 18% of Trans-4-IsoPCHA may have not been replaced by Trans-4-

PCHA[16] since the Trans-4-IsoPCHA molecules were possibly forming multilayers adsorbed on SAL of DA, while Trans-4-PCHA is forming only a single layer hydrophobically bonded to the SAL. Thus, the single layer of Trans-4-PCHA would limit the adsorption capacity of EG as compared to the multilayer of Trans-4-IsoPCHA. After 24 hours, the adsorption of DA (70%) is > Trans-4-PCHA (15%) > Trans-4-IsoPCHA (12%) which is in agreement with both mono/multi-compound adsorptions results and in concordance with the thermodynamic expectations.

For further understanding, several mono/multi-compound solutions were examined at equilibrium conditions (24 h) as indicated in Figure 3-8 and summarized in Table 3-4. Generally, it should be noted that the application of higher  $C_0$  showed higher adsorption capacity (Figure 3-8).[42] The adsorption capacity of EG for NA in the mono-compound solutions ( $C_0 = 50$  mg/L and 10 mg/L) followed the same trend observed previously of DA > Trans-4-PCHA > Trans-4-IsoPCHA with negligible adsorption for HPA and CHA (Figure 3-8a). Increasing the initial concentration for each NA to  $C_0 = 50$  mg/L resulted in the increase of the adsorption of DA, Trans-4-PCHA and Trans-4-IsoPCHA by 468%, 417% and 342% respectively. Overall, the adsorption value increases were directly proportional to the gain in free energy discussed previously ( $\Delta G_{\text{Total}}$ ). Accordingly, the gain in adsorption capacity at higher  $C_0$  for the compounds with similar  $pK_a$  values compounds is only impacted by  $K_{ow}$  of NA and  $NA^{-1}$ . These results might also imply that the mono-compound adsorption could form a multilayer adsorption especially at high initial concentrations of NA assuming that the carboxyl and phenolic sites on the graphite surface are already occupied via  $-CAHB$ .

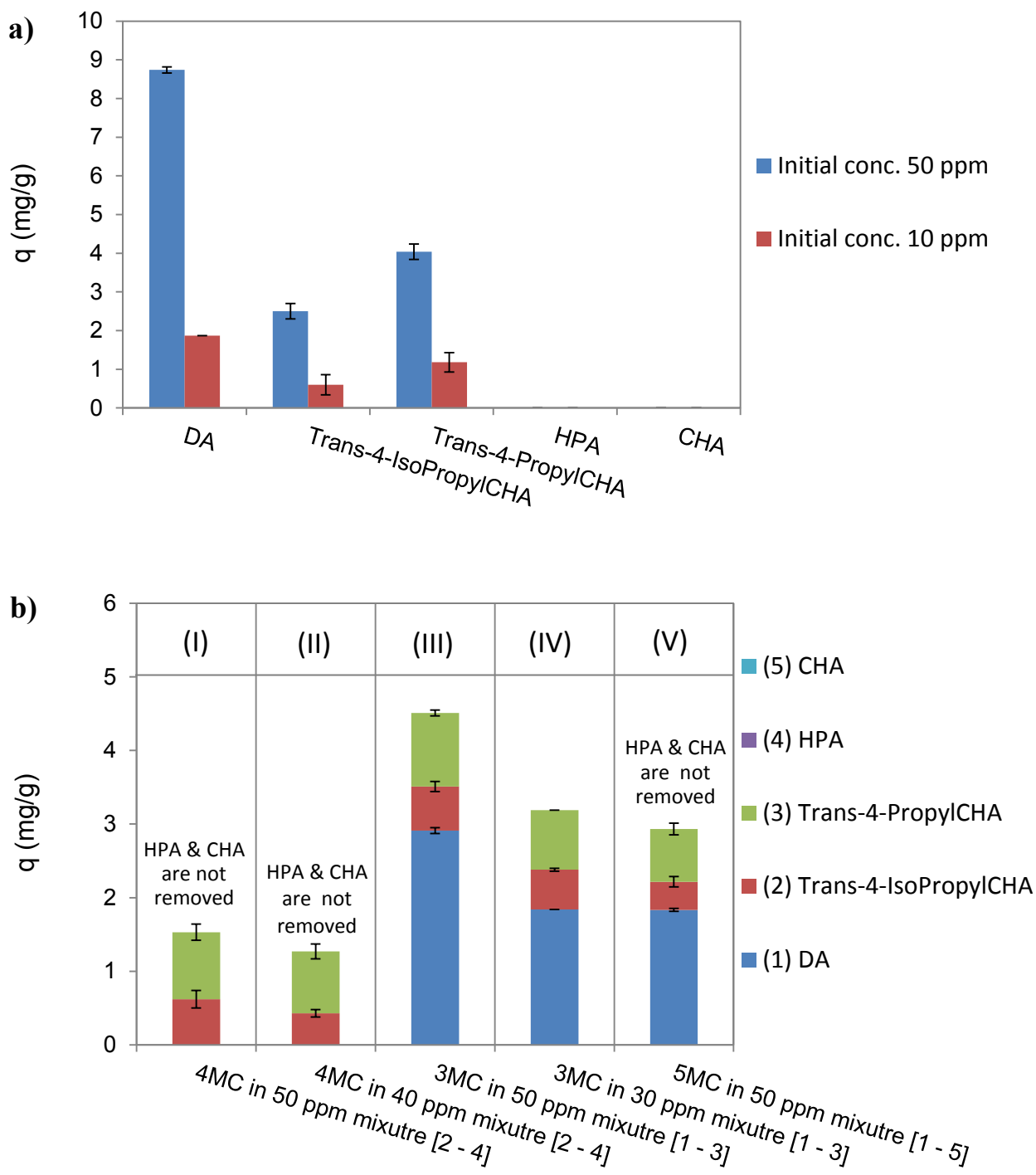


**Figure 3-8.** (a) Mono-compound and (b) multi-compound adsorption of model naphthenic acids after mixing with 2.5 g (EG) /L for 24 hours. MC = model compound

**Table 3-4.** Summary of the adsorption capacities for the mono-compound and multi-compound experiments shown in Figure 3-8

Model NA compounds	DA	Trans-4-IsoPCHA	Trans-4-PCHA	HPA	CHA
1MC (50 ppm)	8.74 ± 0.10				
1MC (10 ppm)	1.87 ± 0.01				
1MC (50 ppm)		2.5 ± 0.20			
1MC (10 ppm)		0.6 ± 0.26			
1MC (50 ppm)			4.04 ± 0.18		
1MC (10 ppm)			1.18 ± 0.21		
1MC (50 ppm)				*	
1MC (10 ppm)				*	
1MC (50 ppm)					*
1MC (10 ppm)					*
3MC (30 ppm)	1.84 ± 0.00	0.54 ± 0.02	0.81 ± 0.00		
3MC (50 ppm)	2.91 ± 0.04	0.60 ± 0.07	1.00 ± 0.04		
4MC (40 ppm)		0.43 ± 0.50	0.84 ± 0.10	*	*
4MC (50 ppm)		0.62 ± 0.12	0.91 ± 0.11	*	*
5MC (50 ppm)	1.83 ± 0.02	0.38 ± 0.07	0.72 ± 0.08	*	*

\* Below detection limit

Various combinations of model NAs mixtures each indicated a similar adsorption pattern as found previously (DA > Trans-4-PCHA > Trans-4-IsoPCHA; CHA/HPA negligible removal after 24 hours) (Figure 3-8b). The 10 mg/L DA adsorption in the C<sub>0</sub> = 50 mg/L (5MC) and 30 mg/L (3MC) mixtures resulted in similar adsorption capacities as in mono-compound solutions with 1 830 mg/kg for 5MC and 1 840 mg/kg for 3MC (Figure 3-8b; IV and V) versus 1 870 mg/kg for mono-compound adsorption (Figure 3-8a). This consistent adsorption is due to the extremely high competition of DA over the other model NAs currently considered (Table 3-3). Additionally, the adsorption capacities of Trans-4-PCHA (5MC: 720 mg/kg; 3MC: 810 mg/kg) and Trans-4-IsoPCHA (5MC: 380 mg/kg; 3MC: 540 mg/kg) were reduced as compared to their mono-compound adsorption capacities of 1 180 mg/kg and 600 mg/kg, respectively (Figure 3-8b; IV and V). The reduction in adsorption for these two compounds in each mixture is primarily due to competition with DA. In contrast, the potential adsorption of these two compounds may

have also been increased due to the potential for hydrophobic bonding with the SAL of DA. Increasing the  $C_0$  of each individual NA (16.7 mg/L /NA) in the mixture 3MC resulted in increased adsorption for each NAs as compared to 10 mg/L /NA (Figure 3-8b III) as reported previously [42]. Experiments excluding the most highly adsorbent DA from the mixture indicated no change in the pattern of adsorption observed for the remaining compounds (adsorption of Trans-4-PCHA > Trans-4-IsoPCHA) which is directly proportional to  $\Delta G_{\text{Total}}$  and to the  $K_{\text{ow}}$  of both species NA and  $\text{NA}^-$  (Figure 3-8b I and II). However, it is suggested that in the absence of DA the Trans-4-PCHA can engage in –CAHB with the EG surface forming a SAL, similar to the adsorption of DA with the EG surface. Given the potential for the formation of a Trans-4-PCHA SAL it would allow Trans-4-IsoPCHA to have a hydrophobic-hydrophobic interaction with the  $\text{CH}_3$  end of Trans-4-PCHA SAL, which would increase adsorption. Overall, the various combinations of compounds competition discussed highlight the possibility of multilayer formation and confirmed the role of  $K_{\text{ow}}$  of NAs on adsorption. As well, the possibility for the synergistic effects of interaction with SAL on the graphite requires further research to fully understand the mechanisms involved in the adsorption.

### **3.4 Environmental significance.**

The recognition of the impact of –CAHB on the adsorption of weak acids on negatively charged carbonaceous surfaces has recently received attention [2, 9, 10]. The current study contributes to the further understanding of the impact of  $\text{pK}_a$ ,  $K_{\text{ow}}$ , molecular structure and competition of weak acids on their adsorption on charged carboxyl/phenolic groups found on carbon surfaces. Additionally, it leads to the elucidation of possible methods of single and multilayer formation of ionized solutes on adsorbent surfaces via –CAHB and hydrophobic bonding. Current results indicate that hydrophobicity of weak ionized acids, as considered by

$K_{ow}$ , is proportional to their adsorption (i.e., increased adsorption with higher  $K_{ow}$ ) and plays a crucial role in the establishment of –CAHB. Although the molecular weight did not show a direct impact on adsorption reported herein, it may indirectly impact the  $K_{ow}$ . Interestingly, the structure reactivity could influence the adsorption of some acids temporarily before equilibrium is reached as observed for Trans-4-IsoPCHA in this study. The current adsorption mechanisms determination will assist in the understanding of the fate and bioavailability of emerging and classical weak ionized acids released into natural water streams. This is in addition to the contribution in the potential optimization of treatment technologies for these compounds using various adsorbents.

### 3.5 References.

- [1] Pan B, Lin D, Mashayekhi H, Xing B. Adsorption and hysteresis of bisphenol A and 17 alpha-ethinyl estradiol on carbon nanomaterials. *Environmental Science & Technology* 2008;42:5480-5485.
- [2] Teixido M, Pignatello JJ, Beltran JL, Granados M, Peccia J. Speciation of the Ionizable Antibiotic Sulfamethazine on Black Carbon (Biochar). *Environmental Science & Technology* 2011;45:10020-10027.
- [3] Cao X, Ma L, Gao B, Harris W. Dairy-Manure Derived Biochar Effectively Sorbs Lead and Atrazine. *Environmental Science & Technology* 2009;43:3285-3291.
- [4] Allen EW. Process water treatment in Canada's oil sands industry: I. Target pollutants and treatment objectives. *Journal of Environmental Engineering and Science* 2008;7:123-138.
- [5] Cornelissen G, Gustafsson O, Bucheli TD, Jonker MTO, Koelmans AA, Van Noort PCM. Extensive sorption of organic compounds to black carbon, coal, and kerogen in sediments and soils: Mechanisms and consequences for distribution, bioaccumulation, and biodegradation. *Environmental Science & Technology* 2005;39:6881-6895.
- [6] Allen-King RM, Grathwohl P, Ball WP. New modeling paradigms for the sorption of hydrophobic organic chemicals to heterogeneous carbonaceous matter in soils, sediments, and rocks. *Advances in Water Resources* 2002;25:985-1016.
- [7] Muller G, Radke CJ, Prausnitz JM. Adsorption of weak organic electrolytes from aqueous-solution on activated carbon - effect of pH. *Journal of Physical Chemistry* 1980;84:369-376.
- [8] Yang K, Wu W, Jing Q, Zhu L. Aqueous Adsorption of Aniline, Phenol, and their Substitutes by Multi-Walled Carbon Nanotubes. *Environmental Science & Technology* 2008;42:7931-7936.
- [9] Li X, Pignatello JJ, Wang Y, Xing B. New Insight into Adsorption Mechanism of Ionizable Compounds on Carbon Nanotubes. *Environmental Science & Technology* 2013;47:8334-8341.
- [10] Ni J, Pignatello JJ, Xing B. Adsorption of Aromatic Carboxylate Ions to Charcoal Black Carbon is Accompanied by Proton Exchange with Water (vol 45, pg 9240, 2012). *Environmental Science & Technology* 2012;46:5633-5633.
- [11] Hyun S, Lee LS. Hydrophilic and hydrophobic sorption of organic acids by variable-charge soils: Effect of chemical acidity and acidic functional group. *Environmental Science & Technology* 2004;38:5413-5419.
- [12] Fontecha-Camara MA, Lopez-Ramon MV, Alvarez-Merino MA, Moreno-Castilla C. Effect of surface chemistry, solution pH, and ionic strength on the removal of herbicides diuron and amitrole from water by an activated carbon fiber. *Langmuir* 2007;23:1242-1247.
- [13] Vinu A, Hossain KZ, Kumar GS, Ariga K. Adsorption of L-histidine over mesoporous carbon molecular sieves. *Carbon* 2006;44:530-536.
- [14] Scott AC, MacKinnon MD, Fedorak PM. Naphthenic acids in athabasca oil sands tailings waters are less biodegradable than commercial naphthenic acids. *Environmental Science & Technology* 2005;39:8388-8394.
- [15] Clemente JS, Fedorak PM. A review of the occurrence, analyses, toxicity, and biodegradation of naphthenic acids. *Chemosphere* 2005;60:585-600.
- [16] Wang H, Lashaki MJ, Fayaz M, Hashisho Z, Philips JH, Anderson JE, et al. Adsorption and Desorption of Mixtures of Organic Vapors on Beaded Activated Carbon. *Environmental Science & Technology* 2012;46:8341-8350.
- [17] Langmuir I. The adsorption of gases on plane surfaces of glass, mica and platinum. *Journal of the American Chemical Society* 1918;40:1361-1403.
- [18] Halsey G, Taylor HS. The adsorption of hydrogen on tungsten powders. *Journal of Chemical Physics* 1947;15:624-630.

- [19] Sheindorf C, Rebhun M, Sheintuch M. Organic pollutants adsorption from multicomponent systems modeled by freundlich type isotherm. *Water Research* 1982;16:357-362.
- [20] Chen GH, Wu DJ, Weng WG, Yan WL. Dispersion of graphite nanosheets in a polymer matrix and the conducting property of the nanocomposites. *Polymer Engineering and Science* 2001;41:2148-2154.
- [21] Krawczyk P. Effect of ozone treatment on properties of expanded graphite. *Chemical Engineering Journal* 2011;172:1096-1102.
- [22] He H, Gao C. General Approach to Individually Dispersed, Highly Soluble, and Conductive Graphene Nanosheets Functionalized by Nitrene Chemistry. *Chemistry of Materials* 2010;22:5054-5064.
- [23] Lashaki MJ, Fayaz M, Niknaddaf S, Hashisho Z. Effect of the adsorbate kinetic diameter on the accuracy of the Dubinin-Radushkevich equation for modeling adsorption of organic vapors on activated carbon. *Journal of Hazardous Materials* 2012;241:154-163.
- [24] Pelekani C, Snoeyink VL. Competitive adsorption in natural water: Role of activated carbon pore size. *Water Research* 1999;33:1209-1219.
- [25] Behera SK, Oh S-Y, Park H-S. Sorption of triclosan onto activated carbon, kaolinite and montmorillonite: Effects of pH, ionic strength, and humic acid. *Journal of Hazardous Materials* 2010;179:684-691.
- [26] Kumar PS, Vincent C, Kirthika K, Kumar KS. Kinetics and equilibrium studies of pb<sup>2+</sup> ion removal from aqueous solutions by use of nano-silversol-coated activated carbon. *Brazilian Journal of Chemical Engineering* 2010;27:339-346.
- [27] Dubus IG, Barriuso E, Calvet R. Sorption of weak organic acids in soils: clofencet, 2,4-D and salicylic acid. *Chemosphere* 2001;45:767-774.
- [28] Aquino AJA, Tunega D, Habephauer G, Gerzabek MH, Lischka H. Interaction of the 2,4-dichlorophenoxyacetic acid herbicide with soil organic matter moieties: a theoretical study. *European Journal of Soil Science* 2007;58:889-899.
- [29] Aristilde L, Sposito G. Binding of ciprofloxacin by humic substances: a molecular dynamics study. *Environmental Toxicology and Chemistry* 2010;29:90-98.
- [30] Iskrenova-Tchoukova E, Kalinichev AG, Kirkpatrick RJ. Metal Cation Complexation with Natural Organic Matter in Aqueous Solutions: Molecular Dynamics Simulations and Potentials of Mean Force. *Langmuir* 2010;26:15909-15919.
- [31] Moreno-Castilla C. Adsorption of organic molecules from aqueous solutions on carbon materials. *Carbon* 2004;42:83-94.
- [32] Ni H-G, Zeng H, Zeng EY. Sampling and analytical framework for routine environmental monitoring of organic pollutants. *Trac-Trends in Analytical Chemistry* 2011;30:1549-1559.
- [33] Wu CH, Kuo CY, Lin CF, Lo SL. Modeling competitive adsorption of molybdate, sulfate, selenate, and selenite using a Freundlich-type multi-component isotherm. *Chemosphere* 2002;47:283-292.
- [34] Maity N, Payne GF. Adsorption from aqueous-solutions based on a combination of hydrogen-bonding and hydrophobic interactions. *Langmuir* 1991;7:1247-1254.
- [35] Gilli G, Gilli P. Towards an unified hydrogen-bond theory. *Journal of Molecular Structure* 2000;552:1-15.
- [36] Gilli P, Pretto L, Bertolasi V, Gilli G. Predicting Hydrogen-Bond Strengths from Acid-Base Molecular Properties. The pK(a) Slide Rule: Toward the Solution of a Long-Lasting Problem. *Accounts of Chemical Research* 2009;42:33-44.
- [37] Lum K, Chandler D, Weeks JD. Hydrophobicity at small and large length scales. *Journal of Physical Chemistry B* 1999;103:4570-4577.
- [38] Berne BJ, Weeks JD, Zhou R. Dewetting and Hydrophobic Interaction in Physical and Biological Systems. *Annual Review of Physical Chemistry* 2009;60:85-103.
- [39] Hua L, Zangi R, Berne BJ. Hydrophobic Interactions and Dewetting between Plates with Hydrophobic and Hydrophilic Domains. *Journal of Physical Chemistry C* 2009;113:5244-5253.

- [40] Mittal J, Hummer G. Interfacial thermodynamics of confined water near molecularly rough surfaces. *Faraday Discussions* 2010;146:341-352.
- [41] Vembanur S, Patel AJ, Sarupria S, Garde S. On the Thermodynamics and Kinetics of Hydrophobic Interactions at Interfaces. *Journal of Physical Chemistry B* 2013;117:10261-10270.
- [42] Knappe DRU, Matsui Y, Snoeyink VL, Roche P, Prados MJ, Bourbigot MM. Predicting the capacity of powdered activated carbon for trace organic compounds in natural waters. *Environmental Science & Technology* 1998;32:1694-1698.



RightsLink®



ACS Publications  
Most Trusted. Most Cited. Most Read.

Title: Probing the Adsorption of Weak Acids on Graphite Using Amplitude Modulation–Frequency Modulation Atomic Force Microscopy  
Author: Ahmed M. A. Moustafa, Jun Huang, Kerry N. McPhedran, et al  
Publication: Langmuir  
Publisher: American Chemical Society  
Date: Mar 1, 2015  
Copyright © 2015, American Chemical Society

Logged in as:

Ahmed Moustafa

LOGOUT

#### PERMISSION/LICENSE IS GRANTED FOR YOUR ORDER AT NO CHARGE

This type of permission/license, instead of the standard Terms & Conditions, is sent to you because no fee is being charged for your order. Please note the following:

- Permission is granted for your request in both print and electronic formats, and translations.
- If figures and/or tables were requested, they may be adapted or used in part.
- Please print this page for your records and send a copy of it to your publisher/graduate school.
- Appropriate credit for the requested material should be given as follows: "Reprinted (adapted) with permission from (COMPLETE REFERENCE CITATION). Copyright (YEAR) American Chemical Society." Insert appropriate information in place of the capitalized words.
- One-time permission is granted only for the use specified in your request. No additional uses are granted (such as derivative works or other editions). For any other uses, please submit a new request.

Copyright © 2015 [Copyright Clearance Center, Inc.](#) All Rights Reserved. [Privacy statement.](#)  
[Terms and Conditions.](#)

Comments? We would like to hear from you. E-mail us at [customer care@copyright.com](mailto:customer care@copyright.com)

## 4 PROBING ADSORPTION OF WEAK ACIDS ON GRAPHITE USING AMPLITUDE MODULATION-FREQUENCY MODULATION ATOMIC FORCE MICROSCOPY<sup>1</sup>

### 4.1 Introduction

Carbonaceous materials, such as graphite-type nanomaterials, have widespread applications for research and industrial purposes including electronic applications [1], biocides [2], and adsorbent surfaces [3]. Recently, the adsorption of environmentally relevant weak ionized acids to carbon surfaces has been attributed to the formation of a negatively charged hydrogen bond (–CAHB) [4, 5]. Following these studies, we evaluated the adsorption to graphite, and competitive interactions, of mixtures of five weakly ionizable naphthenic acids (NAs) with similar  $pK_a$  values which resulted in comparable free energies for –CAHB formation [6]. In this previous study, decanoic acid (DA) had the highest total free energy of the NAs which allowed it to form a self-assembled layer (SAL), via –CAHB, with the negatively charged functional groups on the graphite surface. This SAL formed the base for the establishment of multilayer adsorption of the remaining DA and other mixture NAs. In this previous work, only thermodynamics calculations (revealing the free energy required for bond formations) and adsorption isotherms were conducted; however, direct visualization and characterization of such adsorption behaviour has not been reported previously.

---

<sup>1</sup>A version of this chapter has been published previously: Ahmed M.A. Moustafa, Jun Huang, Kerry N. McPhedran, Hongbo Zeng, and Mohamed Gamal El-Din, Probing Adsorption of Weak Acids on Graphite Using Amplitude Modulation-Frequency Modulation Atomic Force Microscopy. *Langmuir*, 2015. 31 (10), 3069–3075.

Amplitude Modulation - Frequency Modulation Atomic Force Microscopy (AM-FM-AFM) is a technique developed based on multi-frequency and bimodal AFM. The AM-FM viscoelastic mapping mode is a flexible, convenient tool for nano-mechanical characterization of various materials [7, 8]. Basically, the AM-FM mode operates using two cantilever resonances simultaneously. A lower resonance frequency is used to monitor topography changes with a constant amplitude loop feedback (AM). While a higher resonance mode is used to measure frequency shifts and phase changes to provide information about the sample mechanical properties (FM). The amplitude of the excitation signal for FM resonance is typically much smaller than that of the excitation signal for AM resonance, thus it will not impact the standard tapping mode. Overall, this AM-FM signal can be used to quickly identify sample components with different mechanical properties.

Here, AM-FM-AFM was applied to help visualize the adsorption behaviour of decanoic acid on sheets of highly-ordered pyrolytic graphite (HOPG). Firstly, the adsorption potential of DA ( $C_9H_{19}COOH$ ) on graphite was assessed based on thermodynamics. Secondly, AM-FM-AFM was used to image the freshly peeled and functionalized HOPG surfaces before and after DA adsorption. As well, AM-FM-AFM was used to assess the change in surface mechanical properties for the determination of occupied adsorption regions.

## **4.2 Materials and Methods**

### **4.2.1 Chemicals and reagents.**

The HOPG material, mosaic spread 0.4–0.7 degree size ( $10 \times 10 \times 1.5 \text{ mm}^3$ ) was bought from NT-MDT Co. (Russia). Decanoic acid (DA) was purchased from Sigma Aldrich (Malaysia). Methanol, ethanol, and toluene were purchased from Fisher Scientific (Edmonton,

AB, Canada). Ultrapure water was obtained from a Millipore system (France). A 10 mg/L DA solution at pH 5.4 was prepared in MilliQ water (critical micelle concentration > 1,700 mg/L) [9] and used for all experiments.

#### **4.2.2 HOPG functionalization and characterization.**

Water-plasma treatment was employed for functionalizing the surface of HOPG (“F-HOPG”) with oxygenated functional groups. Fresh peeled HOPG surfaces (“HOPG”) were placed in a plasma cleaning chamber (Harrick Plasma, USA) filled with water vapor bubbled in by nitrogen gas (99.99% purity). The chamber pressure was fixed at 170 Pa and the process lasted for 10 min. Duplicate X-ray photoelectron spectroscopy (XPS) analyses (AXIS 165 spectrometer, Japan) were used to characterize the elemental composition and surface functional groups (FGs) of the HOPG and F-HOPG away from the graphene steps as detailed in Appendix C. HOPG and F-HOPG imaging acquisition was conducted by Time of Flight Secondary Ion Mass Spectroscopy (TOF-SIMS; GmbH, Germany).

#### **4.2.3 Adsorption and AM-FM-AFM.**

HOPG and F-HOPG samples were immersed into 60 mL of 10 mg/L DA solutions, respectively. After 24 h the samples were removed, air dried, and glued onto glass slides for imaging with an AFM in AM-FM mode (Asylum MFP-3D, USA). The adsorbed HOPG and F-HOPG surfaces were washed with deionized water (100 mL). The AFM cantilever used was an Olympus AC240TS ( $k=2\text{N/m}$ ) with the normal tapping frequency of 70 kHz, and a high resonance frequency at around 1.2M Hz for frequency modulation. All images were acquired with the same tip and the frequency and height images were adjusted to the same range and offset for direct comparisons.

### 4.3 Results and Discussion

#### 4.3.1 HOPG and F-HOPG characterization.

TOF-SIMS mapping of HOPG/F-HOPG surfaces was performed on a large area ( $120 \times 120 \mu\text{m}^2$ ) to insure the inclusion of a large number of graphene steps (Figure 4-1). For both surfaces,  $\text{C}_2$  groups (C-C/C=C) were dominant with total ion counts (TC) of 283,426 for HOPG being reduced to 218 836 after functionalization with water-plasma treatment to F-HOPG (Figure 4-1a,b) which can be attributed to the increase of oxygenated groups, COH and COOH [1, 10]. Specifically, F-HOPG TCs increased from 249 to 1 461 and 10 861 to 46 825 for COH and COOH groups, respectively (Figure 4-1a,b). XPS results confirmed the TOF-SIMS mapping indicating that HOPG received a significant increase in oxygenated groups after functionalization (Figure 4-1c,d). The deconvolution of the HOPG C1s peak resulted in peaks with binding energies ( $E_B$ ) of 284.2 and 284.6 attributed to C=C and C-C groups, respectively (Figure 4-1c) [2, 3]. The minimal presence of oxygen groups away from the HOPG steps resulted in no oxygenated groups detected in these regions. The F-HOPG C1s peak showed peaks at  $E_B$  values of 284.2, 284.4 and 286.3 resulting from C=C, C-C and C-O groups, respectively (Figure 4-1d). Thus, both techniques confirmed the development of carboxyl and phenolic groups after functionalization. These additional FGs may actively increase the F-HOPG adsorption potential versus the HOPG.

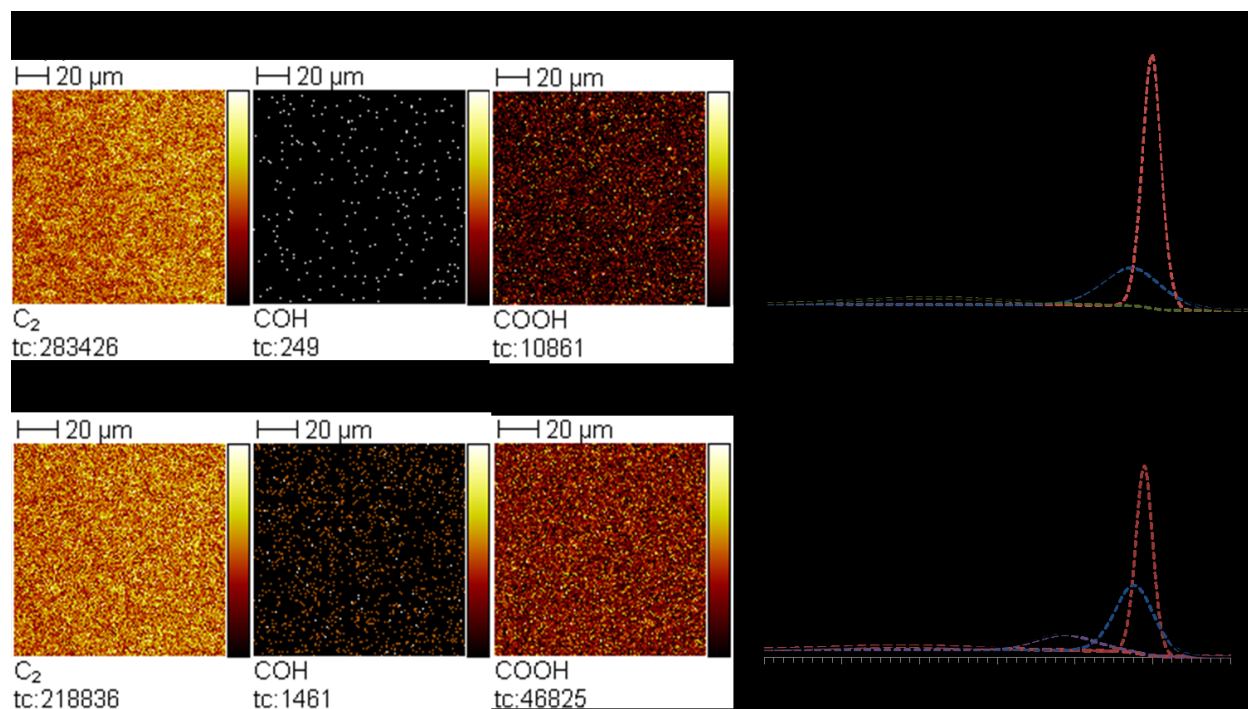


**Figure 4-1.** TOF-SIMS mapping of (a) HOPG and (b) F-HOPG surface. Deconvolution of C1s XPS peak for (c) HOPG and (d) F-HOPG.

### 4.3.2 DA adsorption thermodynamics.

As explained in Chapter 2, the theoretical thermodynamic calculations and adsorption results suggested that the adsorption was driven by the –CAHB formation mechanism for development of a SAL. Unfortunately, HOPG/F-HOPG has insignificant surface area as compared to EG preventing the monitoring of the DA adsorption to HOPG/F-HOPG sheets in solution (i.e., creation of adsorption isotherms) in the present study. However, the HOPG/F-HOPG sheets are ideal for the visualization of adsorption on their surfaces. Currently, it is expected that the –CAHB will be the dominant adsorption mechanism for SAL on HOPG/F-HOPG given the presence of phenolic and carboxylic groups on their surfaces (Figure 4-1) [6, 11]. However, compared with the previously considered work at pH 8.0 [6], the current solution

pH 5.4 might allow for hydrophobic-hydrophobic interaction between DA and HOPG/F-HOPG due to the occurrence of 18% non-ionized DA (Figure 4-2). Thus, the thermodynamics calculations for free energies of adsorption specifically to HOPG/F-HOPG are briefly included herein.

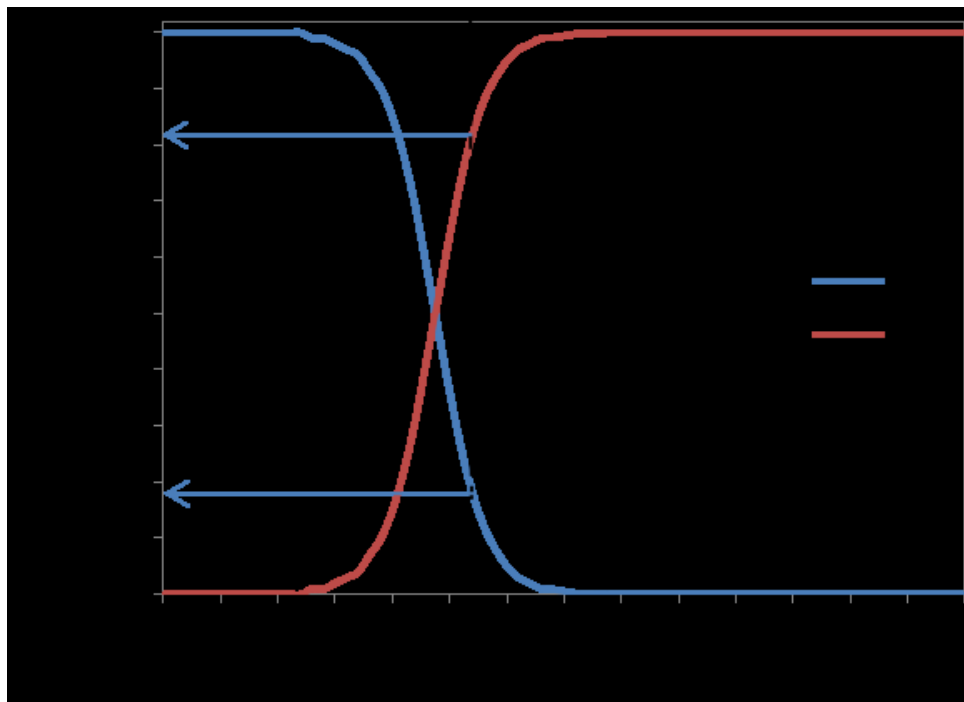


**Figure 4-2.** Speciation diagram for decanoic acid (according to the online SPARC software (<http://archemcalc.com/sparc/index>; accessed January 17<sup>th</sup>, 2014)

The free energy required for  $-CAHB$  formation ( $\Delta G^{-CAHB}$ ) needs to overcome water competition for the HOPG/F-HOPG adsorption sites ( $\Delta G_{H_2O}^{HB}$ ) and the DA solvation energy in water ( $\Delta G_{Solv}$ ):

$$\Delta G^{-CAHB} > \Delta G_{Solv} > \Delta G_{H_2O}^{HB} \quad (1)$$

The high concentration of water (55.5 M) affords an extremely strong competition with DA to bond with HOPG/F-HOPG [4, 5]. Thus, since DA is 82% ionized,  $\Delta G_{H_2O}^{HB}$  for water is calculated by [6]:

$$\Delta G_{H_2O}^{HB} = -RT \ln \left[ \frac{(H_2O)^2}{(DA^- - H^+ - H_2O)} \right] = -44.6 \text{ kJ mole}^{-1} \quad (2)$$

The free energy from the proton exchange of  $DA^-$  with water for solvation ( $\Delta G_{Solv}$ ) is described by [6]:

$$\Delta G_{Solv} = -RT \ln \left[ \frac{K_{a \text{ water}}}{K_{a \text{ DA}}} \right] = -52.0 \text{ kJ mole}^{-1} \quad (3)$$

It is postulated that  $\Delta G^{-CAHB}$  for DA is  $-50.2 \text{ kJ mole}^{-1}$  [12], which is not high enough to overcome  $\Delta G_{Solv}$ , indicating the need for an additional free energy contribution for  $-CAHB$  formation [6]. A hydrophobicity increase of DA due to proton exchange of  $DA^-$  with water could contribute to the required energy gain for  $-CAHB$  formation [5, 6, 13]. To determine this hydrophobicity increase, we assume  $K_{ow}$  (octanol-water partition coefficient) is an adequate hydrophobicity measure (see Figure 4-3), thus the hydrophobic free energy increase supplemented by the occurrence of the  $-CAHB$  ( $\Delta G_{Hydrophobicity}$ ) for DA is:

$$\Delta G_{Hydrophobicity} = -RT \ln \left[ \frac{K_{ow \text{ DA}}}{K_{ow \text{ DA}^-}} \right] = -4.23 \text{ kJ mole}^{-1} \quad (4)$$

The contribution of  $\Delta G_{Hydrophobicity}$  is added to  $\Delta G^{-CAHB}$  resulting in a total free energy gain  $\Delta G_{Total} = \Delta G_{Hydrophobicity} + \Delta G^{-CAHB}$  which is high enough to allow  $-CAHB$  formation [13]. Of note is the possibility of forming  $-CAHB$  between  $DA^-$ - $DA^-$  which can be more advantageous thermodynamically than  $DA^-$ -HOPG/F-HOPG [13-15]; however, the gain in the solvation barrier for hydrophobic compounds increases near hydrophobic surfaces which favors the  $DA^-$ -HOPG/F-HOPG [16]. Therefore, the SAL formation is thermodynamically favorable for

adsorption via –CAHB to the negatively charged FGs sites on the HOPG/F-HOPG surfaces. In addition, multilayer adsorption and possible aggregations would only be expected to occur in the SAL regions.

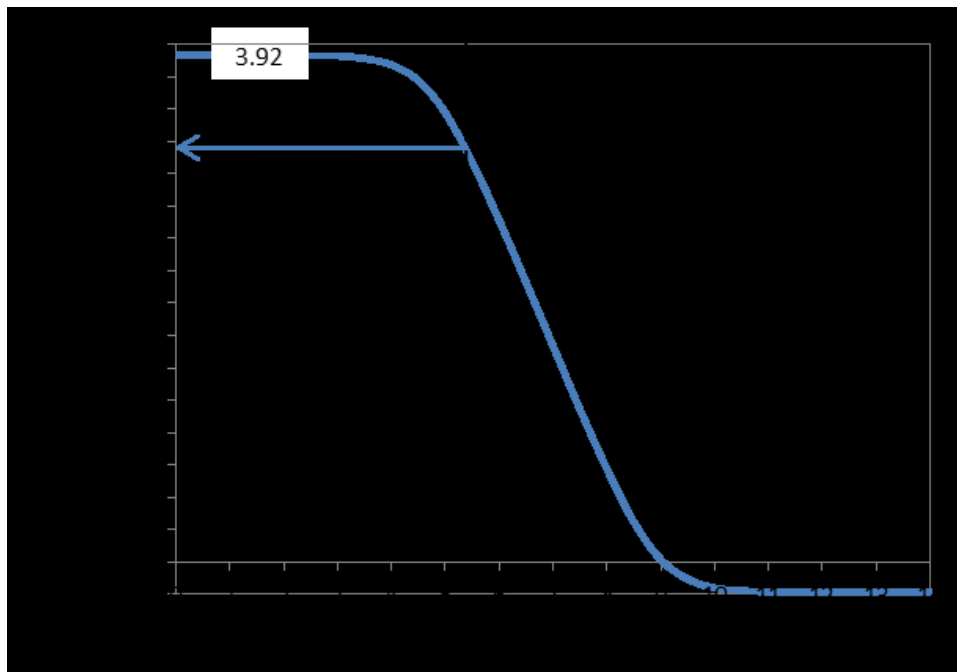


**Figure 4-3.** Log  $K_{ow}$  values for decanoic acid at different pH (according to the online SPARC software (<http://archemcalc.com/sparc/index>; accessed January 17<sup>th</sup>, 2014))

### 4.3.3 AM-FM-AFM imaging before/after DA adsorption.

The HOPG (Figure 4-4) and F-HOPG (Figure 4-5) surfaces were imaged before and after DA adsorption to visualize and discriminate the adsorption behaviour. The AM-FM-AFM images of HOPG surfaces show typical trench and steps topography exist (Figure 4-4a), while the frequency image shows that the mechanical properties at the steps and on the flat surface areas are variable (Figure 4-4b). After DA adsorption (Figure 4-4c,d), it is clear that molecule

aggregates adsorbed to the HOPG surface even after extensive rinsing of the surface with MilliQ water. Considering the adsorption system is quite simple, including water, DA and HOPG, these aggregates must be composed of DA molecules. These molecules are found along the steps of HOPG surfaces as readily observed from the clear contrast on the frequency shift image (Figure 4-4d). The dark areas (Figure 4-4d), which correspond to the higher profile region in the topographic image (Figure 4-4c), have a much lower frequency shift given the DA molecules adsorbed on the HOPG steps are much softer than the flat area of HOPG where no adsorption occurs [4, 17]. A finer, higher resolution scan of the HOPG surface shows a clear morphology (Figure 4-4e) and frequency shift (Figure 4-4f) of the molecular aggregates. The AFM profiles indicated Figures 4-4e,f were used to analyse the height and frequency shift of aggregates along a profile section (Figures 4-4g,h). The height of aggregates reached 7 nm, and the lateral aggregate sizes are around 20 nanometers perpendicular to, and several hundred nanometers along, the steps direction (Figure 4-4e). A large negative frequency shift (-4000 Hz; Figure 4-4h) indicates those regions are softer (i.e., DA adsorbed) as relative to other regions (i.e., hard HOPG).

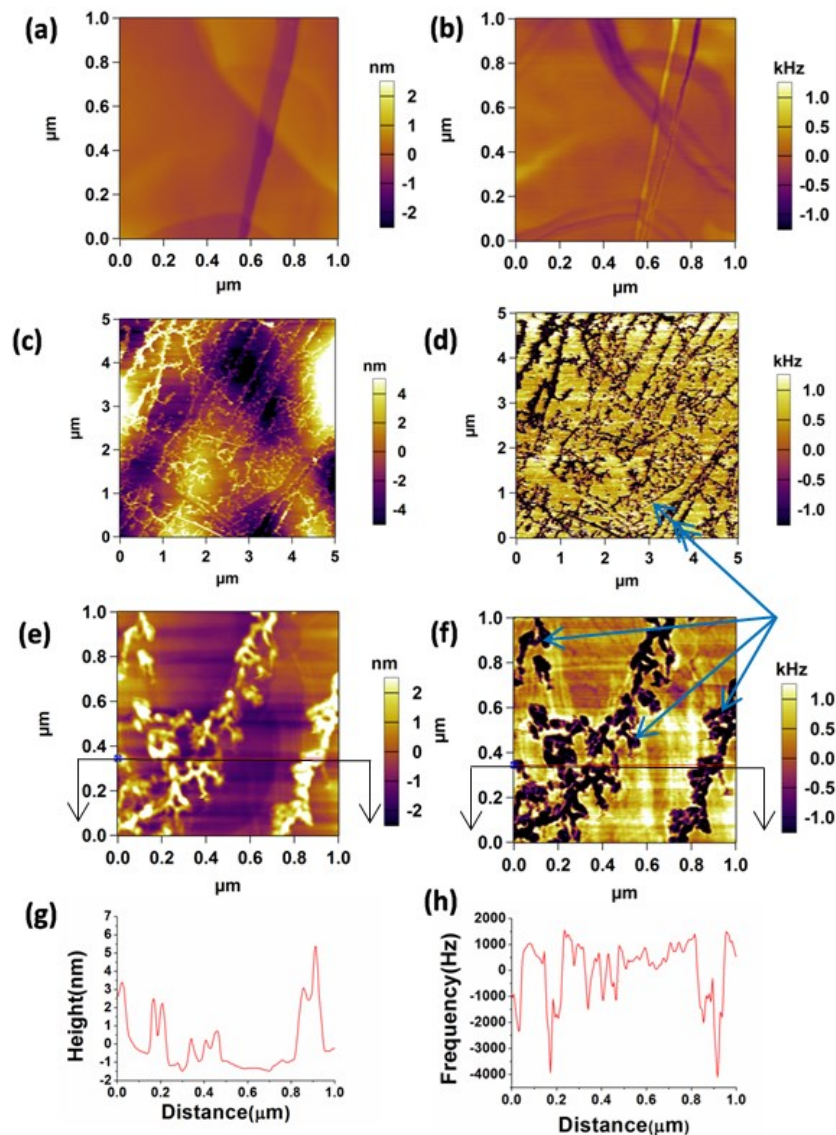


**Figure 4-4.** AM-FM AFM of HOPG surface before functionalization. a) Height image of fresh peeled HOPG surface ( $1\mu\text{m} \times 1\mu\text{m}$ ); b) corresponding frequency shift image of the HOPG surface shown in (a); c) height image of HOPG surface after adsorption of DA for 24h ( $5\mu\text{m} \times 5\mu\text{m}$ ), d) corresponding frequency shift image of HOPG surface shown in (c); e) enlarged fine scan of adsorbed DA on HOPG surface shown in (c) ( $1\mu\text{m} \times 1\mu\text{m}$ ), f) corresponding frequency shift image for surface shown in (e); g) section profile of topography indicated by line and arrows shown in (e); and h) corresponding section of frequency shift of section indicated by line and arrows shown in (f).

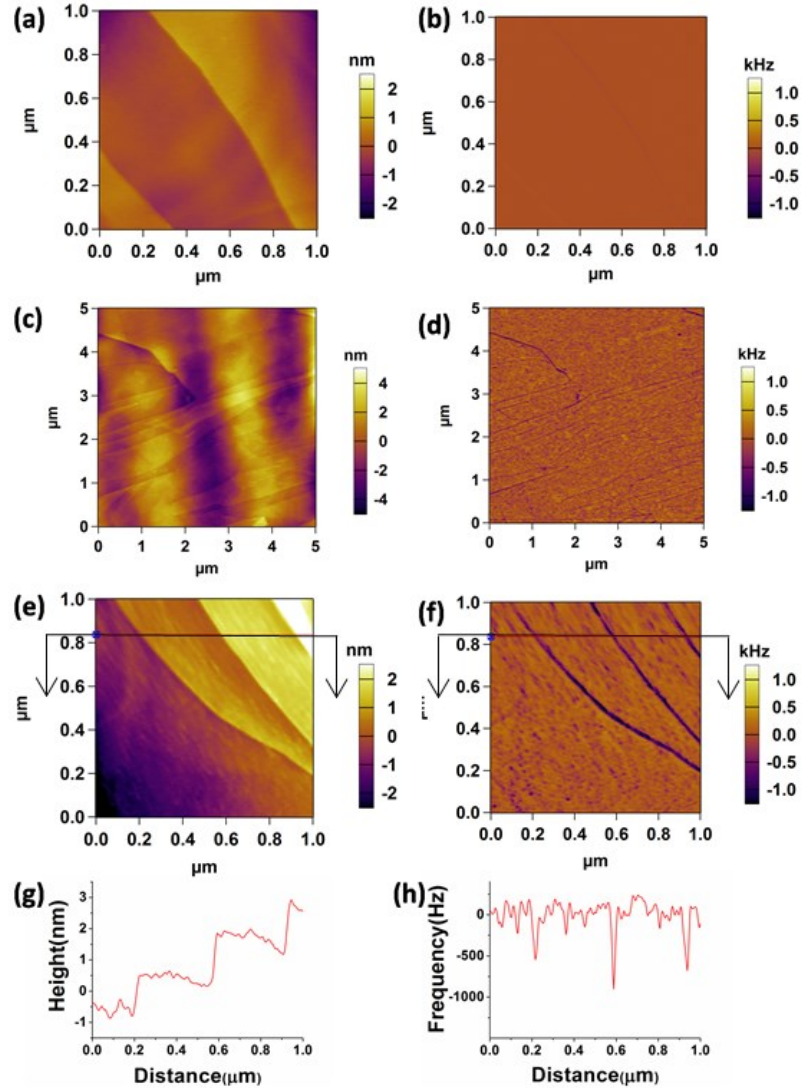


**Figure 4-5.** AM-FM AFM of F-HOPG surface after surface functionalization. a) Height image of fresh peeled F-HOPG surface ( $1\mu\text{m} \times 1\mu\text{m}$ ); b) corresponding frequency shift image of the F-HOPG surface shown in (a); c) height image of F-HOPG surface after adsorption of DA for 24h ( $5\mu\text{m} \times 5\mu\text{m}$ ), d) corresponding frequency shift image of F-HOPG surface shown in (c); e) enlarged fine scan of adsorbed DA on F-HOPG surface shown in (c) ( $1\mu\text{m} \times 1\mu\text{m}$ ), f) corresponding frequency shift image for surface shown in (e); g) section profile of topography indicated by line and arrows shown in (e); and h) corresponding section of frequency shift of section indicated by line and arrows shown in (f).

Given the AM-FM-AFM observations, it is clear that only the HOPG steps are occupied with DA molecules, which is in agreement with the thermodynamics calculations of establishment of a SAL via –CAHB with negatively charged FGs. After SAL formation at the FGs, remaining DA molecules in solution will favor a hydrophobic-hydrophobic interaction with the hydrophobic end of this SAL due to the significant decrease in the density of water molecules around the CH<sub>3</sub> end. This causes a decrease in desolvation hindrance and promotes the adsorption of DA molecules, especially the 18% non-ionized molecules at pH 5.4, into layers at the SAL end [16]. This multilayer DA adsorption at the HOPG steps is readily visualized as the aggregations indicated in Figure 4-4. The height of these aggregates into the solution depends on the declining of the solvation barrier behavior as the aggregates move further away from the HOPG/SAL surfaces. A similar phenomenon would be anticipated at higher pH values; however, with smaller aggregates due to the increase in the hydrophobicity of the dominant DA<sup>-</sup> molecules (Figure 4-2).

To confirm our observations for the occurrence of DA adsorption on the functionalized sites only, water plasma was used to functionalize the HOPG surface (Figure 4-5). This functionalization would theoretically allow the distribution of the negatively charged FGs on the entire HOPG surface (Figure 4-4b). The F-HOPG surface was relatively smooth although some steps were observed (Figure 4-5a); however, the frequency image (Figure 4-5b) indicates almost no frequency shifts across the F-HOPG surface indicating the homogeneity of mechanical properties after functionalization. This is in direct contrast to the variable mechanical properties exhibited prior to functionalization (Figure 4-4b). The schematics shown in Figure 4-6a and 4-6d illustrate the difference between frequency shift images for HOPG (Figure 4-4b) and F-HOPG (Figure 4-5b), respectively. Extra FGs are distributed over the entire F-HOPG surface after

functionalization in addition to those present at the steps of unmodified HOPG. Interestingly, in contrast to the HOPG results, the F-HOPG showed no large adsorbed DA molecule aggregates (Figure 4-5c and 4-5d). DA adsorption on F-HOPG would be expected to be more inclined toward a uniform distribution (as compared to HOPG) over its entire surface given its less variable height and more consistent mechanical properties (Figure 4-5c,d). The enlarged topography scan of the F-HOPG surface (Figure 4-5e) shows a relatively smooth surface between steps as confirmed by the section profile (Figure 4-5g) shown in Figure 4-5e. The change in height at the steps is rapid and has minimal width (Figure 4-5g) as compared to the changes at the HOPG steps (Figure 4-4g); additionally, the height change on the surface in between the steps is minimal which is most probably due to DA distribution on F-HOPG surfaces. Minor aggregations observed between steps might be due to some non-uniformity in functionalization. Interestingly, the F-HOPG frequency shift image (Figure 4-5f) reveals no DA aggregates at the steps as found for HOPG (Figure 4-4f); yet, darker colors at the steps reflects higher DA concentrations within the steps than found between steps due to the increase in FGs concentrations at the steps after functionalization. The section profile of the frequency shift (Figure 4-5h) illustrates a lower frequency shift value at the steps, around 600Hz, much smaller than for HOPG (-4000 Hz; Figure 4-4h), confirming the much lower differences in DA concentrations between various locations on the F-HOPG (Figure 4-5h). The schematics shown in Figure 4-6c and 4-6f illustrate the difference between frequency shift images for HOPG (Figure 4-4f) and F-HOPG (Figure 4-5f), respectively. The DA molecules were distributed over the entire F-HOPG surface as compared to the HOPG steps only due to the presence of extra FGs after the water plasma treatment. Ionized DA are adsorbed first via -CAHB establishing a SAL (Figure 4-6b,e) and the multilayers are adsorbed next forming the observed aggregates on HOPG

steps (Figure 4-6c) or developing more uniform distribution on the F-HOPG surfaces having multiple FGs available for adsorption (Figure 4-6f).

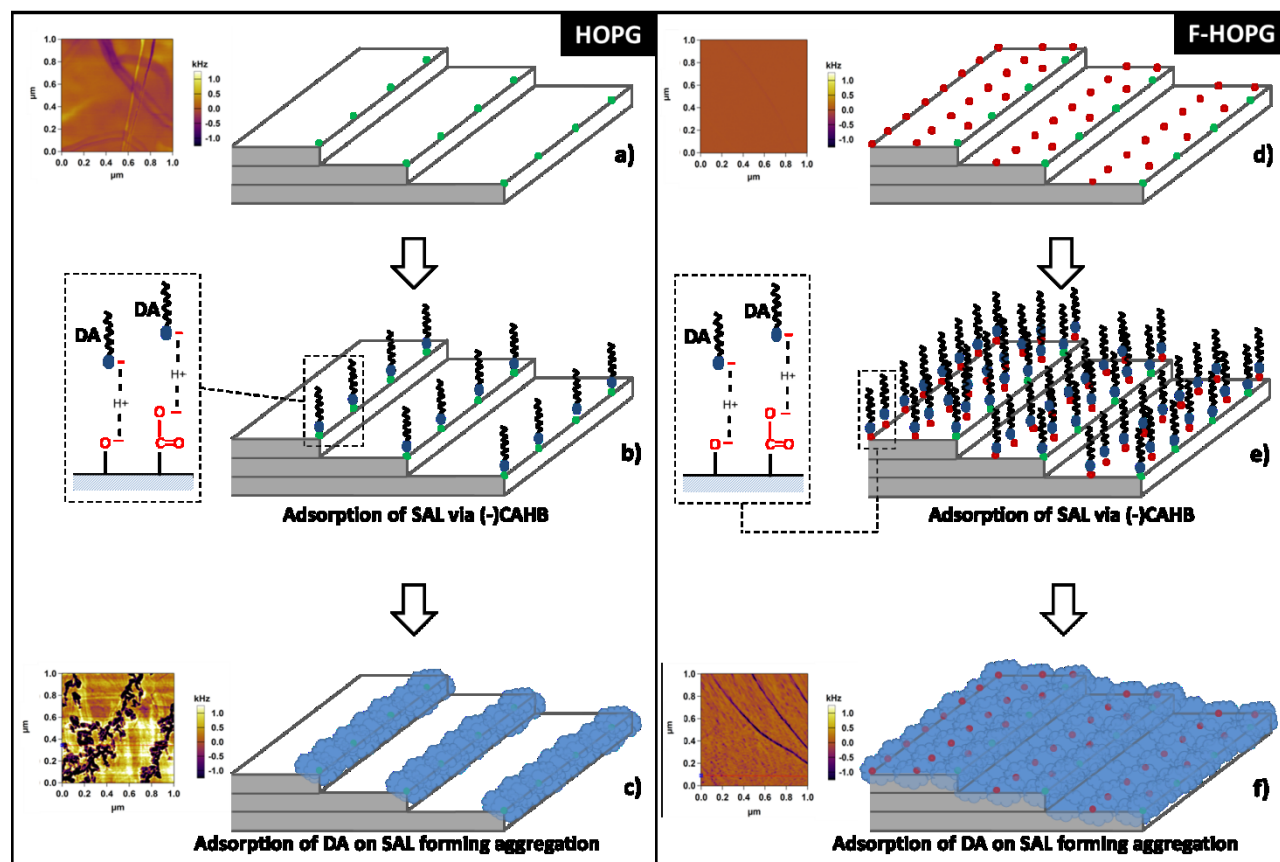


**Figure 4-6.** Frequency shift images of the fine scan ( $1\mu\text{m} \times 1\mu\text{m}$ ) AM-FM AFM and the corresponding schematics for: a) HOPG; b) ionized SAL adsorbed on HOPG steps only (no frequency shift image); c) aggregates of DA adsorbed only on the steps of HOPG d) F-HOPG; e) SAL of DA adsorbed on the whole surface of F-HOPG (no frequency shift image) and f) DA multilayers adsorbed on the whole surface of F-HOPG. (green circles indicate FG on HOPG/F-HOPG steps; red circles indicate FG on the F-HOPG surface after functionalization)

#### **4.4 Environmental significance**

In this work, AM-FM-AFM technique has been applied to discriminate and visualize the adsorption behaviour of DA on HOPG. The adsorption for SAL occurred first via the thermodynamically proven –CAHB in aqueous solution with the FGs found on the HOPG steps and over the entire F-HOPG surface. After this initial SAL formation, multilayers of DA were able to form on the SAL for both HOPG and F-HOPG. Given the FGs were only on the steps of the HOPG, these multilayers appeared as aggregates of molecules. The more even distribution of FGs on the F-HOPG created a more uniform multilayer across its entire surface. A more detailed morphology of these molecular aggregations may be achieved using an even finer scan with a sharper tip for better resolution imaging and is currently being considered for future work. Also, in situ imaging using a variety of compounds in solutions will be the focus of subsequent research.

## 4.5 References.

- [1] Shin YJ, Wang Y, Huang H, Kalon G, Wee ATS, Shen Z, et al. Surface-Energy Engineering of Graphene. *Langmuir* 2010;26:3798-3802.
- [2] Perreault F, Tousley, M.E., Elimelech. Thin-film composite polyamide membranes functionalized with biocidal graphene oxide nanosheets. 2014.
- [3] Pei Z, Li L, Sun L, Zhang S, Shan X-q, Yang S, et al. Adsorption characteristics of 1,2,4-trichlorobenzene, 2,4,6-trichlorophenol, 2-naphthol and naphthalene on graphene and graphene oxide. *Carbon* 2013;51:156-163.
- [4] Ni J, Pignatello JJ, Xing B. Adsorption of Aromatic Carboxylate Ions to Charcoal Black Carbon is Accompanied by Proton Exchange with Water (vol 45, pg 9240, 2012). *Environmental Science & Technology* 2012;46:5633-5633.
- [5] Teixido M, Pignatello JJ, Beltran JL, Granados M, Peccia J. Speciation of the Ionizable Antibiotic Sulfamethazine on Black Carbon (Biochar). *Environmental Science & Technology* 2011;45:10020-10027.
- [6] Moustafa A, McPhedran K, Moreira J, Gamal El-Din M. Investigation of Mono/Competitive Adsorption of Environmentally Relevant Ionized Weak Acids on Graphite: Impact of Molecular Properties and Thermodynamics. *Environmental Science & Technology* 2014;48:14472-14480.
- [7] Herruzo ET, Perrino AP, Garcia R. Fast nanomechanical spectroscopy of soft matter. *Nature Communications* 2014;5.
- [8] Lamour G, Yip CK, Li H, Gsponer J. High Intrinsic Mechanical Flexibility of Mouse Prion Nanofibrils Revealed by Measurements of Axial and Radial Young's Moduli. *Acs Nano* 2014;8:3851-3861.
- [9] Maurer SE, DeClue MS, Albertsen AN, Dorr M, Kuiper DS, Ziock H, et al. Interactions between Catalysts and Amphiphilic Structures and their Implications for a Protocell Model. *Chemphyschem* 2011;12:828-835.
- [10] Robertson J. Diamond-like amorphous carbon. *Materials Science & Engineering R-Reports* 2002;37:129-281.
- [11] Konkena B, Vasudevan S. Understanding Aqueous Dispersibility of Graphene Oxide and Reduced Graphene Oxide through pK(a) Measurements. *Journal of Physical Chemistry Letters* 2012;3:867-872.
- [12] Ni H-G, Zeng H, Zeng EY. Sampling and analytical framework for routine environmental monitoring of organic pollutants. *Trac-Trends in Analytical Chemistry* 2011;30:1549-1559.
- [13] Li X, Pignatello JJ, Wang Y, Xing B. New Insight into Adsorption Mechanism of Ionizable Compounds on Carbon Nanotubes. *Environmental Science & Technology* 2013;47:8334-8341.
- [14] Gilli G, Gilli P. Towards an unified hydrogen-bond theory. *Journal of Molecular Structure* 2000;552:1-15.
- [15] Gilli P, Pretto L, Bertolasi V, Gilli G. Predicting Hydrogen-Bond Strengths from Acid-Base Molecular Properties. The pK(a) Slide Rule: Toward the Solution of a Long-Lasting Problem. *Accounts of Chemical Research* 2009;42:33-44.
- [16] Vembanur S, Patel AJ, Sarupria S, Garde S. On the Thermodynamics and Kinetics of Hydrophobic Interactions at Interfaces. *Journal of Physical Chemistry B* 2013;117:10261-10270.

[17] Fontecha-Camara MA, Lopez-Ramon MV, Alvarez-Merino MA, Moreno-Castilla C. Effect of surface chemistry, solution pH, and ionic strength on the removal of herbicides diuron and amitrole from water by an activated carbon fiber. *Langmuir* 2007;23:1242-1247.



RightsLink®



ACS Publications  
Most Trusted. Most Cited. Most Read.

Title: Investigation of Mono/Competitive Adsorption of Environmentally Relevant Ionized Weak Acids on Graphite: Impact of Molecular Properties and Thermodynamics

Author: Ahmed M. A. Moustafa, Kerry N. McPhedran, Jesús Moreira, et al

Publication: Environmental Science & Technology

Publisher: American Chemical Society

Date: Dec 1, 2014

Copyright © 2014, American Chemical Society

Logged in as:

Ahmed Moustafa

LOGOUT

#### PERMISSION/LICENSE IS GRANTED FOR YOUR ORDER AT NO CHARGE

This type of permission/license, instead of the standard Terms & Conditions, is sent to you because no fee is being charged for your order. Please note the following:

- Permission is granted for your request in both print and electronic formats, and translations.
- If figures and/or tables were requested, they may be adapted or used in part.
- Please print this page for your records and send a copy of it to your publisher/graduate school.
- Appropriate credit for the requested material should be given as follows: "Reprinted (adapted) with permission from (COMPLETE REFERENCE CITATION). Copyright (YEAR) American Chemical Society." Insert appropriate information in place of the capitalized words.
- One-time permission is granted only for the use specified in your request. No additional uses are granted (such as derivative works or other editions). For any other uses, please submit a new request.

Copyright © 2015 Copyright Clearance Center, Inc. All Rights Reserved. Privacy statement. Terms and Conditions.

Comments? We would like to hear from you. E-mail us at [customer care@copyright.com](mailto:customer care@copyright.com)

## 5 INVESTIGATION OF THE ADSORPTION OF IONIZED CARBOXYLIC ACIDS ON GRAPHITE: USING SIMPLE MODEL COMPOUNDS TO UNDERSTAND COMPLEX MIXTURES<sup>1</sup>

### 5.1 Introduction

The continuing increase in the use of nanomaterials, such as graphene, creates an environmental risk due to the release of graphene constituents to natural water streams [1]. Graphene can be found in materials including graphite, while the most common forms used include pure graphene, graphene oxide, and reduced graphene oxide [2]. These nanomaterials have two potentially negative environmental impacts in receiving waters including affecting the fate and transport of organic pollutants and/or natural organic matter and toxicity to organisms [3]. Despite their environmental risks, graphite-type materials such as graphene [4] and carbon nanotubes (CNTs) [4] have been used extensively in applications including adsorption of various compounds such as pesticides and antibiotics [5, 6]. The investigation of adsorption mechanisms has been of current interest with adsorption being considered through the establishment of  $\pi$ - $\pi$  bonds [4, 5, 7-9].

---

<sup>1</sup>A version of this chapter has been submitted previously: Ahmed M.A. Moustafa, Kerry N. McPhedran and Mohamed Gamal El-Din, Investigation of the adsorption of ionized carboxylic acids on graphite: Using simple model compounds to understand complex mixtures. Journal of Hazardous Materials (Submitted; 30 March 2015)

The interactions of the functionalized ends of the ionized organic pollutants with graphitic carbon materials have received recent attention; however, the mechanism and competition of adsorption from mixtures of several model compounds and natural mixtures is still lacking consideration [6, 10-14]. Previously, metal ion bridging was thought to be the only mechanism governing the adsorption of the negatively charged end of ionized weak acids to the negatively charged carbon surface functional groups (FGs) [15, 16]. However, Li et al. [11] found that this type of adsorption caused a rise in the solution pH which made them question the validity of the metal ion bridging mechanism as being the sole method for adsorption as this mechanism would not impact solution pH. Following this discovery, they determined that the increase in pH could be assigned to the formation of a hydrogen bond between the negatively charged end of ionized weak acids and the negatively charged FGs called the negatively charged assisted hydrogen bond (-CAHB) [6, 12].

Of current interest among ionized organic pollutants mixtures are the naphthenic acids (NAs) found in the alkaline oil sands process-affected waters (OSPW). These NAs are found at concentrations ranging from 10 to 120 mg/L in wastewaters created during the bitumen extraction process of the oil sands deposits in Alberta, Canada [17-21]. Although there are hundreds of NAs in OSPW that of known molecular weights their specific structures are not known due to the difficulty of assessing such a large variety of molecular species. Given this difficulty, the investigation of the interaction of OSPW NAs with graphitic adsorbents cannot be used to directly assess adsorption mechanisms. Accordingly, the use of model compound NAs and commercial NAs mixtures are useful in gaining further insight into adsorption mechanisms that may then be extrapolated to more complex mixtures such as OSPW.

Currently, we investigated the adsorption behaviour of individual model compounds (decanoic acid, C<sub>9</sub>H<sub>19</sub>COOH, DA; trans-4-isopropylcyclohexane carboxylic acid, C<sub>9</sub>H<sub>17</sub>COOH, Trans-4-IsoPCHA; and trans-4-propylcyclohexane carboxylic acid, C<sub>9</sub>H<sub>17</sub>COOH, Trans-4-PCHA), mixtures of the three NAs, a commercial NAs mixture (Merichem) and raw OSPW. For the model NAs mixtures, the compounds were chosen to have the same molecular weight but different structures that allows for a comprehensive study of the impact of structure and other molecular properties on interaction with the graphite adsorbent. The commercial NAs mixture contains tens of NAs, some of which may be found in raw OSPW. The advantage of using this mixture is the isolation of the possible impact on adsorption of dissolved salts and minerals found in OSPW [19]. The overall objective of the current study is to evaluate and determine the adsorption mechanisms of complex NAs mixtures on graphite. The fundamental understanding of these interactions is essential to the development of engineered adsorbents for the efficient removal of NAs from OSPW. The expanded graphite (EG) used as the current adsorbent [14] contains mesopores that will not allow for the exclusion removal of NAs due to size. The EG has FGs including phenols and carboxyls on their surfaces that will allow for the development of the –CAHB as we have determined previously [14].

## **5.2 Materials and Methods**

### **5.2.1 Chemicals, Reagents and Oil Sands Process-Affected Water (OSPW).**

The decanoic acid (DA) was purchased from Sigma Aldrich (Malaysia). The trans-4-propylcyclohexanecarboxylic acid (Trans-4-PCHA) and trans-4-isopropylcyclohexanecarboxylic acid (Trans-4-IsoPCHA) were purchased from TCI Japan Organic Chemicals (Japan). The sodium hydroxide (50-52% NaOH) was purchased from Sigma-Aldrich Canada (Oakville, ON).

The acetic acid, ammonium acetate, dichloromethane (DCM), methanol (MeOH), potassium phosphate dibasic ( $K_2HPO_4$ ) and potassium phosphate monobasic ( $KH_2PO_4$ ) were purchased from Fisher Scientific Canada (Edmonton, AB). Ultrapure water was obtained from a Millipore and Elga Synergy<sup>®</sup> UV instrument (France). Refined Merichem NAs were provided by Merichem Chemicals and Refinery Services LLC (Houston, TX, USA). OSPW (pH 8.7) was obtained from a settling basin of an oil sands company located in Fort McMurray, Alberta, Canada in September 2012. The graphite intercalated compounds (GIC) (Grade 3772, Lot# 6319-3) were a gift from Asbury Carbons (NJ, USA).

Stock solutions including 10 and 50 mg/L for each model NA and 50 mg/L for Merichem NAs were prepared in MilliQ water adjusted to pH 8 using 0.1 M phosphate buffer. The OSPW was used as received without further processing.

## **5.2.2 Expanded Graphite Characterization and Analytical Methods.**

The preparation of the expanded graphite (EG) from the GIC has been prepared as explained in Chapter 2. Briefly, the GIC was shocked at  $1000 \pm 25$  °C for one minute to produce the EG. The GIC and EG were characterized for pore volume and BET surface area (IQ2MP Quantachrome system; ATS Scientific Inc., Canada); elemental composition and surface functional groups by XPS analyses (AXIS 165 spectrometer; Kratos Analytical, Japan); morphology (Hitachi Scanning electron microscopy S-2500; Tokyo, Japan; and imaging acquisition was conducted using a Time of Flight Secondary Ion Mass Spectroscopy (TOF-SIMS) instrument (GmbH, Germany).

Model NAs samples were quantified using an HPLC/MS coupled to an ion trap mass spectrometer (Varian500-MS) with chromatographic separation using Phenomenex  $C_8$  column. Solution A was 100% methanol and solution B was 4 mM ammonium acetate (aqueous) with

0.1% acetic acid. The separation method included a gradient elution from 45% to 15% A over 30 min and returned to 45% A for 10 min. The injection volume was 20  $\mu\text{L}$ , the flow rate was 200  $\mu\text{L min}^{-1}$ , and the column temperature was kept at 40  $^{\circ}\text{C}$ . The acid extractable fraction (AEF) concentration of Merichem NAs and OSPW was used to determine their NAs adsorption isotherms using FTIR (PerkinElmer<sup>®</sup>) as described previously [14] .

Quantification of NAs in Merichem and OSPW solutions was performed using a Waters Acquity ultra-pressure high performance liquid chromatography (UPLC) System (Milford, MA, USA chromatographically separate NAs. The UPLC system was connected to a high resolution Synapt G2 HDMS mass spectrometer equipped with an electrospray ionization source operating in the negative ion mode (HRMS). Triplicate sample aliquots of 2 mL were centrifuged for 5 min at 10 000 RPM to remove residual particles with 500  $\mu\text{L}$  of the centrifuge supernatant placed in a 2 mL glass vial with 400  $\mu\text{L}$  of MeOH and 100  $\mu\text{L}$  of 400 mg/L tetradecanoic acid-1-<sup>13</sup>C (internal standard) to make a final 1 mL sample solution. More details on the UPLC/HRMS method can be found in Appendix A.

### 5.2.3 Sorption Experiments.

Experimental treatments considered included:

- 10 mg/L individual model NAs (DA, Trans-4-IsoPCHA and Trans-4-PCHA)
- 50 mg/L individual model NAs (DA, Trans-4-IsoPCHA and Trans-4-PCHA)
- 30 mg/L model NAs mixture (10 mg/L each of DA, Trans-4-IsoPCHA and Tans-4-PCHA)
- 50 mg/L model NAs mixture (16.7 mg/L each of DA, Trans-4-IsoPCHA and Trans-4-PCHA)

- 50 mg/L Merichem AEF
- 50 mg/L OSPW AEF (as received)

For each experiment, triplicate samples of EG (0.3, 0.6, 0.9, and 1.5 g) were added to 60 mL of each treatment contained in a 250 mL glass vial sealed with a Teflon screw cap with resultant EG concentrations of 5, 10, 15, and 25 g/L, respectively. Samples were mixed for 24 hours using a wrist action shaker (Model 75; Burrell Scientific, Pittsburgh, PA, USA) at room temperature ( $22 \pm 2$  °C). Initial control experiments without EG indicated no loss of NAs (e.g., to surfaces, degraded, volatilized) after 24 h. Three EG masses (0.3, 0.6, 0.9 g) were used for fitting Langmuir and Freundlich isotherm models for the individual model NAs. Four EG masses (0.3, 0.6, 0.9, and 1.5 g) were used to fit the adsorption models for the Merichem NAs and OSPW. Further details on the Langmuir and Freundlich models can be found in Appendix D.

## **5.3 Results and Discussion**

### **5.3.1 EG characterization.**

The GIC as received are isolated plate-like particles with a dark grey surface (Figure 5-1a). The GIC expands rapidly due to thermal shock, creating the EG that has a significantly larger worm-like appearance having numerous pores on its surface (Figure 5-1b). Due to this expansion, the density decreases markedly to less than 1% of the initial 630 g/L [22]. As well, the expansion creates an increase in surface area with EG at  $76.9 \pm 1.4$  m<sup>2</sup> g<sup>-1</sup> containing exclusively large mesopores [14, 23] that allow for fast kinetics for adsorption [24]. However, these mesopores will also potentially increase competition for adsorption sites when considering compound mixtures [24]. This surface area is similar to graphene oxide at 65.0 m<sup>2</sup> g<sup>-1</sup>, however, is lower than graphene at 239.1 m<sup>2</sup> g<sup>-1</sup> [4]. Additionally, the surface area of the various CNTs

used by Li et al. [11] ranged from 117 to 228 m<sup>2</sup> g<sup>-1</sup>. Given the surface area impacts the adsorption capabilities of the adsorbents, it would be expected that EG would have similar adsorption capabilities as graphene oxide and lower than graphene or CNTs. The XPS and TOF-SIMS results (Figure 5-2) were similar to our previous findings [14] indicating that the C<sub>2</sub> (C-C and C=C) groups at 284.8 eV were most dominant with total counts of 255 752. The oxygen containing groups CHO (C-OH at 286.2 eV) and CHO<sub>2</sub> (COOH at 288.7 eV) group total counts were only 51 and 294, respectively [25]. Overall, the elemental analysis indicated that EG is composed of 96% carbon and 4% oxygen which is similar to the proportions found in carbon nano-tubes (CNT) used by Li et al. [11] for examining the fate and transport of ionized organic acids. Clearly, given the characteristics of the porous EG are similar to those of CNTs there is potential for the development of this graphitic EG material for the removal of the emerging organic acids pollutants from various wastewater streams.

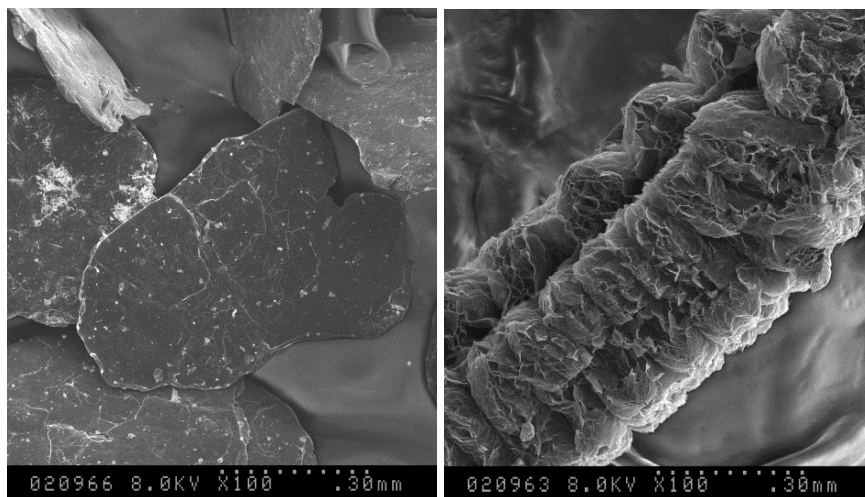


**Figure 5-1.** SEM images for (a) graphite intercalated compounds and (b) expanded graphite (EG)

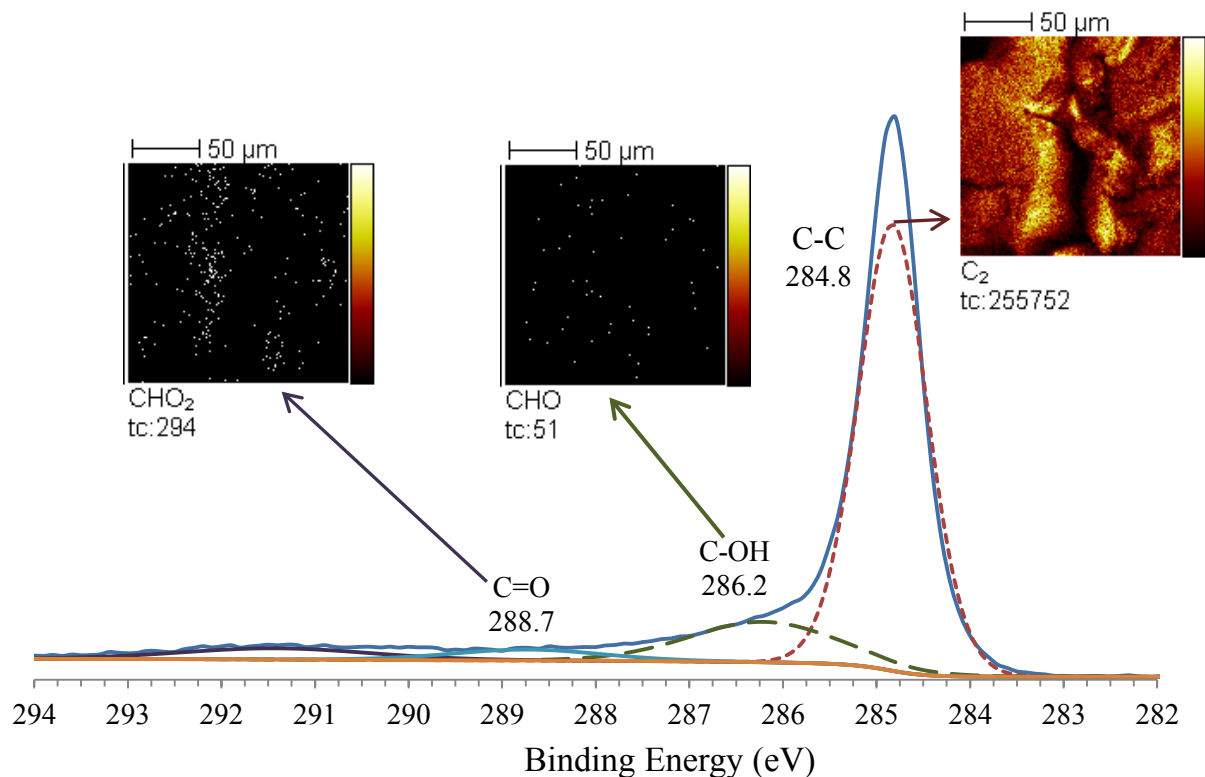


**Figure 5-2.** Deconvolution of C1s peak using XPS for the expanded graphite (figure) and TOF-SIMS (images).

### 5.3.2 Mono- and multi-compound model NA adsorption.

Building upon our previous findings for five model NAs (the current NAs plus heptanoic acid and cyclohexanecarboxylic acid) [14], the knowledge gained from the three current assessed model NAs (DA, Trans-4-IsoPCHA and Trans-4-PCHA) will be used to improve the understanding, and aid in the evaluation of, the adsorption of more complex mixtures including the Merichem NAs and OSPW NAs (see following sections). The two concentrations of the mono-compounds considered at 10 and 50 mg/L (Figure 5-3) were chosen to be similar to actual ranges of NAs found in OSPW (10 to 120 mg/L) measured previously [19-21] without exceeding solubility limits.

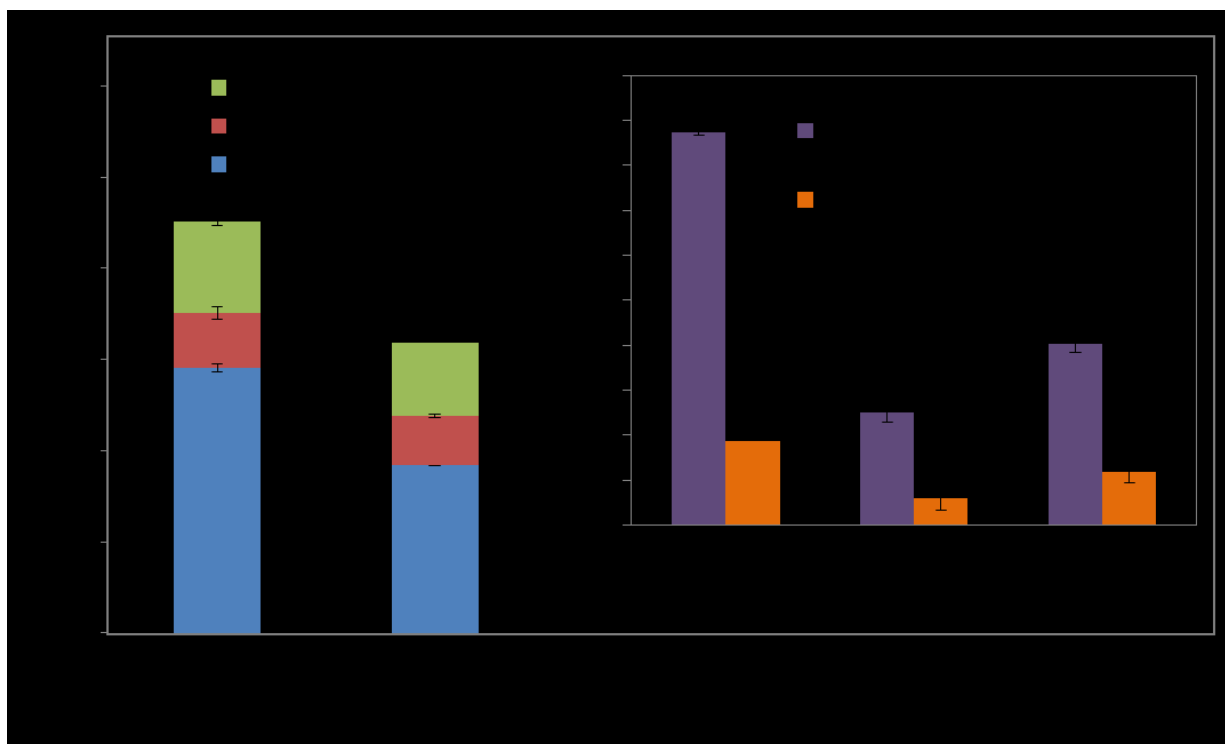


**Figure 5-3.** Multi-compound and mono-compound adsorption of model compound (MC) naphthenic acids after mixing with 2.5 g/L EG for 24 hours. (graph bars represent average of  $n = 3$  and error bars represent standard deviations)

The adsorption capacities for mono-compounds at initial concentration ( $C_0$ ) of 10 mg/L were 1.87, 1.18 and 0.60 mg g<sup>-1</sup> for DA, Trans-4-PCHA and Trans-4-IsoPCHA, respectively. At  $C_0 = 50$  mg/L, the adsorption capacities were 8.74, 4.04 and 2.50 mg g<sup>-1</sup> for DA, Trans-4-PCHA and Trans-4-IsoPCHA, respectively. Overall, the adsorption of the mono-compounds increased linearly with the concentration indicating that either the EG sorption sites were not saturated or multilayer adsorption was occurring (Figure 5-3). Generally, both the Langmuir and Freundlich isotherm models fit the mono-adsorption data for the three model compounds (DA, Trans-4-IsoPCHA and Trans-4-PCHA;  $R^2 \geq 0.91$ ) (Table 5-1). The exception being the Langmuir isotherm for Trans-4-IsoPCHA that is considered invalid with a negative  $q_{\max} = -24.8$ . It should be noted that the Langmuir model would indicate a homogenous EG surface for adsorption [26].

Given the current XPS and TOF-SIMS results indicate a heterogeneous EG surface, the Freundlich model is more representative of the adsorption as it assumes a heterogeneous surface with a diversity of adsorption sites. Li et al. [11] found a similar better fit using the Freundlich versus the Langmuir model for weak acids on CNT, while Pei et al. [4] used the Freundlich model exclusively for aromatic pollutants on graphene and graphene oxide where the isotherms were well-fitted.

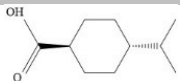
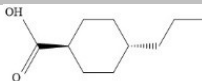
**Table 5-1.** Monocompound Langmuir and Freundlich adsorption isotherm parameters for DA, Trans-4-IsoPCHA and Trans-4-PCHA as obtained from Chapter 2.

Compounds	Langmuir adsorption isotherm			Freundlich adsorption isotherm		
	$q_{max}$	b	$R^2$	K	n	$R^2$
<b>DA</b>	7.14	0.33	0.99	2.22	2.42	0.99
<b>Trans-4-IsoPCHA</b>	8.1	0.33	0.92	0.13	1.33	0.91
<b>Trans-4-PCHA</b>	-24.8	-0.0038	0.97	0.08	0.94	0.98

For the multi-compound adsorption, the 3 model compounds at 30 mg/L (10 mg/L each) and 50 mg/L (16.67 mg/L each) had adsorption capacities of 3 190 mg/kg and 4 510 mg/kg, respectively. Based on these results for mono and multi-compound adsorption, the affinity of NAs to the EG surface is DA > Trans-4-PCHA > Trans-4-IsoPCHA (Figure 5-3). This adsorption follows the order of hydrophobicity as indicated by the anionic Log  $K_{ow}$  values at pH 8 with DA (0.72) > Trans-4-PCHA (-0.12) > Trans-4-IsoPCHA (-0.28) (Table 5-2). A similar adsorption capacity pattern was found by Li et al. [11] for weak acids on CNTs. Overall, the very low Log  $K_{ow}$  values indicate higher hydrophilicity of the anionic NAs at pH 8 versus the neutral forms at pH 7. The EG has a negative surface charge due to deprotonated surface functional groups, thus, the decreased hydrophobicity coupled with the negative charge of the anionic

model compounds would tend to suggest minimal adsorption potential due to electrostatic repulsion impacts [11, 27, 28]. In contrast to the expected behaviour, the model compounds NAs had appreciable EG adsorption capacities based on the mono/multi-compound adsorption (Figure 5-3). This behaviour is the result of the –CAHB as discussed further in the Thermodynamics section below.

**Table 5-2.** Physiochemical properties of the 3 model naphthenic acids calculated using SPARC software (<http://archemcalc.com/sparc/index>; accessed November 15, 2014)

Model NA compounds	Decanoic acid	Trans-4-Isopropyl Cyclohexanoic acid	Trans-4-propyl Cyclohexanoic acid
Abbreviation	DA	Trans-4-IsoCHA	Trasn-4-PCHA
Structure			
Formula	C <sub>10</sub> H <sub>20</sub> O <sub>2</sub>	C <sub>10</sub> H <sub>18</sub> O <sub>2</sub>	C <sub>10</sub> H <sub>18</sub> O <sub>2</sub>
MW	172.3 (g/mol)	170.3 (g/mol)	170.3 (g/mol)
pK <sub>a</sub>	4.9	4.82	4.82
Log K <sub>ow</sub>	3.92	2.89	3.05
Log K <sub>ow</sub> at pH 8	0.72	-0.28	-0.12
Water solubility	47.9 (mg/L)	109 (mg/L)	94 (mg/L)

### 5.3.3 EG adsorption of Merichem and OSPW NAs.

The assessment of adsorption isotherms of various individual NAs in mixtures including the Merichem and OSPW treatments are not possible due to the extreme diversity of detected NAs. Instead, the linear regressions of the adsorption data for the entire NAs mixtures were obtained (Figure 5-4). Results indicated that the Langmuir isotherm models did not fit the adsorption data with negative  $q_{\max}$  values for both Merichem ( $q_{\max} = -16.7$ ) and OSPW ( $q_{\max} = -1.47$ ) isotherms (Table 5-3). Alternatively, the Freundlich isotherm models better represented the

adsorption data (Figure 5-4a,c and Table 5-3) for both Merichem and OSPW treatments which indicates the potential for multilayer adsorption of these NAs on EG [26, 29]. The consideration of the Freundlich isotherm model as being more representative of NAs adsorption is in agreement with the previous model compound findings. It should be noted that the parameter K of the Freundlich isotherms is extremely higher for Merichem NAs versus the OSPW NAs which indicates a higher adsorption capacity for Merichem NAs to the EG (Table 5-3) [29].

**Table 5-3.** Langmuir and Freundlich adsorption isotherm parameters for AEF in Merichem and OSPW.

Compounds	Freundlich adsorption isotherm			Langmuir adsorption isotherm		
	K	n	R <sup>2</sup>	q <sub>max</sub>	b	R <sup>2</sup>
<b>AEF (Merichem)</b>	0.13	0.68	0.90	-16.7	-0.19	0.96
<b>AEF (OSPW)</b>	0.00011	0.36	0.89	-1.47	-0.017	0.91

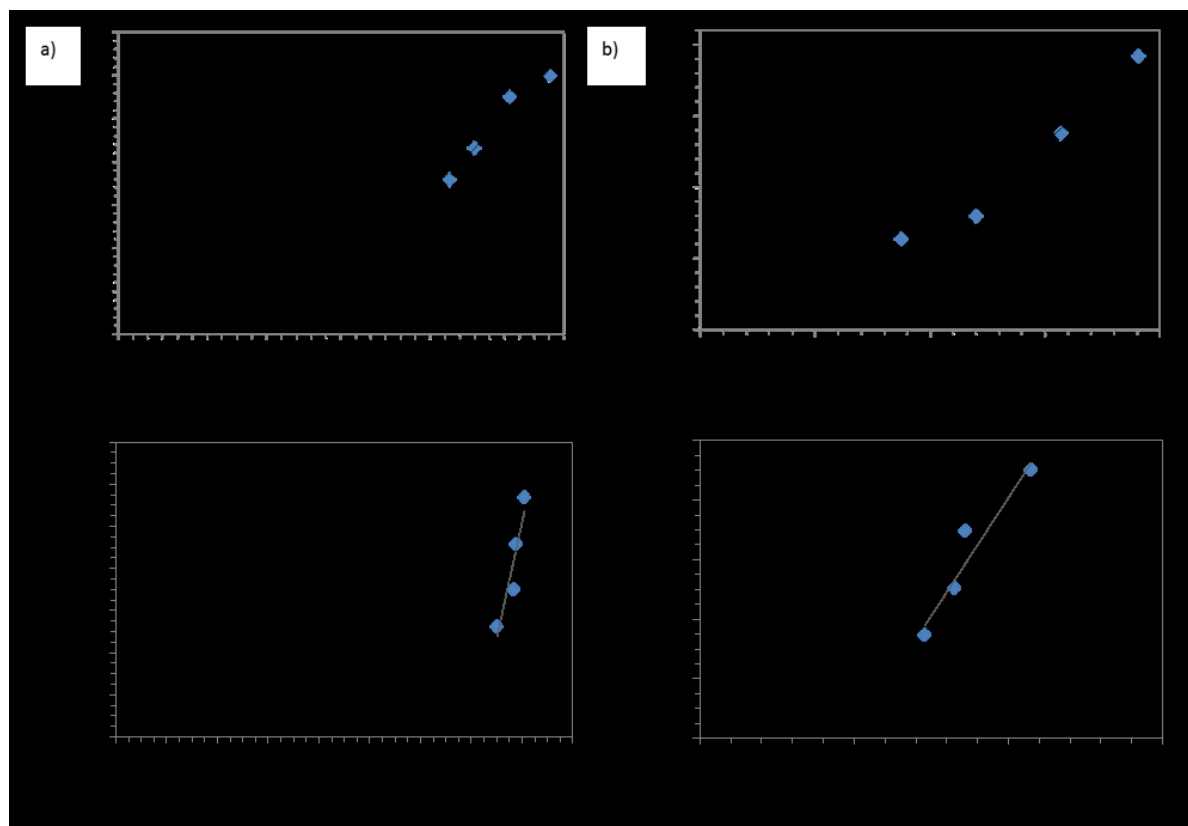


**Figure 5-4.** Freundlich adsorption isotherm (a & c) and Langmuir adsorption isotherm (b & d) for the acid extractable fraction from Merichem NAs solution ( $C_i=50.3 \pm 0.7$ ) (a & b) and OSPW ( $C_0=50.6 \pm 1.2$ ) (c & d) (FTIR results)

The Merichem NAs distributions before and after adsorption are shown in Figure 5-5a,b. The x-axis represents the carbon number and z-axis represents hydrogen deficiency ( $-Z$ ) where  $-Z/2$  represents the number of rings for each NA. Merichem NAs have the most significant concentrations for linear ( $-Z = 0$ ), one ( $-Z = 2$ ), two ( $-Z = 4$ ) and three ( $-Z = 6$ ) ring compounds (total NAs = 41.7 mg/L). In contrast, compounds with four ( $-Z = 8$ ), five ( $-Z = 10$ ) and six ( $-Z = 12$ ) rings have very low initial concentrations  $< 0.15$  mg/L each. These latter compounds were not considered for the following calculations for removal efficiencies due to concentrations approaching or below instrumental detection limits. For OSPW, the distribution of NAs is

diverse but markedly different from the Merichem NAs (Figure 5-6a,b). The insignificant concentrations ( $< 0.10$  mg/L) of linear ( $-Z = 0$ ) and one ( $-Z = 2$ ) ring compounds before adsorption did not allow the consideration of their removal efficiencies as for the Merichem NAs at low concentrations.

Given the diversity of NAs in the two mixtures, the discussion of removal efficiencies may be simplified by considering the removal % of NAs concentrations calculated using the initial ( $C_0$ ) and final ( $C_i$ ) concentrations after adsorption by  $[(C_0 - C_i)/C_0]$  according to individual carbon number and  $-Z$  number (Figures 5-5c and 5-6c). For the Merichem NAs, there was an increasing removal % with increasing carbon number at a constant  $-Z$ ; however, NAs of carbon numbers  $> 16$  were completely removed regardless of  $-Z$  values (Figure 5-5c).

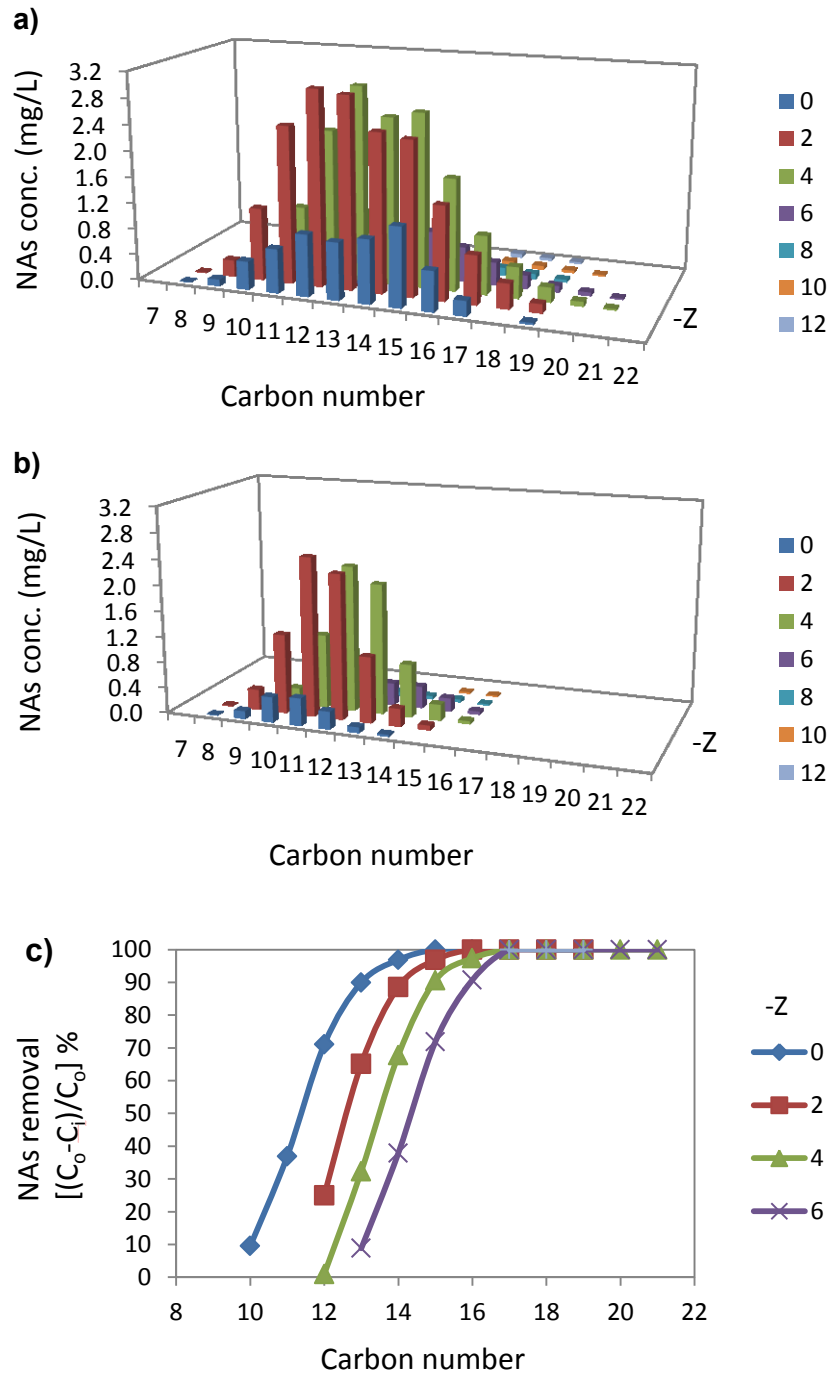


**Figure 5-5.** NAs distribution in Merichem solution ( $C_i = 43$  mg/L) a) before adsorption b) after adsorption after mixing with 2.5 g/L EG for 24 hours and c) % removal of NAs (see text for further details)

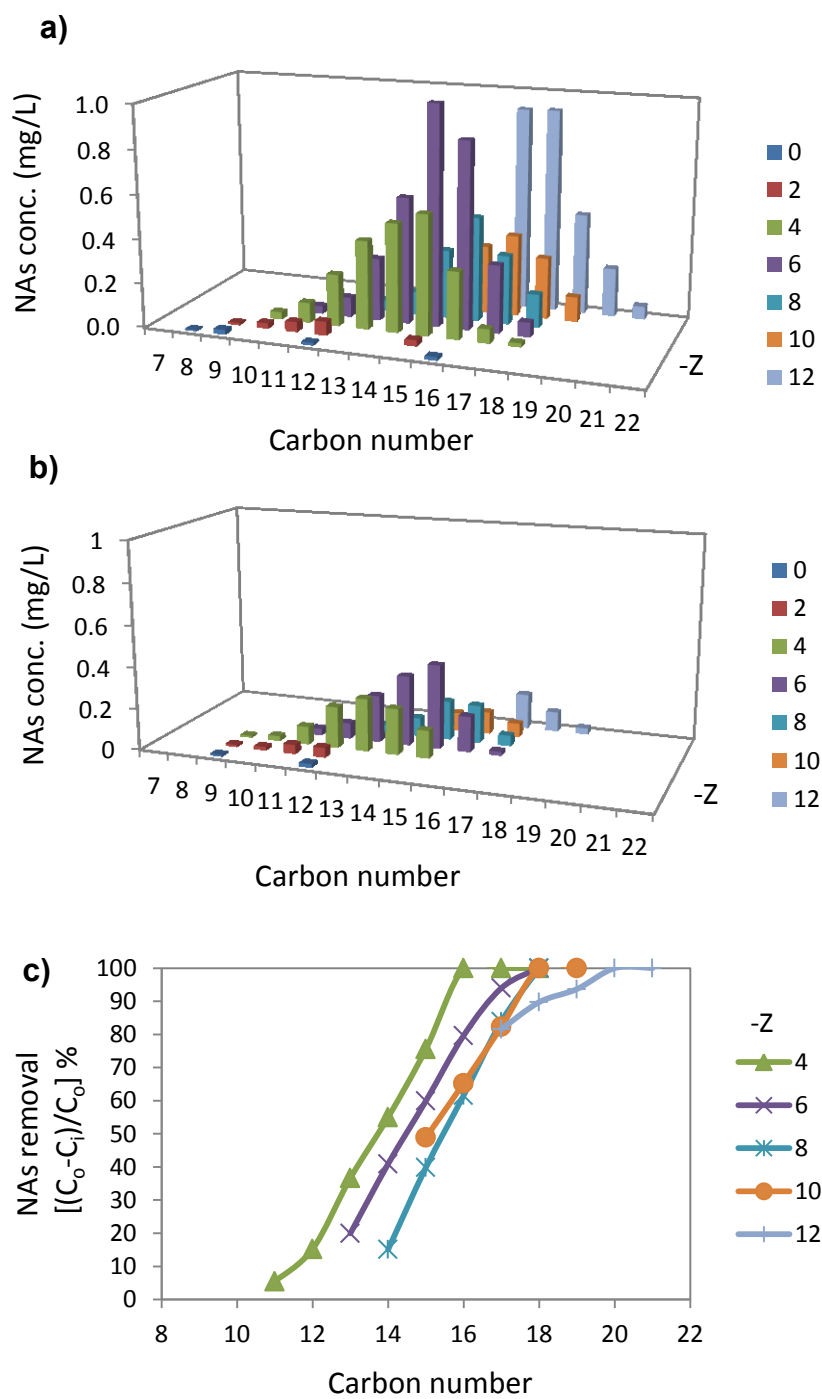


**Figure 5-6.** NAs distribution in OSPW solution ( $C_i = 10.9$  mg/L) a) before adsorption b) after adsorption after mixing with 2.5 g/L EG for 24 hours and c) % removal of NAs (see text for further details).

In addition, the linear compounds ( $Z = 0$ ) for the Merichem NAs have the highest removal % with over 70% removal for carbon numbers  $\geq 12$ . With a constant carbon number, the removal of NAs decreased as the number of rings increased. For example, at carbon number = 12 the  $Z = 0$  NAs had 70% removal while the  $Z = 4$  NAs had no removal. For the OSPW NAs, the observed removal % trends were similar to the Merichem NAs. However, fewer compounds were completely removed for the OSPW NAs than those for Merichem NAs (Figure 5-6c).

The trend of NAs removal for Merichem (Figure 5-5c) and OSPW (Figure 5-6c) NAs may be further explained using their hydrophobicity as determined by Log  $K_{ow}$  values. The theoretical Log  $K_{ow}$  values for the majority of the NAs indicated in Figures 5-5 and 5-6 were identified based on the values of  $n$ ,  $-Z$  and calculated molecular weight using the ChemSpider chemical database (<http://www.chemspider.com>; accessed October, 15, 2014) and plotted in Figure 5-7 [30]. The use of calculated Log  $K_{ow}$  values was needed given that few measured values are available for NAs of lower number of rings (0, 1, 2 and 3), while, little or no information on measured values are available for NAs of higher number of rings (4, 5 and 6). Clearly, there is an increasing trend of Log  $K_{ow}$  values with increasing carbon number for each  $Z$ -value series (Figure 5-7). Thus, the higher the Log  $K_{ow}$  values, the higher the removal % of NAs shown in Figures 5-5c and 5-6c. In addition, for NAs with similar carbon numbers the lower the number of rings (lower  $Z$  values) the higher are the Log  $K_{ow}$  value, and the higher the removal % of NAs. Clearly, the hydrophobicity as indicated by Log  $K_{ow}$  values is playing a critical role in the adsorption of the NAs in both Merichem and OSPW mixtures. To further understand this adsorption, additional experiments were considered including the monitoring of individual carbon number species over time in an attempt to elucidate the adsorption mechanisms.

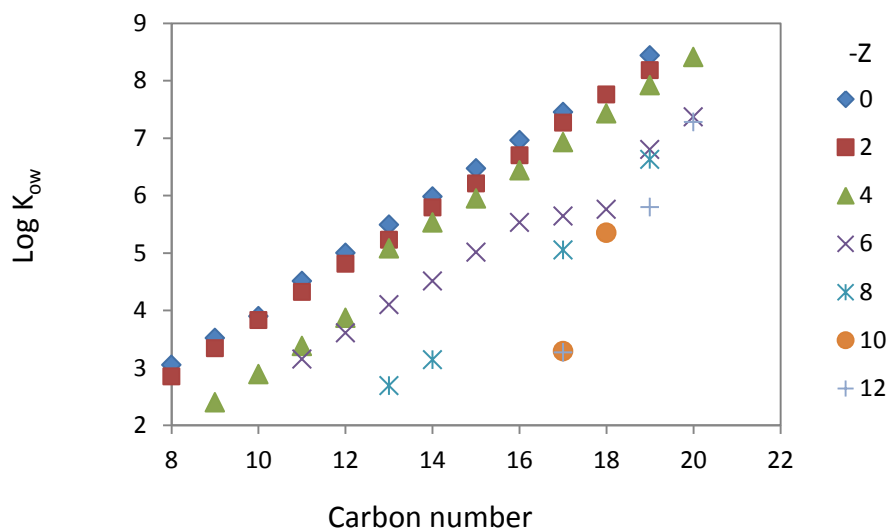


**Figure 5-7.** The Log  $K_{ow}$  of expected NAs in Merichem solution and OSPW

The competition for adsorption sites between Merichem NAs with the same carbon number but different -Z number (i.e.,  $C_{14}$ ,  $C_{15}$  and  $C_{16}$  NAs) were monitored for 24 hours (Figure 5-8). Exceptionally high adsorption kinetics were observed after the first 5 minutes for all carbon numbers which was expected given the large pores sizes of the EG surface that assist the molecular diffusion [24]. Overall, the removal % increased according to the order  $C_{16} > C_{15} > C_{14}$  and decreased according to ( $Z = 8 < 6 < 4 < 2 < 0$ ). Close to 100% removal was observed for  $Z = 0$  for all n values,  $Z = 2$  for  $C_{15}$  and  $C_{16}$ , and  $Z = 4$  for  $C_{16}$ , these results indicate increasing removals with increasing carbon numbers and decreasing Z numbers which corroborates the previous discussion. The OSPW NAs were also evaluated considering the adsorption competition for  $C_{14}$ ,  $C_{15}$  and  $C_{16}$  NAs (Figure 5-9). As for the Merichem NAs, the adsorption kinetics were high initially after the first 10 minutes; however, the removal % were much lower for the OSPW NAs versus the analogous Merichem NAs which confirms the obtained values of the K parameter in the Freundlich equation (Table 5-3). Given the lack of  $Z = 0$  and  $Z = 2$

species in the OSPW NAs, comparisons between the Merichem and OSPW NAs can be made using the  $Z \geq 4$  species. For any carbon number the removals are at least 25% higher for the Merichem versus OSPW species. The lower removals for the OSPW NAs may be due to the presence of more constituents in OSPW matrix than in the Merichem which may be in direct competition with the NAs for the adsorption sites [31].

Overall, it is experimentally confirmed in the current study that removal of NAs (model compounds, Merichem and OSPW) followed the  $\text{Log } K_{ow}$  values which can lead to the assignment of the NAs removals to the hydrophobic interaction between the NAs and EG. However, at alkaline pH values of the current solutions (pH 8 to 8.7) there is a negative surface charge for EG due to the deprotonation of surface functional groups (C-OH and O=C-OH) as confirmed by zeta potential measurements ( $-25.6 \pm 2.3$  mV) [14]. In addition, NAs are weak acids that are 99.9% ionized at these pH values making them negatively charged [14]. Both of these conditions would indicate that adsorption of NAs on EG would be unlikely to occur thermodynamically due to electrostatic repulsion. However, this unexpected behaviour has been noted previously (as discussed in the following section) and has been attributed to -CAHB which mitigates the adsorption of weak acids onto carbon adsorbents [6, 14, 32, 33].

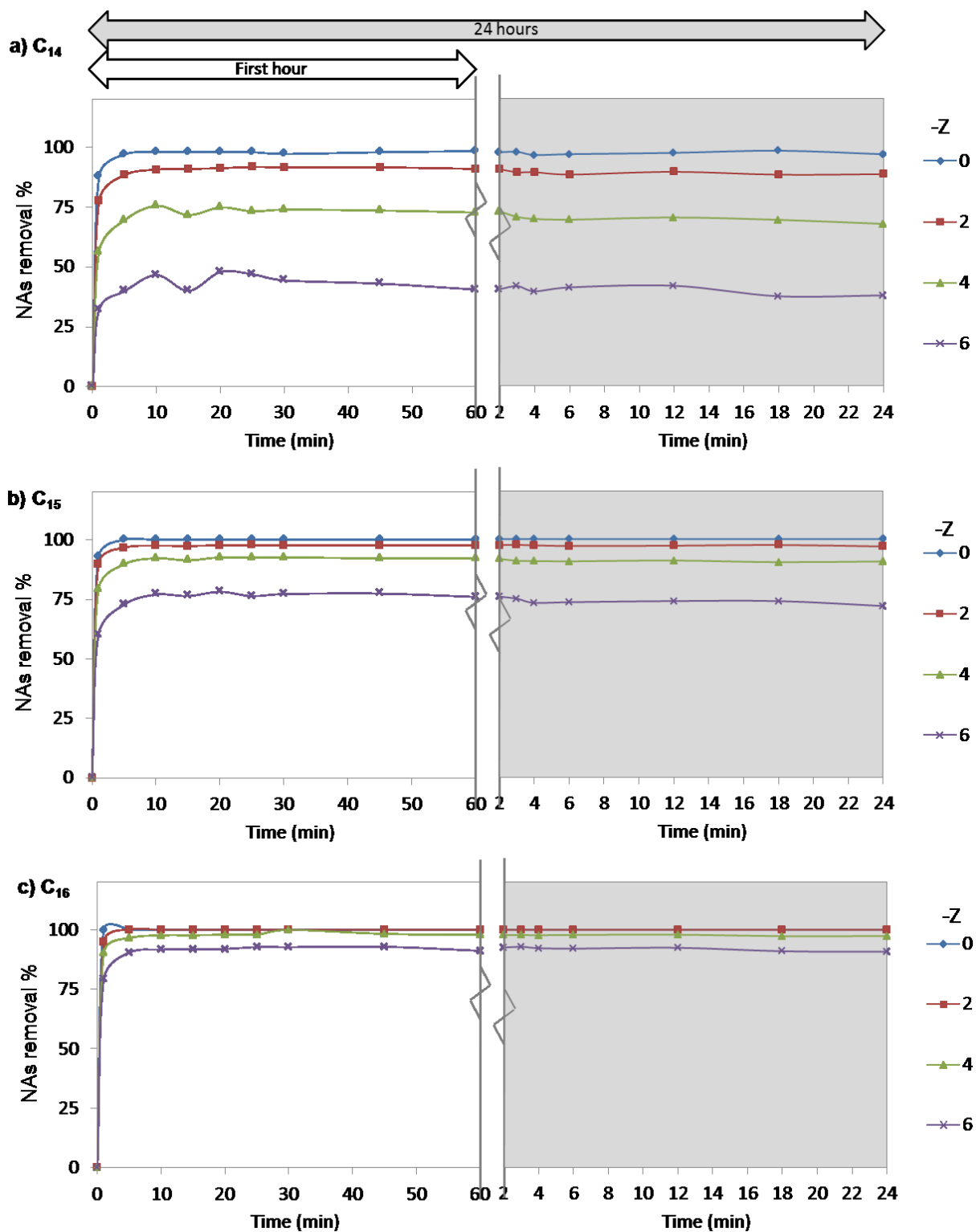


**Figure 5-8.** Impact of number of rings (-Z) on the removal of a) C<sub>14</sub>, b) C<sub>15</sub> and c) C<sub>16</sub> NAs in the Merichem solution during the mixing with EG for 24 hours.

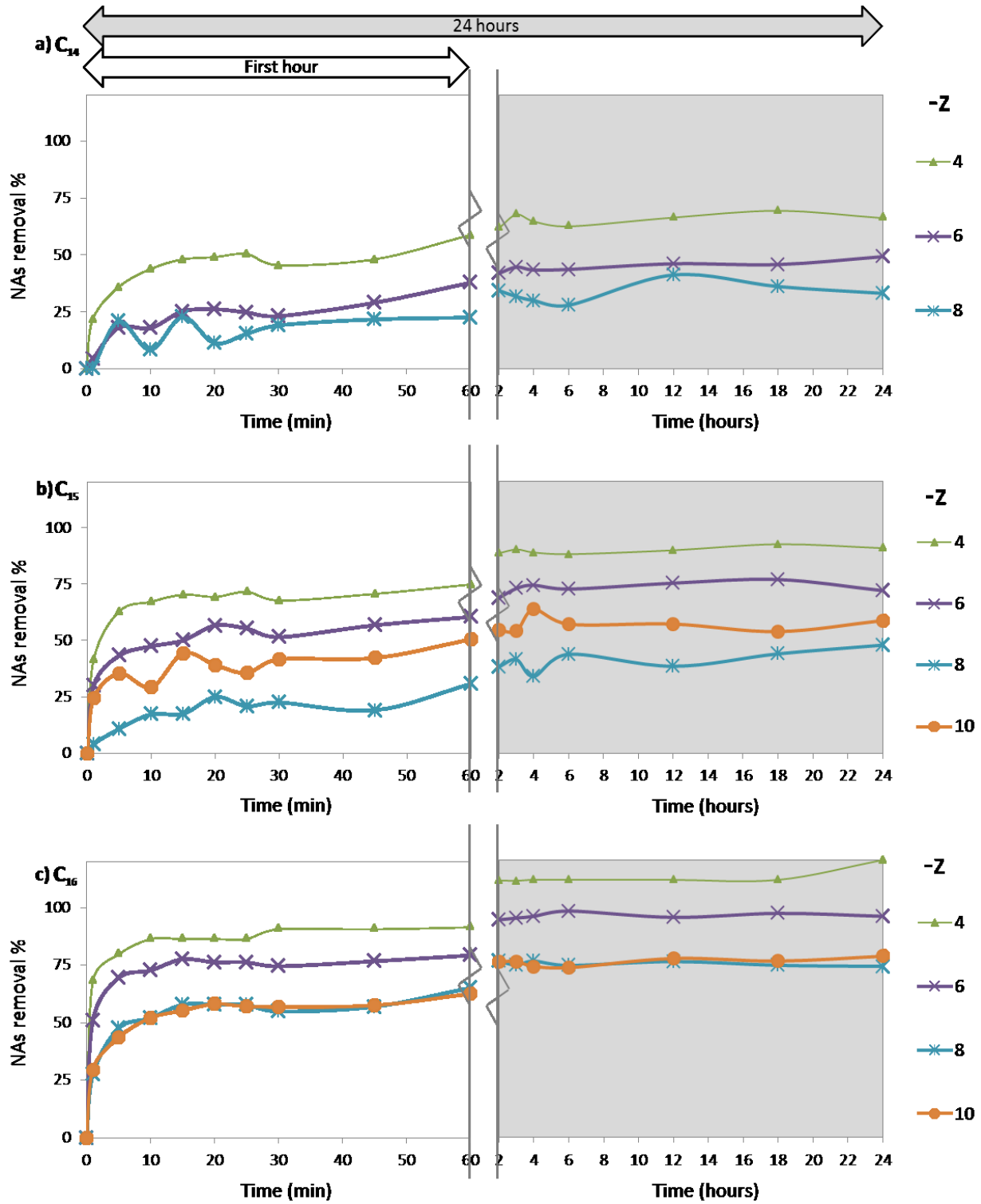
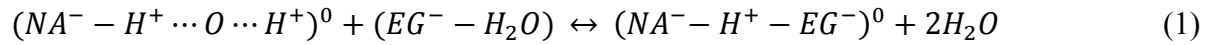


**Figure 5-9.** The impact of the number of rings (-Z) on the removal of a) C<sub>14</sub>, b) C<sub>15</sub> and c) C<sub>16</sub> NAs in OSPW during the mixing with EG for 24 hours

### 5.3.4 Thermodynamics of adsorption of model compounds.

We presented the full derivation of the thermodynamics theory for –CAHB in Chapter 2. In this section only a brief overview of this theory relevant to the current study will be presented according to the schematic shown in Figure 5-10. As a solvent, the concentration of water is high enough to allow water molecules to outcompete NAs trying to bond with the EG surface [34]. This competition is shown moving from before adsorption to after adsorption in Figure 5-10, namely [14] :



Prior to adsorption (Figure 5-10), the free energy required for –CAHB formation ( $\Delta G^{-CAHB}$ ) needs to overcome water competition for the adsorption sites at  $\Delta G_{H_2O}^{HB} = -40$  kJ mo/L for each of  $DA^-$ , Trans-4-IsoPCHA $^-$  and Trans-4-PCHA $^-$ , in addition to the solvation energy in water of  $\Delta G_{Solv} = -52.8$  kJ mo/L for  $DA^-$  and  $-52.4$  kJ mole $^{-1}$  for Trans-4-IsoPCHA $^-$  and Trans-4-PCHA $^-$ , respectively as explained in Chapter 2. Thus, for adsorption to happen the following relationship needs to occur:

$$\Delta G^{-CAHB} > \Delta G_{Solv} > \Delta G_{H_2O}^{HB} \quad (2)$$

The  $\Delta G^{-CAHB}$  has not been determined previously for the current compounds, however, reported  $\Delta G^{-CAHB}$  values were found to rely on the  $pK_a$  difference of the bonded species with  $\Delta G^{-CAHB} = -50.2$  kJ mole $^{-1}$  observed for acetate/phenol having a  $\Delta pK_a = 5.2$  and  $-56.2$  kJ mole $^{-1}$  for carboxyl/carboxyl having a  $\Delta pK_a = 0$  [33]. Based on our previous study (where other compounds with similar  $pK_a$  values did not adsorb on graphite),  $\Delta G^{-CAHB}$  values for the current compounds are expected to be  $\Delta G^{-CAHB} = -50.2$  kJ mole $^{-1}$  (Figure 5-10) [11, 14, 35, 36]. Clearly, this  $G^{-CAHB}$  does not exceed the required  $\Delta G_{Solv}$  for any of the current NAs and more energy is required for

the NAs to bond to the EG surface. To achieve this extra energy, it has been suggested that a portion of the increase in the hydrophobicity of NAs due to proton exchange of  $NA^-$  with water (hydrophobic free energy) could contribute to the energy gain required for the  $-CAHB$  formation (Figure 5-10). Using  $K_{ow}$  as a hydrophobicity surrogate, the following equation describes the hydrophobic free energy ( $\Delta G_{Hydrophobicity}$ ):

$$\Delta G_{Hydrophobicity} = -RT \ln \left[ \frac{K_{ow} NA}{K_{ow} NA^-} \right] \quad (3)$$

Therefore, using values found in Table 5-2 the  $\Delta G_{Hydrophobicity} = -18.3, -18.1$  and  $-18.1, \text{ kJ mole}^{-1}$  for  $DA^0$ ,  $Trans-4-IsoPCHA^0$  and  $Trans-4-PCHA^0$ , respectively. However, the contributions of the  $\Delta G_{Hydrophobicity}$  for each  $NA^0$  toward  $-CAHB$  formation will not be equal since they depend on the water affinity (as expressed by  $\text{Log } K_{ow}$ ) and bond lengths of each NA [37, 38]. However, the assumption of equal bond lengths can be made for the current NAs and using the  $\text{Log } K_{ow}$  values from Table 5-2, the partial contribution of  $\Delta G_{Hydrophobicity}$  ( $\Delta\Delta G_{Hydrophobicity}$ ) would be expected to follow  $DA^0 > Trans-4-PCHA^0 > Trans-4-IsoPCHA^0$ . Finally, the result of this new contribution to  $-CAHB$  creates a total free energy gain  $\Delta G_{Total} = \Delta\Delta G_{Hydrophobicity} + \Delta G^{-CAHB}$  shown in Figure 5-10, which can be substituted into eq. 2 as:

$$\Delta G_{Total} > \Delta G_{Solv} > \Delta G_{H_2O}^{HB} \quad (4)$$

Given the similar  $\Delta G^{-CAHB}$  values for the current model NAs, the  $\Delta G_{Total}$  values would be  $DA^0 > Trans-4-PCHA^0 > Trans-4-IsoPCHA^0$  which is confirmed by the currently observed and previous adsorption results [14] and following the same trend of  $\text{Log } K_{ow}$  for those compounds.

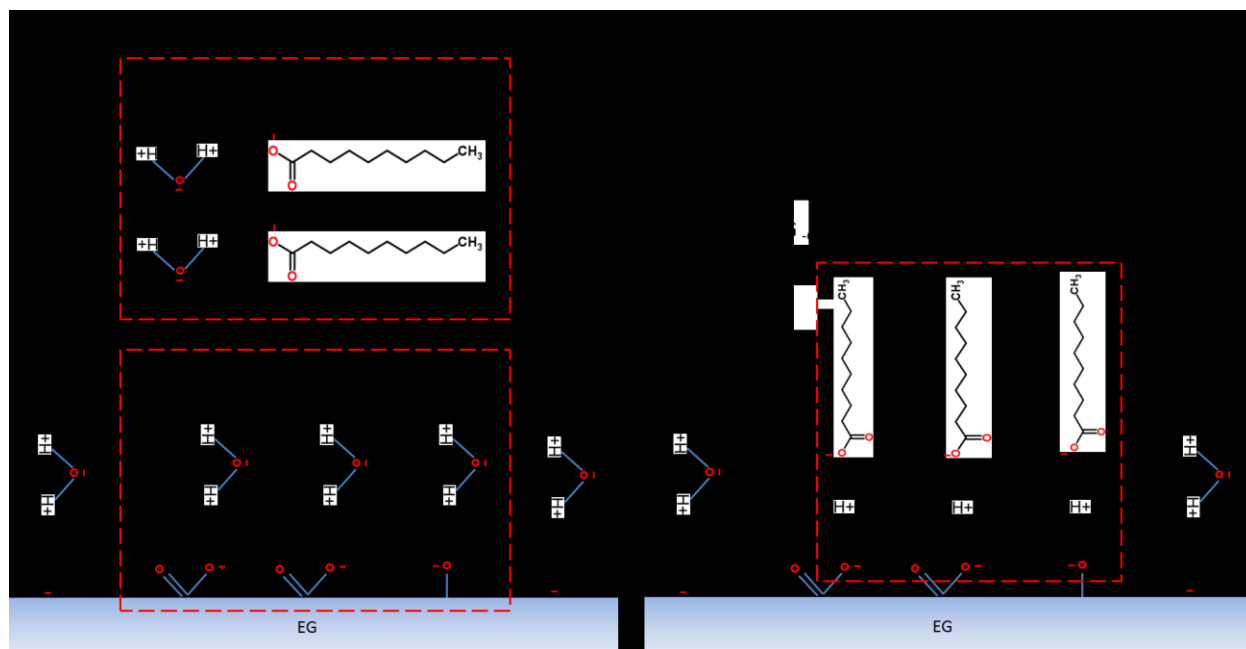


**Figure 5-10.** Schematics for EG surface molecular properties in water and Gibbs free energies before and after adsorption.

### 5.3.5 Thermodynamics of adsorption of NAs in Merichem and OSPW.

Following the previous discussion, the thermodynamics of adsorption for the Merichem and OSPW NAs can also be determined for the  $-CAHB$ . Given the  $pK_a$  values of Merichem and OSPW NAs are around 5 [39] then the average solvation free energy at  $pH \geq 8$  will be:

$$\Delta G_{Solv} (Merichem/ospw) = -RT \ln \left[ \frac{K_{a\ water}}{K_{a\ NA}} \right] = -51.3 \text{ kJ mole}^{-1} \quad (5)$$

Accordingly, the  $\Delta G^{-CAHB} = -50.2 \text{ kJ mole}^{-1}$  for the current NAs is not enough thermodynamically to allow the adsorption via  $-CAHB$  making extra energy required for this bonding to occur. As explained previously, a portion of the increase in the hydrophobicity of NAs due to proton exchange of  $NA^-$  with water in the  $-CAHB$  contributes to the energy gain required for the bond formation. For the current discussion, the lowest  $\text{Log } K_{ow}$  values for the

Merichem and OSPW NAs (Figure 5-7) was considered given it will result in the lowest, most conservative calculated  $\Delta G_{Hydrophobicity}$ . All other NAs will have higher calculated  $\Delta G_{Hydrophobicity}$  values, which will result in a greater contribution to the  $\Delta G_{Total}$ . The lowest Log  $K_{ow}$  value is for the two ringed compound (NA =  $C_9H_{14}O_2$ ) (Figure 5-11) calculated at 1.97 at pH 7 and -1.2 at pH 8 (<http://archemcalc.com/sparc/index>; accessed December, 15, 2014). Thus:

$$\Delta G_{Hydrophobicity} = -RT \ln \left[ \frac{K_{ow NA}}{K_{ow NA^-}} \right] = -18 \text{ kJ mole}^{-1} \quad (6)$$

Accordingly, the lowest  $\Delta G_{Total}$  for  $C_9H_{14}O_2$ ,  $\Delta G^{-CAHB} + \Delta \Delta G_{Hydrophobicity}$  ( $-50.2 \text{ kJ mole}^{-1}$  plus a portion of  $-18 \text{ kJ mole}^{-1}$ ) is higher than the constant  $\Delta G_{Solv} = -51.3 \text{ kJ mo/L}$  for NAs in Merichem and OSPW. Thermodynamics calculations are in pronounced agreement with our observation for the removal of NAs shown in Figures 5-5c and 5-6c that follows Log  $K_{ow}$  values in Figure 5-7. Consequently, it is confirmed that the  $-CAHB$  governs the interaction of ionized NAs with functionalized surfaces in Merichem and OSPW mixture in the current study.

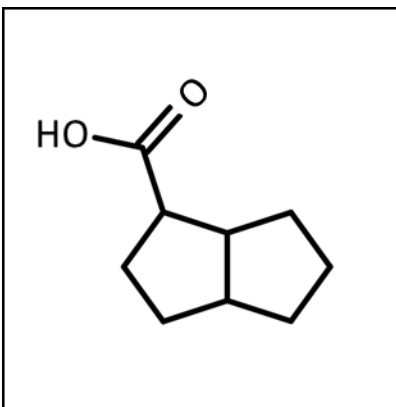


**Figure 5-11.** Expected structure for the  $C_9H_{14}O_2$  (octahydro-1-pentalenecarboxylic acid) in the Merichem mixture as obtained from Chemspider accessed accessed December, 15, 2014

## 5.4 Conclusions.

The adsorption behaviour of ionized weak acids on negatively charged functionalized graphite surfaces was reported for mono-compound solutions and three different mixtures with varied complexities. The results showed that -CAHB is the thermodynamically proven mechanism for adsorption of these ionized weak acids on graphite. Since the  $pK_a$  values of the individual NAs are all similar ( $\Delta pK_a \sim 0$ ), the bond formation relies on the gain in hydrophobic free energy ( $\Delta G_{\text{Hydrophobicity}}$ ) due to proton exchange of  $NA^-$  with water in the -CAHB resulting in higher energy than the  $\Delta G_{\text{Solv}}$ . This was also validated as the NAs adsorption increased with increasing  $\text{Log } K_{ow}$  values. The presence of a large number of NAs species in complex mixtures such as the current Merichem solution and OSPW did not impact the reported mechanism. This work is essential for the development of possible engineered adsorbents for the removal of ionized weak acids from contaminated natural water streams, groundwater and waste waters. It is also contributing to the understanding of the fate and transports of such compounds in the environments as affected by graphene constituents released to natural water streams.

## 5.5 References.

- [1] Chowdhury I, Duch MC, Mansukhani ND, Hersam MC, Bouchard D. Colloidal Properties and Stability of Graphene Oxide Nanomaterials in the Aquatic Environment. *Environmental Science & Technology* 2013;47:6288-6296.
- [2] Compton OC, Nguyen ST. Graphene Oxide, Highly Reduced Graphene Oxide, and Graphene: Versatile Building Blocks for Carbon-Based Materials. *Small* 2010;6:711-723.
- [3] Liu S, Zeng TH, Hofmann M, Burcombe E, Wei J, Jiang R, et al. Antibacterial Activity of Graphite, Graphite Oxide, Graphene Oxide, and Reduced Graphene Oxide: Membrane and Oxidative Stress. *Acc Nano* 2011;5:6971-6980.
- [4] Pei Z, Li L, Sun L, Zhang S, Shan X-q, Yang S, et al. Adsorption characteristics of 1,2,4-trichlorobenzene, 2,4,6-trichlorophenol, 2-naphthol and naphthalene on graphene and graphene oxide. *Carbon* 2013;51:156-163.
- [5] Gao Y, Li Y, Zhang L, Huang H, Hu J, Shah SM, et al. Adsorption and removal of tetracycline antibiotics from aqueous solution by graphene oxide. *Journal of Colloid and Interface Science* 2012;368:540-546.
- [6] Teixido M, Pignatello JJ, Beltran JL, Granados M, Peccia J. Speciation of the Ionizable Antibiotic Sulfamethazine on Black Carbon (Biochar). *Environmental Science & Technology* 2011;45:10020-10027.
- [7] Maliyekkal SM, Sreeprasad TS, Krishnan D, Kouser S, Mishra AK, Waghmare UV, et al. Graphene: A Reusable Substrate for Unprecedented Adsorption of Pesticides. *Small* 2013;9:273-283.
- [8] Xu J, Wang L, Zhu Y. Decontamination of Bisphenol A from Aqueous Solution by Graphene Adsorption. *Langmuir* 2012;28:8418-8425.
- [9] Wang J, Chen Z, Chen B. Adsorption of Polycyclic Aromatic Hydrocarbons by Graphene and Graphene Oxide Nanosheets. *Environmental Science & Technology* 2014;48:4817-4825.
- [10] Yang K, Wu W, Jing Q, Zhu L. Aqueous Adsorption of Aniline, Phenol, and their Substitutes by Multi-Walled Carbon Nanotubes. *Environmental Science & Technology* 2008;42:7931-7936.
- [11] Li X, Pignatello JJ, Wang Y, Xing B. New Insight into Adsorption Mechanism of Ionizable Compounds on Carbon Nanotubes. *Environmental Science & Technology* 2013;47:8334-8341.
- [12] Ni J, Pignatello JJ, Xing B. Adsorption of Aromatic Carboxylate Ions to Charcoal Black Carbon is Accompanied by Proton Exchange with Water (vol 45, pg 9240, 2012). *Environmental Science & Technology* 2012;46:5633-5633.
- [13] Hyun S, Lee LS. Hydrophilic and hydrophobic sorption of organic acids by variable-charge soils: Effect of chemical acidity and acidic functional group. *Environmental Science & Technology* 2004;38:5413-5419.
- [14] Moustafa A, McPherdan K, Moreira J, Gamal El-Din M. Investigation of Mono/Competitive Adsorption of Environmentally Relevant Ionized Weak Acids on Graphite: Impact of Molecular Properties and Thermodynamics. *Environmental Science & Technology* 2014;48:14472-14480.
- [15] Fontecha-Camara MA, Lopez-Ramon MV, Alvarez-Merino MA, Moreno-Castilla C. Effect of surface chemistry, solution pH, and ionic strength on the removal of herbicides diuron and amitrole from water by an activated carbon fiber. *Langmuir* 2007;23:1242-1247.
- [16] Vinu A, Hossain KZ, Kumar GS, Ariga K. Adsorption of L-histidine over mesoporous carbon molecular sieves. *Carbon* 2006;44:530-536.
- [17] MacKinnon M, Van Meer T, Verbeek A. Assessment of biological impact from a wet landscape option for the reclamation of fine tails from oil sands. *Canadian Technical Report of Fisheries and Aquatic Sciences* 1993;0:258.

- [18] Mackinnon MD, Retallack JT. Preliminary characterization and de toxification of tailings pond water at the syncrude canada limited oil sands plant. Proceedings of the 4th Annual Meeting of the International Society of Petroleum Industry Biologists, 1981 1982:P185-210.
- [19] Allen EW. Process water treatment in Canada's oil sands industry: I. Target pollutants and treatment objectives. *Journal of Environmental Engineering and Science* 2008;7:123-138.
- [20] Scott AC, MacKinnon MD, Fedorak PM. Naphthenic acids in athabasca oil sands tailings waters are less biodegradable than commercial naphthenic acids. *Environmental Science & Technology* 2005;39:8388-8394.
- [21] Clemente JS, Fedorak PM. A review of the occurrence, analyses, toxicity, and biodegradation of naphthenic acids. *Chemosphere* 2005;60:585-600.
- [22] Chen GH, Wu DJ, Weng WG, Yan WL. Dispersion of graphite nanosheets in a polymer matrix and the conducting property of the nanocomposites. *Polymer Engineering and Science* 2001;41:2148-2154.
- [23] Lashaki MJ, Fayaz M, Niknaddaf S, Hashisho Z. Effect of the adsorbate kinetic diameter on the accuracy of the Dubinin-Radushkevich equation for modeling adsorption of organic vapors on activated carbon. *Journal of Hazardous Materials* 2012;241:154-163.
- [24] Pelekani C, Snoeyink VL. Competitive adsorption in natural water: Role of activated carbon pore size. *Water Research* 1999;33:1209-1219.
- [25] Krawczyk P. Effect of ozone treatment on properties of expanded graphite. *Chemical Engineering Journal* 2011;172:1096-1102.
- [26] Langmuir I. The adsorption of gases on plane surfaces of glass, mica and platinum. *Journal of the American Chemical Society* 1918;40:1361-1403.
- [27] Behera SK, Oh S-Y, Park H-S. Sorption of triclosan onto activated carbon, kaolinite and montmorillonite: Effects of pH, ionic strength, and humic acid. *Journal of Hazardous Materials* 2010;179:684-691.
- [28] Kumar PS, Vincent C, Kirthika K, Kumar KS. Kinetics and equilibrium studies of pb<sup>2+</sup> ion removal from aqueous solutions by use of nano-silversol-coated activated carbon. *Brazilian Journal of Chemical Engineering* 2010;27:339-346.
- [29] Halsey G, Taylor HS. The adsorption of hydrogen on tungsten powders. *Journal of Chemical Physics* 1947;15:624-630.
- [30] Pourrezaei P, Alpatova A, Chelme-Ayala P, Perez-Estrada LA, Jensen-Fontaine M, Le XC, et al. Impact of petroleum coke characteristics on the adsorption of the organic fractions from oil sands process-affected water. *International Journal of Environmental Science and Technology* 2014;11:2037-2050.
- [31] Wang H, Lashaki MJ, Fayaz M, Hashisho Z, Philips JH, Anderson JE, et al. Adsorption and Desorption of Mixtures of Organic Vapors on Beaded Activated Carbon. *Environmental Science & Technology* 2012;46:8341-8350.
- [32] Moreno-Castilla C. Adsorption of organic molecules from aqueous solutions on carbon materials. *Carbon* 2004;42:83-94.
- [33] Ni H-G, Zeng H, Zeng EY. Sampling and analytical framework for routine environmental monitoring of organic pollutants. *Trac-Trends in Analytical Chemistry* 2011;30:1549-1559.
- [34] Maity N, Payne GF. Adsorption from aqueous-solutions based on a combination of hydrogen-bonding and hydrophobic interactions. *Langmuir* 1991;7:1247-1254.
- [35] Gilli G, Gilli P. Towards an unified hydrogen-bond theory. *Journal of Molecular Structure* 2000;552:1-15.
- [36] Gilli P, Pretto L, Bertolasi V, Gilli G. Predicting Hydrogen-Bond Strengths from Acid-Base Molecular Properties. The pK(a) Slide Rule: Toward the Solution of a Long-Lasting Problem. *Accounts of Chemical Research* 2009;42:33-44.

- [37] Lum K, Chandler D, Weeks JD. Hydrophobicity at small and large length scales. *Journal of Physical Chemistry B* 1999;103:4570-4577.
- [38] Mittal J, Hummer G. Interfacial thermodynamics of confined water near molecularly rough surfaces. *Faraday Discussions* 2010;146:341-352.
- [39] Kaur K, Bhattacharjee S, Pillai R, Ahmed S, Azmi S. Peptide arrays for detecting naphthenic acids in oil sands process affected water. *RSC Advances* 2014;4:60694-60701.

## 6 CONCLUSIONS AND RECOMMENDATIONS

### 6.1 Thesis overview

An enormous amount of fresh water is used for the extraction of bitumen from the oil sands deposits in northern Alberta. By the end of 2015, the expected production of bitumen is around 4.5 million barrel per day resulting in over 500 million m<sup>3</sup>/year of water consumption taken from the Athabasca River. OSPW recycling for further re-use in bitumen extraction reduces the dependency on these fresh waters. However, it leads to a significant reduction in the OSPW quality and leaves it with higher concentrations of NAs which will need to be treated before release into receiving environments. Currently, OSPW is being stored in vast tailings ponds until economically feasible and environmentally-safe treatment processes are available prior to its release. Several treatment techniques have been considered previously for the removal of NAs including membrane filtration, advanced oxidation, biological treatment, constructed wetland, and adsorption. Currently, the consideration of the potential for biological treatment prior to adsorption was considered.

The research herein, focused on the understanding of mechanisms governing the adsorption of NAs on carbonaceous materials. The currently considered adsorbent was EG that contains mesopores which will not allow for the removal of NAs due to size. The 0.45 µm membrane filters normally used to remove the suspended solids from OSPW prior to NAs analysis were evaluated prior to the assessment of adsorption behaviour given losses found in preliminary research work. Following this work, the adsorption behaviour of 5 model NA compounds onto EG in mono/multi compounds solutions were assessed both experimentally and thermodynamically to elucidate the adsorption mechanism. To visualize and characterize the model NAs adsorption on the surface of HOPG, a novel AM-FM-AFM technique was used.

Based on the understanding of the model NAs adsorption on EG and HOPG and the calculated thermodynamics, the adsorption of NAs from complex matrices including Merichem mixture and OSPW were investigated with the mechanism of adsorption assessed and reported.

## **6.2 Conclusions**

The following conclusions were established based on the current research:

### **6.2.1 Chapter 2: Preliminary membrane study**

- The use of membranes for removal of insoluble compounds before NAs quantification can bias the results especially at pH values  $< 6.2$ . The presence of OSPW constituents with  $pK_a \sim 5$  to  $6$  (suggested to be NAs) can be protonated at  $pH < 6.2$  resulting in the reduction of NAs solubility and reduced NAs concentration in the filtrates. Thus OSPW and other commercial mixtures should be filtered at alkaline pH values similar to the pH of natural OSPW ( $\sim 8.0$ ).
- The nylon membranes were the most hydrophilic among tested membranes with a contact angle of  $34.5 \pm 3.1$  as compared to PTFE membrane ( $82.0 \pm 5.5$ ) and the PVDF membrane ( $69.8 \pm 1.5$ ). The nylon membranes were found to be the most efficient for filtration of insoluble compounds from OSPW at its natural pH without impacting the AEF quantification and removing an insignificant amount of the NAs.
- The use of similar membrane filters for OSPW and a Merichem NAs solution (originally contain the same concentrations of AEF) did not result in comparable AEF concentrations (no removal for AEF in OSPW but more than 20% removal for Merichem solutions). Therefore, the use of membranes for filtration of any wastewaters with high organic content for the quantification analysis of organics

should be thoroughly investigated before their application. This is including but not limited to the tailings water for the conventional oil and gas industries and contaminated groundwater impacted by leaking underground and above ground storage tanks.

### 6.2.2 Chapters 3, 4 and 5: Adsorption study

- Adsorption of NAs followed their Log  $K_{ow}$  values (i.e., higher adsorption with higher  $K_{ow}$ ), despite the complete dissociation of the current model NAs and the negative zeta potential of EG ( $-25.6 \pm 2.3$  mV). It was concluded that hydrophobic interaction has a vital role in adsorption but cannot govern the adsorption mechanism.
- The  $-CAHB$  between the negatively charged groups of NAs and the negatively charged FG on adsorbent surface governs the SAL formation. Three compounds, DA, Trans-4-IsoPCHA and Trans-4-PCHA, were adsorbed, in spite of  $\Delta G^{-CAHB}$  values being lower than  $\Delta G_{Solv} = -52.8$  kJ mole<sup>-1</sup>. The increase in the hydrophobicity of NAs due to proton exchange of  $NA^-$  with water could contribute to the energy gain required for the  $-CAHB$  formation. Consequently, two other model NAs with lower Log  $K_{ow}$  values (lower hydrophobicity), CHA and HPA, did not show significant adsorption on EG.
- This study leads to the elucidation of possible methods for multilayer formation of NAs on adsorbent surfaces via the initial  $-CAHB$  followed by subsequent hydrophobic bonding with the  $CH_3$  ends of the SAL.

- Structure reactivity could influence the adsorption of some acids temporarily before equilibrium is reached. For example, after 6 hours of adsorption there was negligible removal of Trans-4-PCHA compared to 52% removal of Trans-4-IsoPCHA which was not expected given the higher  $\Delta G_{\text{Total}}$  for Trans-4-PCHA. The presence of two  $\text{CH}_3$  groups at the hydrophobic end of the Trans-4-IsoPCHA, as compared to only one  $\text{CH}_3$  groups for Trans-4-PCHA, can increase the possibility for Trans-4-IsoPCHA to bond with the hydrophobic end of the DA SAL already adsorbed via  $-\text{CAHB}$ .
- The AM-FM-AFM images showed that DA molecules form aggregates on HOPG. This confirms the ability for multilayer adsorption as anticipated from NAs fitting the Freundlich adsorption isotherms and from the competitive adsorption results.
- The AM-FM-AFM technique revealed that adsorption occurred almost exclusively on the functionalized steps of HOPG and on the entire F-HOPG surfaces. The more even distribution of FGs on the F-HOPG surfaces created a more uniform adsorbed multilayer across the entire surface. This confirmed the vital role of  $-\text{CAHB}$  for the establishment of a SAL which can then act as a base layer for adsorption of other NAs.
- The adsorption of NAs from Merichem and OSPW on EG followed their  $\text{Log } K_{\text{ow}}$  values as was observed previously for the model NAs. It is concluded that  $-\text{CAHB}$  is the thermodynamically plausible mechanism for adsorption of these ionized weak acids on EG for both of these mixtures. The presence of large numbers of NAs species in both mixtures, in addition to the other soluble constituents in OSPW, did not impact the adsorption mechanism.

- The adsorption capacities for NAs from Merichem solutions and OSPW were less than 20% of the reported capacity for AC. As for AC, the application of EG in its current form is not considered to be cost effective for the treatment of OSPW; however, the adsorption mechanism revealed in this study will significantly contribute to the development of more efficient and cost effective engineered adsorbents.
- The determination of the current adsorption mechanism indicated that the fate and bioavailability of emerging and classical weak ionized acids released into natural water streams are impacted mainly by the attachment to functionalized nano-materials as they can adsorb weak ionized acids via –CAHB on the negatively charged functional groups.

To this end, the work approach herein showed experimentally and thermodynamically that the attraction between the two negatively charged ends of adsorbate and adsorbent surface can occur via HB. This was true for mono/multi compound solutions and complex mixtures. The visual characterization of the graphite surface after adsorption indicated adsorption to only the negatively charged regions. This work enhances our understanding for the adsorption of ionized weak acids that is essential for the development of efficient adsorbents for the removal of this class of compounds in any wastewater matrix.

### 6.3 Recommendations

Based on the research presented herein, the following recommendations for future studies can be drawn:

- Given the OSPW recycling by the oil sands industry for bitumen extraction, there is a potential for metal bridging to compete with the –CAHB at higher concentrations of dissolved metals. Future studies should consider the examination of this concern at higher concentrations of these dissolved metals.
- The examination of the adsorption of higher molecular weight and higher number of rings NAs is required to elucidate a full image of the behaviour of different classes of NAs in OSPW. Most of those NAs are not commercially available; therefore these future studies might be preceded by NAs synthesis and characterization.
- The development and regeneration of functionalized adsorbents should be investigated and cost should be assessed in order to reduce the capital and running cost of treatment. In-situ ozone generation using water plasma currently used by the oil sands industry can be used to functionalize the available PC for adsorption of NAs.
- The investigation of biodegradation of OSPW revealed that lower molecular weights with lower Log Kow NAs were removed. An optimized adsorbent should precede a biological treatment process to remove the recalcitrant NAs and to investigate the impact of the combination on the removal of NAs from OSPW.
- A detailed morphology of NAs' molecular aggregations may be achieved by using an even finer scan with a sharper tip for better resolution imaging using the AM-

FM-AFM or AFM-AFM techniques. This would confirm our finding for multilayer adsorption and reveal necessary information regarding the arrangement of NAs on HOPG and can be applied at different intervals before equilibrium to improve our understanding for the structural reactivity of NAs.

- In the current study, two model compounds, CHA and HPA, never adsorbed on the EG surface or on the SAL. The investigation of possible approaches to adsorb these and similar compounds on EG will increase the scope of using the graphite or other carbonaceous materials for treatment. This could be done by exploring the use of polymers to increase the steric interactions with these NAs and may be done also by investigating the occurrence of NAs dimers in solution which may offer increased hydrophobicity of these dimers which can possibly assist the adsorption of these compounds.

**7 APPENDIX A (SUPPORTING MATERIALS FOR CHAPTER 2)**

## **Identification of functional groups in acid-extractable fraction (AEF) by acid-base titration with linear programming method (LPM)**

The charge excess due to the deprotonation of binding sites during the acid-based titration is modeled using LPM to obtain the corresponding  $pK_a$  values and relative intensities [1, 2](Brassard et al., 1990; Smith et al., 1999). The 0.05 M NaOH titrant was prepared and standardized using  $C_8H_5KO_4$  as a primary standard. A 50 mL of OSPW 1 and Merichem NAs mixture (50 mg/L) were titrated using an autotitrator (Model DL53, Mettler Toledo, Switzerland) at a room temperature ( $20 \pm 1$  °C). A 100-mL closed glass graduated cylinder was placed on a stirring plate (Fisher Scientific, Model 120M, USA) and mixed using a magnetic stirring bar. Before titration, the pH of each sample was adjusted to pH 2.5 with 0.1 M  $H_2SO_4$ , and the samples were titrated until pH 11.6. Atmospheric dissolution of carbon dioxide in solutions during titration could bias the titration results. Therefore, the effect of carbon dioxide was eliminated by the subtraction of the blank generated by the titration of Milli-Q water. Titration data were then analyzed using a mathematical model based on LPM to estimate the  $pK_a$  values and intensities of the titrated functional groups [1, 3](Brassard et al., 1990; Cox et al., 1999). Analysis was performed in triplicate and the results are reported as  $avg \pm SD$ .

## **Quantification of classical NAs**

A Waters Acquity UPLC System (Milford, MA, USA) was used for the chromatographic separation of classical NAs. The UPLC system was connected to a high resolution Synapt G2 HDMS mass spectrometer equipped with an electrospray ionization source operating in the negative ion mode. The MassLynx ver. 4.1 and TargetLynx ver. 4.1 were used to control the system and to analyze the data of the target compounds, respectively. The tuning and calibration

were performed with leucine enkephalin standard solution and sodium formate, respectively

A UPLC Phenyl BEH column (1.7  $\mu\text{m}$ , 150 mm  $\times$  1 mm) was used for the chromatographic separation. The mobile phase consisted of: solution A, 10 mM ammonium acetate in Optima-grade water, and solution B, 10 mM ammonium acetate in 50% methanol/50% acetonitrile. The gradient elution was patterned as follows: 1% B for the first 2 min then ramped to 60% B by 3 min, to 70% B by 7 min, to 95% B by 13 min, followed by a hold until 14 min and finally returned to 1% B, followed by a further 5.8 min re-equilibration time. A 100  $\mu\text{L}/\text{min}$  constant flow was maintained through the system and the column temperature was kept at 50  $^{\circ}\text{C}$ . All samples were preserved at 4  $^{\circ}\text{C}$ . Only classical NAs (non-oxidized) were estimated in this study.

- [1] Brassard P, Kramer JR, Collins PV. Binding-site analysis using linear-programming-method. *Environmental Science & Technology* 1990;24:195-201.
- [2] Smith DS, Adams NWH, Kramer JR. Resolving uncertainty in chemical speciation determinations. *Geochimica Et Cosmochimica Acta* 1999;63:3337-3347.
- [3] Cox JS, Smith DS, Warren LA, Ferris FG. Characterizing heterogeneous bacterial surface functional groups using discrete affinity spectra for proton binding. *Environmental Science & Technology* 1999;33:4514-4521.

**8 APPENDIX B (SUPPORTING MATERIALS FOR CHAPTER 3)**

### **Naphthenic acids (NAs) quantification**

Duplicate NAs samples were quantified using a high performance liquid chromatograph coupled to an ion trap mass spectrometer (HPLC/MS) (Varian500-MS) equipped with a Phenomenex C<sub>8</sub> column as described by Afzal et al. (2012). The separating method was: A, 100% methanol, and B, 4 mM ammonium acetate (aqueous) with 0.1% acetic acid, gradient elution from 45% to 15% A over 30 min and returned to 45% A for 10 min. The flow was 200  $\mu\text{L min}^{-1}$  with 20  $\mu\text{L}$  injection volume, and column temperature was 40 °C. The detection limit expressed as the lowest concentration 3 times higher than the noise level for the current model NAs and HPLC/MS method ranged from 0.02 to 0.1 ppm[1].

### **Nonlinear least-squares regression using MATLAB software (R2013a)**

Two built-in available subroutines were used including LSQCURVEFIT for the minimization of the objective function and NLPARCI for the estimation of the 95% confidence intervals. The evaluation of model parameters was conducted using duplicate experimental datasets. The solution for the determined coefficients (a's and n's) must be positive. The optimization criteria used was based on a minimum sum of squares (SSQ) defined as:

$$\text{SSQ} = \sqrt{\sum_{i=1}^N ((x_{i,\text{exp}} - x_{i,\text{pred}})^2)}$$

Where  $x_{i,\text{exp}}$  and  $x_{i,\text{pred}}$  are the  $q_e$  of compound  $i$  obtained experimentally and predicted by the multi-compound Freundlich adsorption model, respectively.

[1] Afzal A, Drzewicz P, Martin JW, El-Din MG. Decomposition of cyclohexanoic acid by the UV/H<sub>2</sub>O<sub>2</sub> process under various conditions. Science of the Total Environment 2012;426:387-392.

**9 APPENDIX C (SUPPORTING MATERIALS FOR CHAPTER 4)**

## **XPS analysis**

The as received fresh peeled and treated HOPG were characterized away from the graphene steps to monitor the development of oxygenated groups at a depth = 2–5 mm. The analytical chamber was sustained under  $3 \times 10^{-8}$  Pa and a monochromatic Al K $\alpha$  source ( $h\nu = 1486.6$  eV) was used at 210 W, while survey scans were collected for binding energies from 1100 to 0 eV with analyzer pass energy of 160 eV and a step of 0.4 eV. For high-resolution spectra, pass energy was 20 eV with a 0.1 eV step with no charge neutralization required for conducting samples.

**10 APPENDIX D (SUPPORTING MATERIALS FOR CHAPTER 5)**

## Adsorption Isotherm Calculations

The Langmuir model was developed to describe monolayers on homogenous surfaces[1], while the Freundlich model considers the heterogenic nature of adsorbent surfaces and could represent mono and mono/multilayer adsorption[2]. Linear regression was employed to determine the adsorption parameters for isotherm models according to the following:

$$\text{Langmuir model: } q_e = (q_{max}bC_e)/(1 + bC_e) \quad (1)$$

Where  $q_e$  ( $\text{mg g}^{-1}$ ) and  $C_e$  ( $\text{mg/L}$ ) are the mass of sorbed NA on EG and NAs concentration in solution; respectively, at equilibrium.  $q_{max}$  ( $\text{mg g}^{-1}$ ) is the maximum adsorption capacity at equilibrium and  $b$  ( $\text{L mg}^{-1}$ ) is a constant related to the strength of the adsorption bond.

$$\text{Freundlich model: } q_e = KC_e^{(1/n)} \quad (2)$$

Where  $K$  ( $\text{mg/L}$ ) is an adsorption capacity related constant and  $n$  is an adsorption strength related constant.

[1] Langmuir I. The adsorption of gases on plane surfaces of glass, mica and platinum. *Journal of the American Chemical Society* 1918;40:1361-1403.

[2] Halsey G, Taylor HS. The adsorption of hydrogen tungsten powders. *Journal of Chemical Physics* 1947;15:624-630.

[3] Moustafa A, McPhedran K, Moreira J, Gamal El-Din M. Investigation of Mono/Competitive Adsorption of Environmentally Relevant Ionized Weak Acids on Graphite: Impact of Molecular Properties and Thermodynamics. *Environmental Science & Technology* 2014;48:14472–14480.

## 11 Bibliography

- [1] Allen EW. Process water treatment in Canada's oil sands industry: I. Target pollutants and treatment objectives. *Journal of Environmental Engineering and Science* 2008;7:123-138.
- [2] Smith BE, Lewis CA, Belt ST, Whitby C, Rowland SJ. Effects of Alkyl Chain Branching on the Biotransformation of Naphthenic Acids. *Environmental Science & Technology* 2008;42:9323-9328.
- [3] Holowenko FM, MacKinnon MD, Fedorak PM. Characterization of naphthenic acids in oil sands wastewaters by gas chromatography-mass spectrometry. *Water Research* 2002;36:2843-2855.
- [4] Kannel PR, Gan TY. Naphthenic acids degradation and toxicity mitigation in tailings wastewater systems and aquatic environments: a review. *Journal of environmental science and health Part A, Toxic/hazardous substances & environmental engineering* 2012;47:1-21.
- [5] Ityokumbul MT, Kasperski KL. Reactivity of caustic treated oil sand coke residues. *Fuel Processing Technology* 1994;37:281-294.
- [6] El-Din MG, Fu H, Wang N, Chelme-Ayala P, Perez-Estrada L, Drzewicz P, et al. Naphthenic acids speciation and removal during petroleum-coke adsorption and ozonation of oil sands process-affected water. *Science of the Total Environment* 2011;409:5119-5125.
- [7] Quagraine EK, Peterson HG, Headley JV. In situ bioremediation of naphthenic acids contaminated tailing pond waters in the Athabasca oil sands region-demonstrated field studies and plausible options: A review. *Journal of Environmental Science and Health Part a-Toxic/Hazardous Substances & Environmental Engineering* 2005;40:685-722.
- [8] Han X, MacKinnon MD, Martin JW. Estimating the in situ biodegradation of naphthenic acids in oil sands process waters by HPLC/HRMS. *Chemosphere* 2009;76:63-70.
- [9] MacKinnon M, Van Meer T, Verbeek A. Assessment of biological impact from a wet landscape option for the reclamation of fine tails from oil sands. *Canadian Technical Report of Fisheries and Aquatic Sciences* 1993;0:258.
- [10] Nelson PN, Baldock JA, Oades JM. Concentration and composition of dissolved organic-carbon in streams in relation to catchment soil properties. *Biogeochemistry* 1993;19:27-50.
- [11] Headley JV, McMartin DW. A review of the occurrence and fate of naphthenic acids in aquatic environments. *Journal of Environmental Science and Health Part a-Toxic/Hazardous Substances & Environmental Engineering* 2004;39:1989-2010.
- [12] Mackinnon MD, Retallack JT. Preliminary characterization and de toxification of tailings pond water at the syncrude canada limited oil sands plant. *Proceedings of the 4th Annual Meeting of the International Society of Petroleum Industry Biologists* 1982:P185-210.
- [13] Scott AC, MacKinnon MD, Fedorak PM. Naphthenic acids in athabasca oil sands tailings waters are less biodegradable than commercial naphthenic acids. *Environmental Science & Technology* 2005;39:8388-8394.
- [14] Clemente JS, Fedorak PM. A review of the occurrence, analyses, toxicity, and biodegradation of naphthenic acids. *Chemosphere* 2005;60:585-600.
- [15] Kaur K, Bhattacharjee S, Pillai RG, Ahmed S, Azmi S. Peptide arrays for detecting naphthenic acids in oil sands process affected water. *Rsc Advances* 2014;4:60694-60701.
- [16] Brient JA. Commercial utility of naphthenic acids recovered from petroleum distillates. *Abstracts of Papers of the American Chemical Society* 1998;215:018-PETR.
- [17] Barrow MP, Headley JV, Peru KM, Derrick PJ. Data Visualization for the Characterization of Naphthenic Acids within Petroleum Samples. *Energy & Fuels* 2009;23:2592-2599.
- [18] Pourrezaei P, Alpatova A, Chelme-Ayala P, Perez-Estrada LA, Jensen-Fontaine M, Le XC, et al. Impact of petroleum coke characteristics on the adsorption of the organic fractions from oil sands

process-affected water. *International Journal of Environmental Science and Technology* 2014;11:2037-2050.

[19] Frank RA, Fischer K, Kavanagh R, Burnison BK, Arsenault G, Headley JV, et al. Effect of carboxylic acid content on the acute toxicity of oil sands naphthenic acids. *Environmental Science & Technology* 2009;43:266-271.

[20] Frank RA, Sanderson H, Kavanagh R, Burnison BK, Headley JV, Solomon KR. Use of a (Quantitative) Structure-Activity Relationship (Q)SAR Model to Predict the Toxicity of Naphthenic Acids. *Journal of Toxicology and Environmental Health-Part a-Current Issues* 2010;73:319-329.

[21] Jones D, Scarlett AG, West CE, Rowland SJ. Toxicity of Individual Naphthenic Acids to *Vibrio fischeri*. *Environmental Science & Technology* 2011;45:9776-9782.

[22] Birkholz DA, Rogers RE, MacKinnon M. Molecular toxicology associated with natural naphthenic acids isolated from Syncrude tailings pond water and commercially available naphthenic acids. *Canadian Technical Report of Fisheries and Aquatic Sciences* 1997;0:109.

[23] Quagraine EK, Headley JV, Peterson HG. Is biodegradation of bitumen a source of recalcitrant naphthenic acid mixtures in oil sands tailing pond waters? *Journal of Environmental Science and Health Part a-Toxic/Hazardous Substances & Environmental Engineering* 2005;40:671-684.

[24] McKenzie N, Yue S, Liu X, Ramsay BA, Ramsay JA. Biodegradation of naphthenic acids in oils sands process waters in an immobilized soil/sediment bioreactor. *Chemosphere* 2014;109:164-172.

[25] Stackelberg PE, Gibs J, Furlong ET, Meyer MT, Zaugg SD, Lippincott RL. Efficiency of conventional drinking-water-treatment processes in removal of pharmaceuticals and other organic compounds. *Science of the Total Environment* 2007;377:255-272.

[26] Randtke SJ. Organic contaminant removal by coagulation and related process combinations. *Journal American Water Works Association* 1988;80:40-56.

[27] Rengaraj S, Moon SH, Sivabalan R, Arabindoo B, Murugesan V. Agricultural solid waste for the removal of organics: adsorption of phenol from water and wastewater by palm seed coat activated carbon. *Waste Management* 2002;22:543-548.

[28] Bousher A, Shen XD, Edyvean RGJ. Removal of coloured organic matter by adsorption onto low-cost waste materials. *Water Research* 1997;31:2084-2092.

[29] Zhang MM, Li C, Benjamin MM, Chang YJ. Fouling and natural organic matter removal in adsorbent/membrane systems for drinking water treatment. *Environmental Science & Technology* 2003;37:1663-1669.

[30] Iranmanesh S, Harding T, Abedi J, Seyedejn-Azad F, Layzell DB. Adsorption of naphthenic acids on high surface area activated carbons. *Journal of Environmental Science and Health Part a-Toxic/Hazardous Substances & Environmental Engineering* 2014;49:913-922.

[31] Mohamed MH, Wilson LD, Headley JV, Peru KM. Sequestration of naphthenic acids from aqueous solution using beta-cyclodextrin-based polyurethanes. *Physical Chemistry Chemical Physics* 2011;13:1112-1122.

[32] Lashaki MJ, Fayaz M, Wang H, Hashisho Z, Philips JH, Anderson JE, et al. Effect of Adsorption and Regeneration Temperature on Irreversible Adsorption of Organic Vapors on Beaded Activated Carbon. *Environmental Science & Technology* 2012;46:4083-4090.

[33] Zubot W, MacKinnon MD, Chelme-Ayala P, Smith DW, El-Din MG. Petroleum coke adsorption as a water management option for oil sands process-affected water. *Science of the Total Environment* 2012;427:364-372.

[34] Inagaki M, Suwa T. Pore structure analysis of exfoliated graphite using image processing of scanning electron micrographs. *Carbon* 2001;39:915-920.

[35] Toyoda M, Moriya K, Inagaki M. Temperature dependence of heavy oil sorption on exfoliated graphite. *Sekiyu Gakkaishi-Journal of the Japan Petroleum Institute* 2001;44:169-172.

- [36] Tryba B, Morawski AW, Kaleczuk RJ, Inagaki M. Exfoliated graphite as a new sorbent for removal of engine oils from wastewater. *Spill Science & Technology Bulletin* 2003;8:569-571.
- [37] Vieira F, Cisneros I, Rosa NG, Trindade GM, Mohallem NDS. Influence of the natural flake graphite particle size on the textural characteristic of exfoliated graphite used for heavy oil sorption *Carbon* 2006;44:2590-2592
- [38] Hristea G, Budrugaec P. Characterization of exfoliated graphite for heavy oil sorption *Journal of Thermal Analysis and Calorimetry* 2008;91:817-823.
- [39] Kalaitzidou K, Fukushima H, Drzal LT. Mechanical properties and morphological characterization of exfoliated graphite-polypropylene nanocomposites. *Composites Part a-Applied Science and Manufacturing* 2007;38:1675-1682.
- [40] Fukushima H, Drzal LT. Enhancement of the mechanical, electrical and thermal properties of nylon nanocomposites via addition of exfoliated graphite nanoplatelets (xGnP). *Proceedings of the Twelfth US-Japan Conference on Composite Materials* 2006:793-807.
- [41] Toyoda M, Inagaki M. Heavy oil sorption using exfoliated graphite - New application of exfoliated graphite to protect heavy oil pollution. *Carbon* 2000;38:199-210.
- [42] Inagaki M, Toyoda M, Kang FY, Zheng YP, Shen WC. Pore structure of exfoliated graphite - A report on a joint research project under the scientific cooperation program between NSFC and JSPS. *New Carbon Materials* 2003;18:241-249.
- [43] Inagaki M, Nagata T, Suwa T, Toyoda M. Sorption kinetics of various oils onto exfoliated graphite. *New Carbon Materials* 2006;21:97-102.
- [44] Toyoda M, Iwashita N, Inagaki M. Sorption of Heavy Oils into Carbon Materials. *Chemistry and Physics of Carbon, Vol 30* 2008;30:177-237.
- [45] Moustafa A. Fabrication characterization and oil spills remediation properties of the exfoliated graphite. *The Pennsylvania State University-Electronic thesis directory*; 2009.
- [46] Song Y-L, Li J-T, Chen H. Removal of acid brown 348 dye from aqueous solution by ultrasound irradiated exfoliated graphite. *Indian Journal of Chemical Technology* 2008;15:443-448.
- [47] Li JT, Li M, Li JH, Sun HW. Removal of disperse blue 2BLN from aqueous solution by combination of ultrasound and exfoliated graphite. *Ultrasonics Sonochemistry* 2007;14:62-66.
- [48] Ramesha GK, Kumara AV, Muralidhara HB, Sampath S. Graphene and graphene oxide as effective adsorbents toward anionic and cationic dyes. *Journal of Colloid and Interface Science* 2011;361:270-277.
- [49] Cornelissen G, Gustafsson O, Bucheli TD, Jonker MTO, Koelmans AA, Van Noort PCM. Extensive sorption of organic compounds to black carbon, coal, and kerogen in sediments and soils: Mechanisms and consequences for distribution, bioaccumulation, and biodegradation. *Environmental Science & Technology* 2005;39:6881-6895.
- [50] Allen-King RM, Grathwohl P, Ball WP. New modeling paradigms for the sorption of hydrophobic organic chemicals to heterogeneous carbonaceous matter in soils, sediments, and rocks. *Advances in Water Resources* 2002;25:985-1016.
- [51] Muller G, Radke CJ, Prausnitz JM. Adsorption of weak organic electrolytes from aqueous-solution on activated carbon - effect of pH. *Journal of Physical Chemistry* 1980;84:369-376.
- [52] Yang K, Wu W, Jing Q, Zhu L. Aqueous Adsorption of Aniline, Phenol, and their Substitutes by Multi-Walled Carbon Nanotubes. *Environmental Science & Technology* 2008;42:7931-7936.
- [53] Li X, Pignatello JJ, Wang Y, Xing B. New Insight into Adsorption Mechanism of Ionizable Compounds on Carbon Nanotubes. *Environmental Science & Technology* 2013;47:8334-8341.
- [54] Ni J, Pignatello JJ, Xing B. Adsorption of Aromatic Carboxylate Ions to Charcoal Black Carbon is Accompanied by Proton Exchange with Water (vol 45, pg 9240, 2012). *Environmental Science & Technology* 2012;46:5633-5633.

- [55] Teixido M, Pignatello JJ, Beltran JL, Granados M, Peccia J. Speciation of the Ionizable Antibiotic Sulfamethazine on Black Carbon (Biochar). *Environmental Science & Technology* 2011;45:10020-10027.
- [56] Hyun S, Lee LS. Hydrophilic and hydrophobic sorption of organic acids by variable-charge soils: Effect of chemical acidity and acidic functional group. *Environmental Science & Technology* 2004;38:5413-5419.
- [57] Fontecha-Camara MA, Lopez-Ramon MV, Alvarez-Merino MA, Moreno-Castilla C. Effect of surface chemistry, solution pH, and ionic strength on the removal of herbicides diuron and amitrole from water by an activated carbon fiber. *Langmuir* 2007;23:1242-1247.
- [58] Vinu A, Hossain KZ, Kumar GS, Ariga K. Adsorption of L-histidine over mesoporous carbon molecular sieves. *Carbon* 2006;44:530-536.
- [59] Del Rio LF, Hadwin AKM, Pinto LJ, MacKinnon MD, Moore MM. Degradation of naphthenic acids by sediment micro-organisms. *Journal of Applied Microbiology* 2006;101:1049-1061.
- [60] Grewer DM, Young RF, Whittal RM, Fedorak PM. Naphthenic acids and other acid-extractables in water samples from Alberta: What is being measured? *Science of the Total Environment* 2010;408:5997-6010.
- [61] Pourrezaei P, Drzewicz P, Wang Y, El-Din MG, Perez-Estrada LA, Martin JW, et al. The Impact of Metallic Coagulants on the Removal of Organic Compounds from Oil Sands Process-Affected Water. *Environmental Science & Technology* 2011;45:8452-8459.
- [62] Kavanagh RJ, Burnison BK, Frank RA, Solomon KR, Van Der Kraak G. Detecting oil sands process-affected waters in the Alberta oil sands region using synchronous fluorescence spectroscopy. *Chemosphere* 2009;76:120-126.
- [63] Frank RA, Kavanagh R, Burnison BK, Headley JV, Peru KM, Van Der Kraak G, et al. Diethylaminoethyl-cellulose clean-up of a large volume naphthenic acid extract. *Chemosphere* 2006;64:1346-1352.
- [64] Martin JW, Barri T, Han XM, Fedorak PM, El-Din MG, Perez L, et al. Ozonation of Oil Sands Process-Affected Water Accelerates Microbial Bioremediation. *Environmental Science & Technology* 2010;44:8350-8356.
- [65] Jivraj MN, MacKinnon, M.D., Fung, B. Naphthenic acid extraction and quantitative analysis with FTIR spectroscopy. Technical report; 1995 1995.
- [66] Martin JW, Han XM, Peru KM, Headley JV. Comparison of high- and low-resolution electrospray ionization mass spectrometry for the analysis of naphthenic acid mixtures in oil sands process water. *Rapid Communications in Mass Spectrometry* 2008;22:1919-1924.
- [67] He Y, Wiseman SB, Hecker M, Zhang X, Wang N, Perez LA, et al. Effect of Ozonation on the Estrogenicity and Androgenicity of Oil Sands Process-Affected Water. *Environmental Science & Technology* 2011;45:6268-6274.
- [68] Anderson JC, Wiseman SB, Wang N, Moustafa A, Perez-Estrada L, Gamal El-Din M, et al. Effectiveness of Ozonation Treatment in Eliminating Toxicity of Oil Sands Process-Affected Water to *Chironomus dilutus*. *Environmental science & technology* 2012;46:486-493.
- [69] Bataineh M, Scott AC, Fedorak PM, Martin JW. Capillary HPLC/QTOF-MS for characterizing complex naphthenic acid mixtures and their microbial transformation. *Analytical Chemistry* 2006;78:8354-8361.
- [70] Brassard P, Kramer JR, Collins PV. Binding-site analysis using linear-programming. *Environmental Science & Technology* 1990;24:195-201.
- [71] Cox JS, Smith DS, Warren LA, Ferris FG. Characterizing heterogeneous bacterial surface functional groups using discrete affinity spectra for proton binding. *Environmental Science & Technology* 1999;33:4514-4521.

- [72] Peuravuori J, Koivikko R, Pihlaja K. Characterization, differentiation and classification of aquatic humic matter separated with different sorbents: synchronous scanning fluorescence spectroscopy. *Water Research* 2002;36:4552-4562.
- [73] Fein JB, Daughney CJ, Yee N, Davis TA. A chemical equilibrium model for metal adsorption onto bacterial surfaces. *Geochimica Et Cosmochimica Acta* 1997;61:3319-3328.
- [74] Ni H-G, Zeng H, Zeng EY. Sampling and analytical framework for routine environmental monitoring of organic pollutants. *Trac-Trends in Analytical Chemistry* 2011;30:1549-1559.
- [75] Xie R, Li Y, Chu L-Y. Preparation of thermo-responsive gating membranes with controllable response temperature. *Journal of Membrane Science* 2007;289:76-85.
- [76] Chandler-Temple A, Wentrup-Byrne E, Whittaker AK, Grondahl L. Graft Copolymerization of Methoxyacrylethyl Phosphate onto Expanded Poly(tetrafluoroethylene) Facial Membranes. *Journal of Applied Polymer Science* 2010;117:3331-3339.
- [77] Chebbi R, Beicha A, Daud WRW, Zaamouche R. Surface analysis for catalyst layer (PT/PTFE/C) and diffusion layer (PTFE/C) for proton exchange membrane fuel cells systems (PEMFCs). *Applied Surface Science* 2009;255:6367-6371.
- [78] Wang X, Tian Y, Wang Z, Tao Y. A Novel Hydrophilic Modification of PTFE Membranes Using In Situ Deposited PANI. *Journal of Macromolecular Science Part B-Physics* 2011;50:172-178.
- [79] Wang L, Zhang X, Hou S, Wang X, Wang A, Liu S. Preparation and Characterization of Hydrophilic PVDF Membrane via graft modification by Maleic Anhydride. In: Wang PCALLYGSXMBJL, editor. *Manufacturing Science and Technology, Pts 1-3*; 2011. p. 286-291.
- [80] Yang X, Zhang B, Liu Z, Deng B, Yu M, Li L, et al. Preparation of the antifouling microfiltration membranes from poly(N,N-dimethylacrylamide) grafted poly(vinylidene fluoride) (PVDF) powder. *Journal of Materials Chemistry* 2011;21:11908-11915.
- [81] Han MJ, Barona GNB, Jung B. Effect of surface charge on hydrophilically modified poly(vinylidene fluoride) membrane for microfiltration. *Desalination* 2011;270:76-83.
- [82] Lin A, Shao S, Li H, Yang D, Kong Y. Preparation and characterization of a new negatively charged polytetrafluoroethylene membrane for treating oilfield wastewater. *Journal of Membrane Science* 2011;371:286-292.
- [83] Cabaniss SE, Shuman MS. Synchronous fluorescence-spectra of natural-waters - tracing sources of dissolved organic-matter. *Marine Chemistry* 1987;21:37-50.
- [84] Pullin MJ, Cabaniss SE. Physicochemical variations in DOM-synchronous fluorescence: Implications for mixing studies. *Limnology and Oceanography* 1997;42:1766-1773.
- [85] B.H S. *Infrared Spectroscopy: Fundamentals and Applications*: John Wiley & Sons, Ltd., Chichester, UK; 2004.
- [86] Pan B, Lin D, Mashayekhi H, Xing B. Adsorption and hysteresis of bisphenol A and 17 alpha-ethinyl estradiol on carbon nanomaterials. *Environmental Science & Technology* 2008;42:5480-5485.
- [87] Cao X, Ma L, Gao B, Harris W. Dairy-Manure Derived Biochar Effectively Sorbs Lead and Atrazine. *Environmental Science & Technology* 2009;43:3285-3291.
- [88] Wang H, Lashaki MJ, Fayaz M, Hashisho Z, Philips JH, Anderson JE, et al. Adsorption and Desorption of Mixtures of Organic Vapors on Beaded Activated Carbon. *Environmental Science & Technology* 2012;46:8341-8350.
- [89] Langmuir I. The adsorption of gases on plane surfaces of glass, mica and platinum. *Journal of the American Chemical Society* 1918;40:1361-1403.
- [90] Halsey G, Taylor HS. The adsorption of hydrogen on tungsten powders. *Journal of Chemical Physics* 1947;15:624-630.
- [91] Sheindorf C, Rebhun M, Sheintuch M. Organic pollutants adsorption from multicomponent systems modeled by freundlich type isotherm. *Water Research* 1982;16:357-362.

- [92] Chen GH, Wu DJ, Weng WG, Yan WL. Dispersion of graphite nanosheets in a polymer matrix and the conducting property of the nanocomposites. *Polymer Engineering and Science* 2001;41:2148-2154.
- [93] Krawczyk P. Effect of ozone treatment on properties of expanded graphite. *Chemical Engineering Journal* 2011;172:1096-1102.
- [94] He H, Gao C. General Approach to Individually Dispersed, Highly Soluble, and Conductive Graphene Nanosheets Functionalized by Nitrene Chemistry. *Chemistry of Materials* 2010;22:5054-5064.
- [95] Lashaki MJ, Fayaz M, Niknaddaf S, Hashisho Z. Effect of the adsorbate kinetic diameter on the accuracy of the Dubinin-Radushkevich equation for modeling adsorption of organic vapors on activated carbon. *Journal of Hazardous Materials* 2012;241:154-163.
- [96] Pelekani C, Snoeyink VL. Competitive adsorption in natural water: Role of activated carbon pore size. *Water Research* 1999;33:1209-1219.
- [97] Behera SK, Oh S-Y, Park H-S. Sorption of triclosan onto activated carbon, kaolinite and montmorillonite: Effects of pH, ionic strength, and humic acid. *Journal of Hazardous Materials* 2010;179:684-691.
- [98] Kumar PS, Vincent C, Kirthika K, Kumar KS. Kinetics and equilibrium studies of pb<sup>2+</sup> ion removal from aqueous solutions by use of nano-silversol-coated activated carbon. *Brazilian Journal of Chemical Engineering* 2010;27:339-346.
- [99] Dubus IG, Barriuso E, Calvet R. Sorption of weak organic acids in soils: clofencet, 2,4-D and salicylic acid. *Chemosphere* 2001;45:767-774.
- [100] Aquino AJA, Tunega D, Habephauer G, Gerzabek MH, Lischka H. Interaction of the 2,4-dichlorophenoxyacetic acid herbicide with soil organic matter moieties: a theoretical study. *European Journal of Soil Science* 2007;58:889-899.
- [101] Aristilde L, Sposito G. Binding of ciprofloxacin by humic substances: a molecular dynamics study. *Environmental Toxicology and Chemistry* 2010;29:90-98.
- [102] Iskrenova-Tchoukova E, Kalinichev AG, Kirkpatrick RJ. Metal Cation Complexation with Natural Organic Matter in Aqueous Solutions: Molecular Dynamics Simulations and Potentials of Mean Force. *Langmuir* 2010;26:15909-15919.
- [103] Moreno-Castilla C. Adsorption of organic molecules from aqueous solutions on carbon materials. *Carbon* 2004;42:83-94.
- [104] Wu CH, Kuo CY, Lin CF, Lo SL. Modeling competitive adsorption of molybdate, sulfate, selenate, and selenite using a Freundlich-type multi-component isotherm. *Chemosphere* 2002;47:283-292.
- [105] Maity N, Payne GF. Adsorption from aqueous-solutions based on a combination of hydrogen-bonding and hydrophobic interactions. *Langmuir* 1991;7:1247-1254.
- [106] Gilli G, Gilli P. Towards an unified hydrogen-bond theory. *Journal of Molecular Structure* 2000;552:1-15.
- [107] Gilli P, Pretto L, Bertolasi V, Gilli G. Predicting Hydrogen-Bond Strengths from Acid-Base Molecular Properties. The pK(a) Slide Rule: Toward the Solution of a Long-Lasting Problem. *Accounts of Chemical Research* 2009;42:33-44.
- [108] Lum K, Chandler D, Weeks JD. Hydrophobicity at small and large length scales. *Journal of Physical Chemistry B* 1999;103:4570-4577.
- [109] Berne BJ, Weeks JD, Zhou R. Dewetting and Hydrophobic Interaction in Physical and Biological Systems. *Annual Review of Physical Chemistry* 2009;60:85-103.
- [110] Hua L, Zangi R, Berne BJ. Hydrophobic Interactions and Dewetting between Plates with Hydrophobic and Hydrophilic Domains. *Journal of Physical Chemistry C* 2009;113:5244-5253.
- [111] Mittal J, Hummer G. Interfacial thermodynamics of confined water near molecularly rough surfaces. *Faraday Discussions* 2010;146:341-352.
- [112] Vembanur S, Patel AJ, Sarupria S, Garde S. On the Thermodynamics and Kinetics of Hydrophobic Interactions at Interfaces. *Journal of Physical Chemistry B* 2013;117:10261-10270.

- [113] Knappe DRU, Matsui Y, Snoeyink VL, Roche P, Prados MJ, Bourbigot MM. Predicting the capacity of powdered activated carbon for trace organic compounds in natural waters. *Environmental Science & Technology* 1998;32:1694-1698.
- [114] Shin YJ, Wang Y, Huang H, Kalon G, Wee ATS, Shen Z, et al. Surface-Energy Engineering of Graphene. *Langmuir* 2010;26:3798-3802.
- [115] Perreault F, Tousley, M.E., Elimelech. Thin-film composite polyamide membranes functionalized with biocidal graphene oxide nanosheets. 2014.
- [116] Pei Z, Li L, Sun L, Zhang S, Shan X-q, Yang S, et al. Adsorption characteristics of 1,2,4-trichlorobenzene, 2,4,6-trichlorophenol, 2-naphthol and naphthalene on graphene and graphene oxide. *Carbon* 2013;51:156-163.
- [117] Moustafa A, McPherdan K, Moreira J, Gamal El-Din M. Investigation of Mono/Competitive Adsorption of Environmentally Relevant Ionized Weak Acids on Graphite: Impact of Molecular Properties and Thermodynamics. *Environmental Science & Technology* 2014;48:14472-14480.
- [118] Herruzo ET, Perrino AP, Garcia R. Fast nanomechanical spectroscopy of soft matter. *Nature Communications* 2014;5.
- [119] Lamour G, Yip CK, Li H, Gsponer J. High Intrinsic Mechanical Flexibility of Mouse Prion Nanofibrils Revealed by Measurements of Axial and Radial Young's Moduli. *Acs Nano* 2014;8:3851-3861.
- [120] Maurer SE, DeClue MS, Albertsen AN, Dorr M, Kuiper DS, Ziock H, et al. Interactions between Catalysts and Amphiphilic Structures and their Implications for a Protocell Model. *Chemphyschem* 2011;12:828-835.
- [121] Robertson J. Diamond-like amorphous carbon. *Materials Science & Engineering R-Reports* 2002;37:129-281.
- [122] Konkena B, Vasudevan S. Understanding Aqueous Dispersibility of Graphene Oxide and Reduced Graphene Oxide through pK(a) Measurements. *Journal of Physical Chemistry Letters* 2012;3:867-872.
- [123] Chowdhury I, Duch MC, Mansukhani ND, Hersam MC, Bouchard D. Colloidal Properties and Stability of Graphene Oxide Nanomaterials in the Aquatic Environment. *Environmental Science & Technology* 2013;47:6288-6296.
- [124] Compton OC, Nguyen ST. Graphene Oxide, Highly Reduced Graphene Oxide, and Graphene: Versatile Building Blocks for Carbon-Based Materials. *Small* 2010;6:711-723.
- [125] Liu S, Zeng TH, Hofmann M, Burcombe E, Wei J, Jiang R, et al. Antibacterial Activity of Graphite, Graphite Oxide, Graphene Oxide, and Reduced Graphene Oxide: Membrane and Oxidative Stress. *Acs Nano* 2011;5:6971-6980.
- [126] Gao Y, Li Y, Zhang L, Huang H, Hu J, Shah SM, et al. Adsorption and removal of tetracycline antibiotics from aqueous solution by graphene oxide. *Journal of Colloid and Interface Science* 2012;368:540-546.
- [127] Maliyekkal SM, Sreepasad TS, Krishnan D, Kouser S, Mishra AK, Waghmare UV, et al. Graphene: A Reusable Substrate for Unprecedented Adsorption of Pesticides. *Small* 2013;9:273-283.
- [128] Xu J, Wang L, Zhu Y. Decontamination of Bisphenol A from Aqueous Solution by Graphene Adsorption. *Langmuir* 2012;28:8418-8425.
- [129] Wang J, Chen Z, Chen B. Adsorption of Polycyclic Aromatic Hydrocarbons by Graphene and Graphene Oxide Nanosheets. *Environmental Science & Technology* 2014;48:4817-4825.
- [130] Kaur K, Bhattacharjee S, Pillai R, Ahmed S, Azmi S. Peptide arrays for detecting naphthenic acids in oil sands process affected water. *RSC Advances* 2014;4:60694-60701.
- [131] Smith DS, Adams NWH, Kramer JR. Resolving uncertainty in chemical speciation determinations. *Geochimica Et Cosmochimica Acta* 1999;63:3337-3347.
- [132] Afzal A, Drzewicz P, Martin JW, El-Din MG. Decomposition of cyclohexanoic acid by the UV/H<sub>2</sub>O<sub>2</sub> process under various conditions. *Science of the Total Environment* 2012;426:387-392.